University of Alberta

Deposition of Asphaltene-in-Toluene Droplets in an Impinging Jet Cell

by

Vinod Kumar ©

A thesis submitted to the Faculty of Graduate Studies and Research in partial fulfillment of the requirements for the degree of Master of Science

in

Chemical Engineering

Department of Chemical and Materials Engineering

Edmonton, Alberta

Fall, 2002

National Library
of Canada

Acquisitions and
Bibliographic Services

395 Wellington Street
Ottawa ON K1A 0N4
Canada

Bibliothèque nationale
du Canada

Acquisitions et
services bibliographiques

395, rue Wellington
Ottawa ON K1A 0N4
Canada

Your file Votre référence

Our file Notre référence

The author has granted a non-exclusive licence allowing the National Library of Canada to reproduce, loan, distribute or sell copies of this thesis in microform, paper or electronic formats.

L'auteur a accordé une licence non exclusive permettant à la Bibliothèque nationale du Canada de reproduire, prêter, distribuer ou vendre des copies de cette thèse sous la forme de microfiche/film, de reproduction sur papier ou sur format électronique.

The author retains ownership of the copyright in this thesis. Neither the thesis nor substantial extracts from it may be printed or otherwise reproduced without the author's permission.

L'auteur conserve la propriété du droit d'auteur qui protège cette thèse. Ni la thèse ni des extraits substantiels de celle-ci ne doivent être imprimés ou autrement reproduits sans son autorisation.

0-612-81425-4

Canada

University of Alberta

Library Release Form

Name of Author:	Vinod Kumar
Title of Thesis:	Deposition of Asphaltene-in-Toluene Droplets in an Impinging Jet Cell
Degree:	Master of Science
Year this Degree Granted:	2002

Permission is hereby granted to the University of Alberta Library to reproduce single copies of this thesis and to lend or sell such copies for private or scientific research purposes only.

The author reserves all other publication and other rights in association with the copyright in the thesis, and except as herein before provided, neither the thesis nor any substantial portion thereof may be printed or otherwise reproduced in any material form whatever without the author's prior permission.

Vinod Kumar

Vinod Kumar
11304 – 12 Avenue
Edmonton, AB, T6J 6S4
Canada

Date: September 20, 2002

University of Alberta

Faculty of Graduate Studies and Research

The undersigned certify that they have read, and recommend to the Faculty of Graduate Studies and Research for acceptance, a thesis entitled "Deposition of Asphaltene-in-Toluene Droplets in an Impinging Jet Cell" submitted by Vinod Kumar in partial fulfillment of the requirements for the degree of Master of Science.

J. H. Masliyah
(Supervisor)

Dr. Sean Sanders
(Co-Supervisor)

Dr. Subir Bhattacharjee

Dr. Shijie Liu

Date: August 19, 2002

Acknowledgements

Apart from the principles of colloidal science, many other things were put on trial in the attempt of writing this thesis. If I may begin with myself, first, it was my own resilience to enter into an intense academic discipline after several years of engagement with industrial life. Then I should mention my wife's ability to dream about excellences of life and pursue them. I drew heavily upon her undefeatable spirit and capability for prudent denials of the negatives. Also put on trial was my little children's capacity for making numerous sacrifices, even without understanding it, which includes forgiveness for my long absences for uncountable days. I stand indebted.

I also stand indebted to Dr. Jacob H. Masliyah, my supervisor for providing me this opportunity, his support and his guidance. His confidence in my abilities and encouragement gave me the strength and determination to complete this thesis. I am highly indebted to Dr. Sean Sanders for his keen interest in my work, his advice, stimulating discussions and invaluable help in preparation of this thesis. I also wish to thank Dr. Chun Yang for introducing me to the impinging jet technique used in this study. I would also like to specially acknowledge Dr. Jan Czarnecki of Syncrude Research for providing me the equipment of the impinging jet and all other material help.

I wish to thank members of the examining committee for their time and consideration of this thesis. Lastly, financial support from COURSE and from Albian Sands Energy is gratefully acknowledged.

Abstract

Understanding of asphaltene interaction with asphaltene, bitumen, clay fines and air bubbles is important in the success of the oil sand industry in north Alberta. Interest in this subject stems from its relevance to Albian Sands' new froth treatment process in which asphaltenes will be precipitated along with water, bitumen and clay fines. Although the asphaltene precipitation process is well known, there is very little data available on the precipitated asphaltenes – their interactions with each other to form aggregates, with bitumen, and with hydrophobic and hydrophilic surfaces such as fines and air bubbles.

This thesis presents results of both experimental investigation and theoretical modeling of the deposition process of asphaltene-in-toluene droplets suspended in water onto hydrophilic, hydrophobic, bitumen coated and asphaltene coated surfaces. A well established impinging jet technique is used to study the deposition of a flowing asphaltene-in-toluene droplets suspended in water onto a solid substrate at varying flow rates, pH and electrolyte concentrations. The deposition process is modeled by solving the mass transport equation which includes influences of hydrodynamic convection, Brownian diffusion and migration under gravitational and DLVO forces (e.g. the van der Waals and electrical double layer forces).

The model simulations were found to be in reasonable agreement with the experimental data when electrostatic double layer interactions are neglected. However, the model failed to predict deposition when the electrostatic force is considered.

Contents

Page

Chapter one **Introduction** 1
1.0 Objective of this study 3
1.1 Thesis outline 4

Chapter Two **Colloidal deposition** 5
2.0 Impinging jet technique 7
2.1 Experimental setup 9
2.2 Analysis of deposition experiments 10

Chapter Three **Theory** 15
3.0 Introduction 15
3.1 Solution of mass transport equation 15
3.2 General expression for mass flux 16
3.3 Fluid velocity in the stagnation region 17
3.4 Particle or droplet velocity 20
3.5 Particle or droplet diffusion coefficient 21
3.6 External body forces 22
3.7 Colloidal surface forces 23
3.7.1 van der Waals interaction 23
3.7.2 Electric double layer (EDL) interactions 28
3.8 Mass transport equation 33
3.9 Boundary conditions 35
3.10 Numerical method 36

Chapter Four **Sensitivity analysis and validation** 41
4.0 Introduction 41
4.1 Effect of particle radius 43
4.2 Effect of adhesion number 43
4.3 Effect of electrostatic double layer (EDL) strength parameter Dl 44

4.4 Numerical model validation and testing of experimental apparatus 45
4.5 Deposition experiments using latex particles 46
4.6 Conclusions 47

Chapter Five **Experimental method** 57
5.0 Introduction 57
5.1 Clean bitumen 57
5.2 Production of asphaltenes 58
5.3 Preparation and characterization of asphaltene-in-toluene droplet suspension in water 58
5.3.1 Concentrated suspension 58
5.3.2 Dilute suspension 60
5.3.3 Concentration and size distribution of asphaltene-in-toluene droplets 60
5.4 Collector surface preparation 61
5.4.1 Hydrophilic (untreated) glass slides 61
5.4.2 Hydrophobic (methylated) glass slide 62
5.4.3 Bitumen coated slide 63
5.4.4 Asphaltene coated slide 64
5.5 Zeta potential measurements 64
5.6 Choice of Hamaker constant 65
5.7 List of the conducted experiments 66

Chapter Six **Deposition of asphaltene-in-toluene droplet suspension in water on hydrophilic collectors** 70
6.0 Introduction 70
6.1 Analysis of the experiments with hydrophilic collectors 70

Chapter Seven **Deposition of asphaltene-in-toluene droplet suspension in water on hydrophobic collectors** 77
7.0 Introduction 77

	7.1	Collector surface preparation and characterization	79
	7.2	Analysis of the deposition experiments	79
Chapter Eight		**Deposition of asphaltene-in-toluene droplet suspension in water on coated collectors**	88
	8.0	Introduction	88
	8.1	Preparations	89
	8.2	Analysis of the experiments with asphaltene coated collectors	89
	8.3	Analysis of the experiments with bitumen coated collectors	91
Chapter Nine		**Summary, Conclusions and Recommendations**	97
	9.0	Discrepancy between experimental results and theoretical predictions (non – DLVO behavior)	97
	9.1	Summary	100
	9.2	Conclusions	100
	9.3	Recommendations for future work	101
	9.4	Contributions made by this study	102
References			103
Appendix	A	Computer code	111
Appendix	B	Raw data	130

List of Tables

Page

Table 4-1 Characterization of Sanders' latex depositing experiment. 45

Table 4-2 Characterization of latex deposition experiments. 47

Table 5-1 List of asphaltene-in-toluene deposition experiments. 66

Table 6-1 Experimental conditions for asphaltene-in-toluene droplet deposition onto a hydrophilic (untreated) glass collector. 71

Table 7-1 Experimental conditions for asphaltene-in-toluene droplet deposition onto a methylated (hydrophobic) glass collector. 80

Table 8-1 Experimental conditions for asphaltene coated collectors deposition experiments. 90

Table 8-2 Experimental conditions for bitumen coated collectors deposition experiments. 91

List of Figures

Page

Figure 2-1 Schematic of experimental setup for performing deposition experiments with the impinging jet apparatus. 13

Figure 2-2 Impinging jet cell. 14

Figure 3-1 Geometry of impinging jet cell: R = 1.275 mm; H_o = 2.55 mm; L = 40 mm. 39

Figure 3-2 Schematic diagram representing charge distribution around a negatively charged particle. 40

Figure 4-1 Predicted variation of Sherwood number with particle radius for a system described by Ad = 0.1, M_i = 0.01M (1:1), Dl = 0, Gr = 0, $\overline{H}_o = 2$. 49

Figure 4-2 Predicted variation of Sherwood number with adhesion number for a system described by a_p = 1.0 μm, Dl = 0, M_i = 0.01M (1:1), $\overline{H}_o = 2$, Gr = 0. 50

Figure 4-3 Predicted variation of Sherwood number with double layer strength parameter Dl for a system described by a_p = 1.0 μm, Ad = 0.5, Gr = 0, Re = 200, $\overline{H}_o = 2$ and electrolyte concentration = 0.1M (1:1 type). 51

Figure 4-4 Predicted variation of Sherwood number with double layer strength parameter Dl for a system described by a_p = 1.0 μm, Ad = 0.5, $\overline{H}_o = 2$, Gr = 0, Re = 200 and electrolyte concentration = 0.01M (1:1 type). 52

Figure 4-5 Simulation results (solid line) of the present study model for latex particle deposition experiments conducted by Sanders [1997]. Symbols represent Sanders' experimental results. Parameters used in the model: a_p = 0.416 μm; Ad = 0.2; [NaCl] = 0.01M; Dl = 0 and $\overline{\alpha} = 0.52\,Re^{0.5}$ 53

Figure 4-6 Sherwood number as a function of Reynolds number for the latex particle deposition experiments conducted by Sanders [1997]. Symbols represent experimental results and solid line represents predictions by Sanders' model using a_p = 0.416 μm, Ad = [0.2, 0.8], [NaCl] = 0.01M, Dl = 0 and $\overline{\alpha} = 0.52\,Re^{0.5}$. 54

Figure 4-7 Stagnation Region Coating Density (SRCD) as a function of time for latex particle deposition experiment conducted in this study. a_p = 1.45 μm, $\overline{\alpha} = 5.3\mathrm{Re}^{0.5} - 8.13$ (Re ≥ 5), pH = 5.8, [NaCl] = 0.01M, and $\overline{H}_o = 2$. 55

Figure 4-8 Sherwood number as a function of Reynolds number for the latex particle deposition experiments. Symbols represent experimental results and solid line indicates present study model simulation using a_p = 1.45 μm, Ad = 0.2, [NaCl] = 0.01M, Dl = 0, $\overline{H}_o = 2$ and $\overline{\alpha} = 5.3\mathrm{Re}^{0.5} - 8.13$ (Re ≥ 5). 56

Figure 5-1 Image of asphaltene-in-toluene droplet obtained with 50X objective. 67

Figure 5-2 A typical hemacytometer result of size distribution and concentration measurements of asphaltene-in-toluene droplet suspension in water. 68

Figure 5-3 Schematic diagram of chemical structures for untreated and methylated glass surfaces, proposed by Araujo et al. [1995] 69

Figure 6-1 Stagnation Region Coating Density (SRCD) as a function of time for asphaltene-in-toluene droplet deposition experiments onto hydrophilic (untreated) glass surfaces (Set # 3 in Table 6-1): pH = 3.5, [NaCl] = 0.01M, ζ_p = - 20 mV, ζ_c = - 45 mV, Ad = 0.412. 74

Figure 6-2 Dimensionless mass transfer rate (expressed as Sherwood number) as a function of Reynolds number of asphaltene-in-toluene droplet deposition onto hydrophilic (untreated) glass surfaces (Set # 3 in Table 6-1): pH = 3.5, a_p = 1.5 μm, Ad = 0.412, ζ_p = - 20 mV, ζ_c = - 45 mV, [NaCl] = 0.01M and $\overline{\alpha} = 5.3\mathrm{Re}^{0.5} - 8.13$ (Re ≥ 5). Symbols represent experimental results and solid line indicates model predictions using Dl = 0. 75

Figure 6-3 Dimensionless mass transfer rate (expressed as Sherwood number) as a function of Reynolds number of asphaltene-in-toluene droplet deposition onto hydrophilic (untreated) glass surfaces (Set # 4 in Table 6-1): pH = 8.0, [NaCl] = 0.001M, ζ_p = - 60 mV, ζ_c = - 75 mV, Ad = 0.412. Symbols represent experimental results and solid line indicates model predictions using Dl = 0. 76

Figure 7-1 Stagnation Region Coating Density (SRCD) as a function of time for asphaltene-in-toluene droplet deposition experiments onto hydrophobic (methylated) glass surfaces (Set # 2 in Table 7-1): pH = 8.5, [NaCl] = 0.01M, ζ_p = - 55 mV, ζ_c = - 30 mV, Ad = 0.412. 83

Figure 7-2 Dimensionless mass transfer rate (expressed as Sherwood number) as a function of Reynolds number of asphaltene-in-toluene droplet deposition onto hydrophobic (methylated) glass surfaces (Set # 2 in Table 7-1):pH = 8.5, a_p = 1.5 μm, Ad = 0.412, ζ_p = - 55 mV, ζ_c = - 30 mV, [NaCl] = 0.01M and $\overline{\alpha} = 5.3\mathrm{Re}^{0.5} - 8.13$ (Re ≥ 5). Symbols represent experimental results and solid line indicates model predictions using Dl = 0. 84

Figure 7-3 Stagnation Region Coating Density (SRCD) as a function of time for asphaltene-in-toluene droplet deposition experiments onto hydrophobic (methylated) glass surfaces (Set # 3 in Table 7-1): pH = 3.5, [NaCl] = 0.01M, ζ_p = - 20 mV, ζ_c = - 10 mV, Ad = 0.412. 85

Figure 7-4 Dimensionless mass transfer rate (expressed as Sherwood number) as a function of Reynolds number of asphaltene-in-toluene droplet deposition onto hydrophobic (methylated) glass surfaces (Set # 3 in Table 7-1): pH = 3.5, a_p = 1.5 μm, Ad = 0.412, ζ_p = - 20 mV, ζ_c = - 10 mV, [NaCl] = 0.01M and $\overline{\alpha} = 5.3\mathrm{Re}^{0.5} - 8.13$ (Re ≥ 5). Symbols represent experimental results and solid line indicates model predictions using Dl = 0. 86

Figure 7-5 Dimensionless mass transfer rate (expressed as Sherwood number) as a function of Reynolds number of asphaltene-in-toluene droplet deposition onto hydrophobic (methylated) glass surfaces (Set # 4 in Table 7-1): pH = 8.0, [NaCl] = 0.001M, ζ_p = - 60 mV, ζ_c = - 40 mV, Ad = 0.412. Symbols represent experimental results and solid line indicates model predictions using Dl = 0. 87

Figure 8-1 Stagnation Region Coating Density (SRCD) as a function of time for asphaltene-in-toluene droplet deposition experiments onto asphaltene coated collector (Set # 2 in Table 8-1): pH = 3.5, [NaCl] = 0.01M, ζ_p = - 20 mV, ζ_c = - 20 mV, Ad = 0.132. 93

Figure 8-2 Dimensionless mass transfer rate (expressed as Sherwood number) as a function of Reynolds number of asphaltene-in-toluene droplet deposition onto asphaltene coated glass collectors (Set # 2 in Table 8-1): pH = 3.5, a_p = 1.5 μm, Ad = 0.132, ζ_p = - 20 mV, ζ_c = - 10 mV, [NaCl] = 0.01M and $\overline{\alpha} = 5.3\mathrm{Re}^{0.5} - 8.13$ (Re ≥ 5). Symbols represent experimental results and solid line indicates model predictions using Dl = 0. 94

Figure 8-3 Stagnation Region Coating Density (SRCD) as a function of time for asphaltene-in-toluene droplet deposition experiments onto bitumen coated collector (Set # 4 in Table 8-2): pH = 3.5, [NaCl] = 0.01M, $\zeta_p = -20$ mV, $\zeta_c = -25$ mV, Ad = 0.132. 95

Figure 8-4 Dimensionless mass transfer rate (expressed as Sherwood number) as a function of Reynolds number of asphaltene-in-toluene droplet deposition onto bitumen coated glass collectors (Set # 4 in Table 8-2): pH = 3.5, $a_p = 1.5$ μm, Ad = 0.132, $\zeta_p = -20$ mV, $\zeta_c = -25$ mV, [NaCl] = 0.01M and $\overline{\alpha} = 5.3\,Re^{0.5} - 8.13$ ($Re \geq 5$). Symbols represent experimental results and solid line indicates model predictions using Dl = 0. 96

Nomenclature

a_p	Droplet or particle radius, [m]
Ad	Dimensionless adhesion number, $[A_{132}/(6kT)]$
A_{132}	Hamaker constant for van der Waals force between phase 1 (a particle or droplet of radius a_p) and phase 2 (collector surface) separated by medium 3 (an aqueous solution), [J]
A_{ij}	Hamaker constant for van der Waals force between phase i and phase j in vacuum, [J]
c	Local particle or droplet concentration, $[m^{-3}]$
c_o	Bulk particle or droplet concentration, $[m^{-3}]$
$\overline{\overline{D}}$	Particle or droplet diffusion coefficient tensor, $[m^2\ s^{-1}]$
D_∞	Bulk particle or droplet diffusion coefficient tensor, $(D_\infty = kT/6\pi\mu_f a_p)$, $[m^2\ s^{-1}]$
Da	Dimensionless double layer (EDL) asymmetry parameter, $\left(Da = \frac{(\zeta_p - \zeta_c)^2}{2\zeta_p \zeta_c}\right)$
Dl	Dimensionless double layer (EDL) strength parameter, $\left(Dl = \frac{4\pi\varepsilon_o \varepsilon_r \kappa a_p \zeta_p \zeta_c}{kT}\right)$
d_{rr}, d_{zz}	Diffusion coefficient corrections, dimensionless
DLVO	Derjaguin-Landau-Verwey-Overbeek
e	Elementary charge, $[1.602 \times 10^{-19}\ C]$
f_i	Dimensionless universal hydrodynamic correction coefficients, [i = 1 to 4]
F, $\vec{F}$	Force or force vector, [N]
F_r, F_z	Force components, [N]
F_{Col}	Colloidal force, [N]
F_{Ex}	External force, [N]

ε_r	Dielectric constant
θ	Contact angle, [deg]
κ	Inverse Debye Huckel length, [m^{-1}]
κa_p	Dimensionless double layer (EDL) thickness parameter
λ	London characteristic wavelength or retardation parameter, [$\lambda = 10^{-7}$ m]
$\bar{\lambda}$	Dimensionless retardation parameter, [λ / a_P]
μ_f	Bulk (fluid) viscosity, [Pa s]
ζ_p	Particle or droplet zeta potential, [V]
ζ_c	Collector zeta potential. [V]
ρ_f	Fluid density, [kg m^{-3}]
ρ_p	Particle or droplet mean density, [kg m^{-3}]
ρ_e	Electrostatic charge density, [C m^{-3}]
$\Delta\rho$	Density difference between a particle or droplet and bulk fluid, [$\Delta\rho = (\rho_p - \rho_f)$, kg m^{-3}]
φ	Local potential in the EDL field, [V]
ψ	Stream function, [$m^3\ s^{-1}$]
$\bar{\psi}$	Dimensionless stream function
ψ_o	Surface potential, [V]
ψ_ζ	Stern potential, [V]
∇	Gradient operator
∇^2	Laplacian operator

F_G	Gravitational force, [N]
F_{EDL}	Electrostatic double layer (EDL) force, [N]
F_{VDW}	Van der Waals interaction force, [N]
$\overline{F}_z$	Dimensionless normal (axial) component force, [$F_z a_p / (kT)$]
Gr	Dimensionless gravity number, [$2(\Delta\rho)ga_P^3/(9\mu_f D_\infty)$]
g	Acceleration due to gravity, [ms^{-2}]
h	Separation gap between particle or droplet from the collector, [$h = z - a_P$], [m]
$\overline{h}$	Dimensionless separation distance between a particle from the collector, [h/a_P]
$\overline{H}_o$	Dimensionless separation gap between the capillary exit and the collector, [$\overline{H}_o = H_o / R$]
HHF	Hogg-Healy-Fuerstenau
$\vec{j}$	Particle or droplet mass flux vector, [$m^{-2}s^{-1}$]
J_o	Initial mass transfer flux of particle or droplet to the collector, [$m^{-2}s^{-1}$]
k	Boltzmann constant, [1.381×10^{-23} JK^{-1}]
L	Length of outflow region in the impinging jet cell, [m]
M_i	Molarity of ionic species i, [mol L^{-1}]
N_A	Avogadro's number, [6.023×10^{23} mol^{-1}]
n_{io}	Bulk number concentration of type-i ions, [m^{-3}]
Pe	Peclet number, [$2\alpha (a_p)^3 / D_\infty$]
Q	Volumetric flow rate, [m^3 s^{-1}]
r	Radial cylindrical coordinate
$\overline{r}$	Dimensionless radial cylindrical coordinate, [r/R or r/a_P]
R	Radius of capillary tube, [m]

Re	Reynolds number, [$Re = \rho_f VR/\mu_f$]
S	Stagnation region coating density (SRCD), [m^{-2}]
Sc	Schmidt number, [$(\rho_f/\mu_f)/D_\infty$]
Sh	Sherwood number, [$(J_o a_P)/(D_\infty c_o)$]
t	Time, [s]
T	Absolute temperature, [K]
$\vec{u}$	Particle or droplet velocity vector, [$m\ s^{-1}$]
$\vec{v}$	Fluid velocity vector, [$m\ s^{-1}$]
$\bar{v}_r$	Dimensionless fluid velocity component, [v_r / V]
$\bar{v}_z$	Dimensionless fluid velocity component, [v_z / V]
V	Volume averaged bulk fluid velocity, [$m\ s^{-1}$]
V_{EDL}	Electrostatic double layer interaction potential, [J]
V_{VDW}	Van der Waals interaction potential, [J]
X	Dimensionless particle or droplet flux to the collector surface
$\bar{z}$	Dimensionless axial coordinate, [z/R or z/a_P]
z_i	Valence of type-i ions

Greek Symbols

α	Strength of stagnation point flow in impinging jet, [$m^{-1}s^{-1}$]
$\bar{\alpha}$	Dimensionless strength of stagnation point flow in impinging jet
δ	Location of "perfect sink" boundary condition for particle or droplet attachment to the collector (at primary energy minimum) [m]
$\bar{\delta}$	Dimensionless location of perfect sink boundary location, [δ/a_P]
ε_0	Dielectric constant or permittivity of vacuum, [$8.854\times 10^{-12}\ C\ V^{-1}\ m^{-1}$]

Chapter One

Introduction

Colloidal science deals mainly with the interaction of microscopic bodies such as clay fines and other solids, liquid droplets and air bubbles or the interaction of a dispersed phase with an external body. The interaction between colloidal particles in dispersion or their interaction with a surface is quite complex and depends mainly on the following factors: 1. shape and size of the particle; 2. surface properties of the dispersed particle and the collector (external body) – chemical and physical; and 3. continuous phase chemical and physical properties.

An understanding of colloidal interactions is crucial to the success of many industrial and biological processes such as secondary oil recovery [Soo and Radke, 1984; Soo and Radke, 1986]; packed bed filtration [Rajagopalan and Kim, 1981; Tien, 1989]; fouling of reverse osmosis membranes [Hung and Tien, 1976]; paper and pulp processing [Varennes and van de Ven, 1988]; transport of colloidal contaminates in groundwater [McDowell et al., 1986]; deposition of cells onto surfaces in biological processes [Ruckenstein, and Chen, 1989]; release and re-deposition of corrosion products [Kallay and Matijevic, 1987]; and bio-chemical and pharmaceutical production.

Systems of dispersed particles and droplets are of particular importance in the oil sand industry which extracts bitumen from mined oil sand ore in northern Alberta. This extracted bitumen later is converted to synthetic crude by an upgrading process. The extraction process, based mainly on the Clark Hot Water Extraction Process (CHWE)

[Clark and Pasternack, 1949] is conceptually quite simple and accomplished in four basic steps:

- oil sand is mixed with water to make a slurry
- slurry is conditioned in a tumbler or hydrotransport pipeline
- gravity separation of bitumen froth from the oil sand slurry
- froth treatment

Commercial extraction processes are all water-based, but utilize different process temperatures and process aids. In such water-based extraction processes, complex colloidal phenomena control bitumen recovery and ultimately, the quality of the feed to the upgrading plant.

A good example of the importance of colloidal forces is illustrated by a new bitumen froth treatment process to be used for the first time on a commercial scale by Albian Sands Energy. In this process, asphaltenes are precipitated along with clay fines, other solid materials and water from the bitumen froth. This new technique is interesting as it is based on phase separation and eliminates the need for expensive and maintenance-intensive rotating equipment such as centrifuges (employed by Syncrude and Suncor for froth treatment). Although the asphaltene precipitation process has been studied extensively, there is very little data available on the precipitated asphaltenes – their interactions with each other to form aggregates, with bitumen, and with hydrophobic and hydrophilic surfaces such as fines and air bubbles.

The present study attempts to provide a quantitative method to describe interactions between precipitated asphaltene particles, between asphaltene particles and bitumen and between asphaltenes and hydrophobic or hydrophilic surfaces.

In the present study, asphaltene deposition is investigated based on the DLVO theory. The forces that influence colloidal interactions are mostly but not limited to the London-van der Waals (VDW), electrostatic double layer (EDL), Brownian, viscous, inertia, gravitation and surface tension forces. VDW and EDL interactions form the basis of the well known DLVO theory of colloidal stability developed independently by Derjaguin and Landau of USSR and Verwey and Overbeek of Holland [Masliyah, 1994].

The experimental apparatus used in this study is known as the impinging jet cell and is similar to that developed by Dabros and van de Ven [1983]. Results obtained from impinging jet cell experiments are compared with predictions based on DLVO theory and the governing mass transport equations.

1.0 Objective of this Study

The main objective of this study is to quantify and predict asphaltene-asphaltene interactions and determine the ability to employ a well-established experimental technique to do so. This objective is to be achieved by using the impinging jet technique for the study of asphaltene-asphaltene, asphaltene-bitumen, asphaltene-hydrophobic and asphaltene-hydrophilic surface interactions, while controlling:

- hydrodynamic flow intensities;
- continuous phase properties (ionic strength and pH).

The experimental data are then analyzed and compared with those predicted by a theoretical model based on DLVO theory.

1.1. Thesis Outline

This thesis is divided into the following sections:

1. A discussion and analysis of various experimental techniques normally used to study particle and / or droplet deposition.
2. Development of the numerical model, which simulates impinging jet deposition.
3. Validation of the numerical model by simulating results of previous studies.
4. Validation of the experimental apparatus by conducting latex particle deposition experiments.
5. Analysis of the experimental results.
6. Conclusions and recommendations for future studies.
7. Contributions of the present study.

Chapter Two

Colloidal deposition

Many theoretical and experimental studies of colloidal particle interaction have been conducted. Adamczyk et al. [1983; 1994] provided an excellent review on the subject. Basically, there are two theoretical approaches to predict the kinetics of particle deposition, which take into account both the hydrodynamic interaction and short-range colloidal forces.

The first method is the Eulerian approach developed by Ruckenstein and Prieve [1973] and Spielman and Fitzpatrick [1974] where the distribution of the particles is evaluated within a control volume. The second method is the Lagrangian approach in which attention is focused on the motion of a single particle along a trajectory defined by all combined influences or all relevant forces and torques [Zebel, 1965; Spielman and Goren, 1970; Spielman and Fitzpatrick, 1973]. The Lagrangian approach has limited use where Brownian diffusion is significant, the particle- collector energy barrier is high or where the flow pattern is complex. The Eulerian approach has one more advantage as it gives particle concentration distributions with the combined effect of hydrodynamic flow and surface forces. In addition, this method provides insight into the particle mass transfer process. Therefore, the Eulerian approach is used in the present study.

Numerous experimental techniques that are used to study particle deposition onto collectors of various shape and size are described in the literature. Spherical collectors [Spielman and Fitzpatrick, 1973; Spielman, and Cukor, 1973], cylindrical collectors

[Adamczyk and van de Ven, 1981], and parallel and cylindrical channels [Bowen et al., 1976; Bowen and Epstein, 1979] are described in the literature.

The rotating disc technique [Wnek et al., 1977; Dabros and Adamczyk, 1979; Preive and Lin, 1980; Rajagopalan and Kim, 1981], which uses "Stagnation Point Flow Method" to specify hydrodynamic flow conditions, is widely used for deposition experiments. In this technique, the collector surface is a disc that rotates at a constant angular velocity to create a diffusion boundary layer of constant thickness. The advantage of the rotating disc technique is that the collector surface area is uniformly accessible for mass transfer. In other words, mass transfer flux is not location specific on the collector surface. The disadvantage is that by virtue of the movement of the disc, the deposition process and rates cannot be observed directly and evaluation of the coating density is possible only after completion of the experiment when the disc (collector) can be placed under a microscope. In addition, the disconnection and the physical removal of the disc from the apparatus requires additional handling, which may cast doubt on the validity of the results. The same is true for the other stagnation point flow techniques that utilize spherical or cylindrical collectors.

Another technique, which avoids the shortcomings associated with the rotating disc technique, is the parallel plate channel technique. A comprehensive analysis of the parallel plate channel technique is given by Bowen et al. [1976]. In this technique, a parallel plate flow chamber is used to study particle deposition from a flowing suspension on a stationary collector surface situated parallel to the direction of the flow. The theory of parallel plate channel deposition is similar to that of the rotating disk except it must account for changes in the particle deposition density in the direction of flow as a function of distance from the inlet of the chamber. Bowen and Epstein [1979] used this method to study the deposition of silica particles onto a glass plate. This technique was also used to study polystyrene latex particle deposition [Adamczyk and van de Ven, 1981; Sjollema and Busscher, 1990] and microorganism deposition [Meinders et al., 1995]. Recently, Song and Elimelech [1995] presented a comprehensive theory of particle deposition onto a permeable surface in a parallel plate channel. However, the use of this method is normally limited to conditions where low flow rates are desirable.

Recently, a great deal of information has emerged on the study of particle deposition in complex systems such as packed beds [Elimelech, 1994], cross-flow membranes [Hong et al., 1997; Faibish et al., 1998; Alargova et al., 1998] and periodic arrays of cylindrical collectors [Li and Park, 1997]. In addition, Huisman et al. [1999] presented a more advanced theory incorporating physicochemical particle-particle interactions for the particle deposition in cross flow micro-filtration.

2.0. Impinging jet technique

Another technique that uses stagnation point flow deposition was developed by Dabros and van de Ven [1983]. The advantage of this technique is that since the collector surface is stationary and a microscope can be focused directly on the stagnation region of the collector surface, the researcher is able to observe the deposition process as it occurs. This not only presents a better understanding of the deposition mechanism, but can also provide insight into the behavior of the particle in the vicinity of the collector surface. The advantages of the impinging jet experimental setup are as follows:

1. The collector surface is stationary and on transparent collectors, deposition can be observed directly (by a microscopic arrangement) in real time from start of the experiment to its end. The whole process of mass transfer and deposition can thus be recorded for subsequent analysis.
2. Hydrodynamic conditions are well defined, controlled and reproducible over a wide range of Reynolds numbers. In addition, physicochemical conditions are independently controllable and reproducible. Therefore, the effect of hydrodynamic and colloidal surface forces can be studied separately over a wide range of flow Reynolds numbers.
3. The theoretical analysis is greatly simplified by the use of stagnation point flow because the flux to the collector surface is uniform and is independent of radial distance in a small region surrounding the stagnation point.

Dabros and van de Ven [1983] provided a theoretical model for particle deposition in an impinging jet cell. This technique is used extensively by many researchers for various conditions. Some examples include the effects of surfactants [Adamczyk et al., 1986], the effects of polyelectrolytes [Varennes and van de Ven, 1988], attractive EDL interaction [Adamczyk et al., 1989; Boluk and van de Ven, 1989], polymer adsorption [Dijt et al., 1990], particle detachment [Varennes and van de Ven, 1987], characterization of polymers [van de Ven and Kelemen, 1996], deposition structure and ordering [Adamczyk et al., 1990], deposition of droplets [Sanders, 1997] and bubble attachment [Yang, 2000].

2.1. Experimental Setup

The impinging jet apparatus is shown in Figure 2-1. The heart of the impinging jet apparatus is the cup-shaped cell, which is constructed of Pyrex glass of internal diameter (ID) 40 mm, in which a capillary tube is fixed in the center. The internal diameter (ID) of the capillary is 2.55 mm and its length is 60 mm. At the top of the cell, a glass microscopic slide (75 × 50 × 1 mm) can be placed. The liquid containing colloidal particles or droplets, to be called a suspension, flows through the capillary tube upward toward the collector surface. The exit of the capillary tube and the collector surface are separated by a distance, H, of 2.55 mm, which is equal to the internal diameter of the capillary tube. The dimensionless separation distance between exit of the capillary tube and the collector surface is therefore given as $\overline{H}_o = \frac{H}{R} = 2$.

The liquid suspension flows upward through the capillary tube and impinges on the glass microscopic slide, which is held in place atop the external wall of the cell. No adhesive is required as the cell is under a slight vacuum. After impinging on the surface of the microscopic slide, the suspension flows downward through the annulus between the external wall of the capillary and the internal wall of the cell and flows out the bottom through a flow controlling device to a lower reservoir. The solution is then pumped to the upper reservoir using a peristaltic pump. The level in the upper reservoir is always maintained (by the peristaltic pump) up to the level of the recirculation port and any additional quantity of the solution flows back to the lower reservoir via the re-circulation line. In this way, constant hydrostatic head is maintained for steady flow. The flow control device is actually a replaceable capillary tube. Flow capillary tubes of different diameters and lengths correspond to different flow rates. By changing the flow capillary tube, it is possible to manipulate the flow rates in the impinging jet cell. These capillary tubes were calibrated for Reynolds numbers 45 to 800. Flow tubes were checked and calibrated at least once every month to verify their accuracy.

The deposition process was observed from above using an Olympus microscope fitted with a "10X" objective. A Sony video camera adapter was fitted on the microscope instead of a conventional eyepiece. Three external fiber optic light sources were placed at 45° angles to the microscopic slide to optimize the contrast between the particles and the background field (a similar arrangement of dark field illuminator microscope). The video adapter of the microscope was connected to a Sony CCD color camera. The camera was connected to a Panasonic color monitor and a Panasonic VHS VCR through a timer. The deposition experiments were video recorded for subsequent playback and analysis. The total magnification achieved with the microscope (10X objective) and video camera was 330 times.

2.2. Analysis of deposition experiments

Each experiment was analyzed by counting the number of particles attached in the stagnation region as a function of time. The stagnation region is a circular area having the stagnation point as its center. The radius of the stagnation region is 300 μm and its area is 0.283 mm^2. The stagnation point and the stagnation region are calibrated onto the monitor screen for a 10X microscope objective and the magnification of the video camera. It is possible to move the microscope stage in both lengthwise and transverse directions so that the stagnation region could be precisely located onto the monitor screen.

After counting the number of attached particles in the stagnation region as a function of time, the number of attached particles was converted into stagnation region coating density (SRCD), S, by dividing the number of particles attached in the stagnation region by the area of stagnation region [Sanders, 1997]:

$$S = \frac{\text{Number of particles in the stagnation region}}{\text{Area of the stagnation region}}$$

Initially, S increases linearly with time but levels off due to blocking effects created by the already attached particles in the stagnation region [Dabros et al., 1983; 1987; Sanders et al., 1997]. Therefore, the initial slope of the SRCD curve as a function of time is used to calculate the flux (J_o) of particles to the collector surface [Sanders, 1997], where

$$J_o = \left.\frac{dS}{dt}\right|_{t=0} \qquad (2.1)$$

The dimensionless mass transfer rate to the collector surface, expressed as the Sherwood number, Sh is then calculated as

$$Sh = J_o \frac{a_p}{D_\infty c_o} \qquad (2.2)$$

where a_p is the particle radius, c_o is number concentration of particles in the electrolyte solution and D_∞ is the diffusion coefficient calculated by Stokes-Einstein equation:

$$D_{\infty} = \frac{kT}{6\pi\mu_f a_p} \qquad (2.3)$$

In Equation (2.3), μ_f is the viscosity of the fluid (water), k is the Boltzmann constant and T is the absolute temperature. It is clear from Equations (2.1) and (2.2) that the experimentally determined Sherwood number can be calculated directly from experimental quantities such as the particle radius, viscosity of the fluid, temperature of the fluid and particle deposition rate.

Theoretically, the Sherwood numbers are calculated by solving the mass transport equation, which requires knowledge of the velocity field in the stagnation region. The method used to solve the governing mass transport, Navier-Stokes and continuity equations is discussed in Chapter 3. Predicted values of the Sherwood number are then compared with those determined experimentally to evaluate how effectively a theoretical model based on DLVO theory predicts the rate of particle deposition.

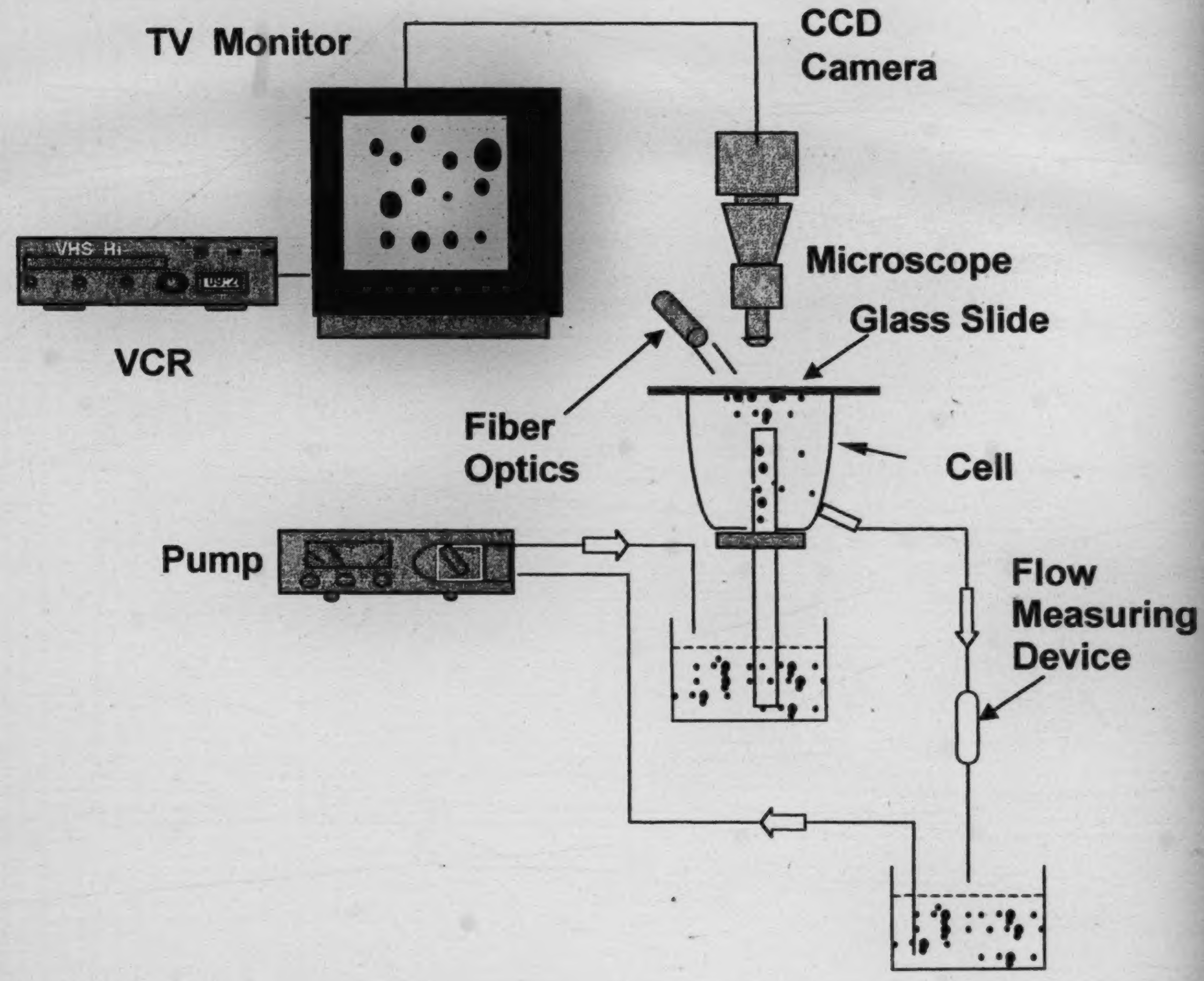
TV Monitor
CCD
Camera
VHS Hi
VCR
Microscope
Glass Slide
Fiber
Optics
Cell
Pump
Flow
Measuring
Device

Figure 2-1. Schematic of experimental setup for performing deposition experiments with the impinging jet apparatus.

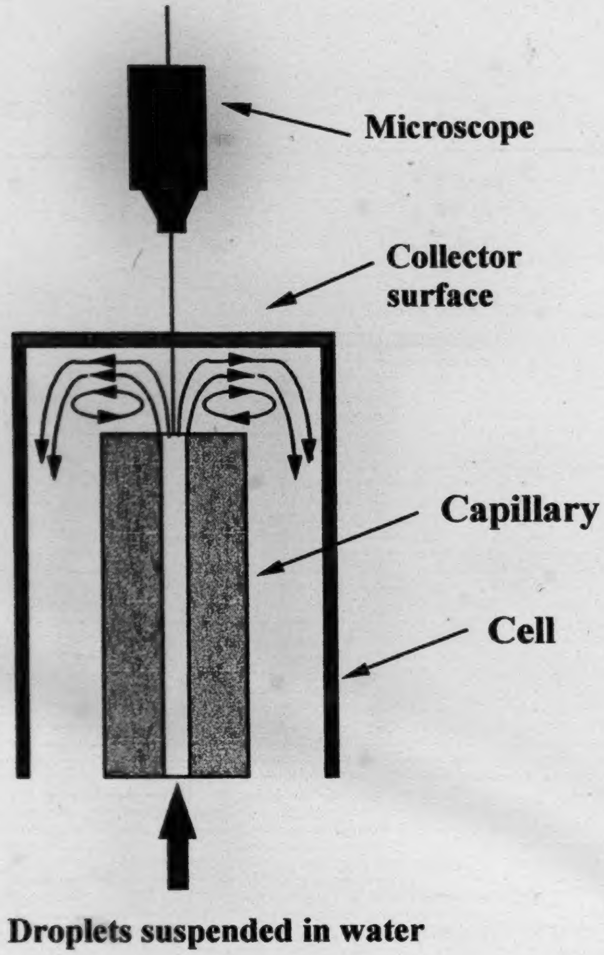
Microscope
Collector surface
Capillary
Cell
Droplets suspended in water

Figure 2-2. Schematic of the impinging jet cell.

Chapter Three

Theory

3.0. Introduction

This chapter focuses on solving the mass transport equation for dispersed droplets in the impinging jet flow on a collector surface. The Eulerian approach is used to derive the droplet transport equation, which includes the effects of convection, Brownian diffusion, hydrodynamic interaction, gravity, as well as van der Waals and electrostatic double layer surface force interactions. The importance of the stagnation region is in being able to evaluate the hydrodynamic conditions. In order to solve the mass transport equation, we need to know the particle or droplet velocity, its mass diffusion coefficient and we must specify all forces acting on the particle or droplet.

3.1. Solution of the mass transport equation

Assuming there is no source term, the mass transfer of a spherical particle or droplet in a dilute suspension is described by

$$\frac{\partial c}{\partial t} + \nabla \bullet \bar{j} = 0 \qquad (3.1)$$

where c is the local concentration of particles or droplets (number of particles or droplets per unit volume), t is the time, ∇ is the gradient operator and $\bar{j}$ is the mass transfer flux vector of the dispersed particle or droplets (space number of particles or droplets per unit area per second) to the collector.

For steady state, which occurs immediately after the onset of deposition in the impinging jet experiments, the mass conservation equation can be simplified to

$$\nabla \bullet \vec{j} = 0 \qquad (3.2)$$

Due to symmetry of the impinging jet flow, the mass conservation equation can be described in a two-dimensional cylindrical coordinate system shown in Figure 3-1 and can be expressed as:

$$\frac{1}{r}\frac{\partial}{\partial r}(r\, j_r) + \frac{\partial}{\partial z}(j_z) = 0 \qquad (3.3)$$

where j_r and j_z are components of flux $\vec{j}$ in the radial and axial directions, respectively.

3.2. General expression for mass flux

Particle or droplet mass flux can be decomposed into contributions from convection, diffusion and migration under colloidal and external force fields. The mass flux is expressed by the following convection-diffusion equation or Fokker-Planck equation [ven de Van, 1989; Masliyah, 1994]:

$$\vec{j} = \vec{u}c - \overline{\overline{D}} \bullet \nabla c + \frac{c}{kT}\overline{\overline{D}} \bullet \vec{F} \qquad (3.4)$$

where $\vec{u}$ is the particle or droplet velocity vector in the absence of diffusion and external forces, $\overline{\overline{D}}$ is particle or droplet diffusion coefficient tensor, kT represents thermal energy (k is the Boltzmann constant and T is absolute temperature) and $\vec{F}$ is the total force acting on the particle or droplet.

In order to solve the mass conservation equation, we need to know the particle or droplet velocity, its mass diffusion coefficient and we must specify all forces acting on a particle or droplet.

In general, the forces acting on a particle or droplet may include external body forces $\vec{F}_{EX}$ (such as gravity) and colloidal surface forces $\vec{F}_{Col}$ (such as van der Waals and electrostatic double layer forces). The total force is given by

$$\vec{F} = \vec{F}_{Ex} + \vec{F}_{Col} \tag{3.5}$$

3.3. Fluid velocity in the stagnation region

The advantage of the impinging jet technique is that fluid flow in the stagnation point region is controlled and can be rigorously described. The hydrodynamic conditions (i.e. Reynolds number) can be readily manipulated to examine their impact on the particle or droplet attachment. The governing equations needed to evaluate the flow field are derived from fundamental fluid dynamic equations, i.e., continuity and Navier-Stokes equations. The scheme of solving the governing equations is well described by Sanders [1997] and Yang [2000]. Here, it is discussed briefly. For details, readers are encouraged to see Sanders [1997] and Yang [2000].

The sole purpose of solving the continuity and Navier-Stokes equations is to characterize the flow field near the stagnation point where the colloidal surface forces between a particle or droplet and the collector surface are expected to play important roles in particle or droplet transport and attachment. Stagnation flow is well documented in fluid mechanics studies. Dabros and van de Ven [1983] showed that the Schmidt number, $\mathrm{Sc} = \frac{(\mu_f / \rho_f)}{D_\infty}$, is usually large for mass transfer of colloidal particle or droplets. Here, D_∞ is the diffusion coefficient of a particle or droplet given by Stokes-Einstein equation,

$D_\infty = \frac{kT}{6\pi\mu_f a_p}$ [van de Ven, 1989].

When $\mathrm{Sc} \gg 1$ the diffusion boundary layer is much thinner than hydrodynamic boundary layer [Dabros and van de Ven, 1983] and only the flow field nearest to the collector needs to be considered because the mass transfer occurs entirely within the hydrodynamic boundary layer.

The flow field near a collector surface [Dabros and van de Ven, 1983] can be described by the axisymmetrical part of a general second order flow as below:

$$\bar{v}_r = \bar{\alpha}\,\bar{z}\,\bar{r} \qquad \text{and} \qquad \bar{v}_z = -\bar{\alpha}\,\bar{z}^2 \tag{3.6}$$

where $\bar{\alpha}$ is a dimensionless impinging jet flow coefficient, which characterizes "the strength of the stagnation flow". The quantities $\bar{v}_r, \bar{v}_z$, $\bar{z}$ and $\bar{r}$ are defined as

$\bar{v}_r = \frac{v_r}{V}$, $\bar{v}_z = \frac{v_z}{V}$, $\bar{z} = \frac{z}{R}$, $\bar{r} = \frac{r}{R}$ and V is the volume averaged fluid velocity.

The value of $\bar{\alpha}$ is evaluated by solving the continuity and Navier – Stokes equations using the stream function – vorticity method with appropriate boundary conditions [Deshpande and Vaishnav, 1982; Dabros et al., 1983; Sanders, 1997; Yang, 2000]. It is interesting to note that for stagnation flow, the flow intensity $\bar{\alpha}$ is independent of both radial $\bar{r}$ and axial $\bar{z}$ coordinates within the stagnant region. However, $\bar{\alpha}$ is found to be strongly dependent on Reynolds number, and on the dimensionless separation distance between the capillary tube exit and the collector surface $\overline{H}_o$ ($\overline{H}_o = \frac{H}{R}$).

Yang [2000] developed an empirical expression for $\overline{\alpha}$ for $\overline{H}_o = 2$, first by numerically solving the continuity and Navier – Stokes equations for different Reynolds numbers and then by performing a regression analysis of $\overline{\alpha}$ vs Re curve which is expressed as

$$\overline{\alpha} = 5.3\mathrm{Re}^{0.5} - 8.13 \qquad (5 \le \mathrm{Re} \le 1000) \tag{3.7}$$

In the present study, $\overline{H}_o = 2$, which is the same as has been used by Yang [2000]. Hence, no attempt is made to solve the Navier-Stokes and the continuity equations to evaluate $\overline{\alpha}$. Equation (3.7) is used to calculate values of $\overline{\alpha}$ for characterizing the flow field in the stagnation region. Equation (3.6) along with Equation (3.7) will represent the stagnation flow field and will be used in the solution of the mass transport equation.

Dabros and van de Ven [1983] have shown that Equations (3.6) and (3.7) could be used to describe fluid flow in the impinging jet region for lateral distances up to 25% of the capillary radius from the stagnation point ($\overline{r} = \frac{r}{R} \le 0.25$). Yang [2000] also performed a series of numerical runs at different Re and confirmed Equation (3.7) is valid for $\overline{r} = \frac{r}{R} \le 0.25$ and $\overline{z} = \frac{z}{R} \le 0.1$.

Recently, Adamczyk et al. [2001] also performed CFD for this flow region and found similar results. Therefore, it is concluded that the flow pattern expressed by Equation (3.6) is valid laterally up to $\overline{r} = \frac{r}{R} \le 0.25$ from the stagnation point at the collector surface in the impinging jet cell. This analysis provides the boundaries for the stagnation region in analyzing results of impinging jet experiments.

3.4. Particle or droplet velocity

Following Spielman and Fitzpatrick [1973], the relationship between the fluid velocity, $\vec{v}$ and the particle or droplet velocity, $\vec{u}$ near a collector surface is given by

$$u_r = v_r f_3 \qquad (3.8a)$$

$$u_z = v_z f_1 f_2 \qquad (3.8b)$$

where f_1, f_2 and f_3 are universal (correction) hydrodynamic functions [Masliyah, 1994] related to deviation from Stokes flow and the Stokes- Einstein relationship due to the presence of a collector. Rigorous derivation of these functions is presented by Brenner [1961], Goldman et al. [1967], Goren [1970] and Goren and O'Neill [1971].

In the stagnation region, the flow field is known [Equations (3.6) and (3.7)] and thus u_r and u_z can be determined by substituting the expressions of v_r [Equation (3.6)] and v_z [Equation (3.7)] in Equations (3.8a) and (3.8b). The particle or droplet velocity can be expressed as

$$u_r = \alpha r z f_3 \qquad (3.9a)$$

$$u_z = -\alpha z^2 f_1 f_2 \qquad (3.9b)$$

In Equations (3.9a) and (3.9b), α is known as "the intensity of the stagnation flow" and is related to $\bar{\alpha}$ (the dimensionless intensity of stagnation point flow for the fluid) by

$$\alpha = \bar{\alpha}(\frac{V}{R^2}) = \bar{\alpha}(\frac{\mu_f \, Re}{\rho_f \, R^3}) \qquad (3.10)$$

where $$Re = \frac{\rho_f VR}{\mu_f}$$

where R is the radius of the capillary and V is the volume average velocity of the fluid at the exit of the capillary.

3.5. Particle or droplet diffusion coefficient

Near the collector surface, hydrodynamic interactions also affect the particle or droplet diffusion coefficient (or diffusivity). The particle or droplet diffusion coefficient becomes dependent on the position and the orientation of the particle or droplet and the collector wall (i.e. it becomes tensorial quantity). Assuming a dilute suspension of spherical particles or droplets, the particle or droplet diffusion coefficient components are formulated [Masliyah, 1994; van de Ven, 1989] as

$$\bar{\bar{D}} = \begin{pmatrix} D_{rr} & D_{rz} \\ D_{zr} & D_{zz} \end{pmatrix} = D_\infty \begin{pmatrix} d_{rr} & 0 \\ 0 & d_{zz} \end{pmatrix} \qquad (3.11)$$

where $D_{zr} = D_{rz} = 0$ (as there is no coupling between the axial and radial terms of diffusion), $D_{rr}(z) = D_\infty d_{rr} = D_\infty f_4(z)$ and $D_{zz}(z) = D_\infty d_{zz} = D_\infty f_1(z)$.

Here, z represents the distance from the center of the particle or droplet to the collector surface and μ_f and a_p are the viscosity of the aqueous solution and radius of the particle or droplet, respectively.

The universal hydrodynamic correction functions $d_{rr} = f_4(z)$ and $d_{zz} = f_1(z)$ take into account deviation from Stokes flow and Stokes-Einstein equation caused by the presence of the collector surface. These universal hydrodynamic functions $f_1(z)$ to $f_4(z)$ are tabulated in the literature [Brenner, 1961; Goren, 1970; Goren and O'Neill, 1971; Preive and Lin, 1982]. Masliyah [1994] gave empirical curve-fitted expressions of the universal hydrodynamic functions $f_1(z)$ to $f_4(z)$.

3.6. External body forces

Normally external body forces acting on the particle or droplet include gravitational and electrical forces, when a charged particle or droplet is subjected to an external electric field. In the present study, no external electric field was present and thus only the gravitational body force is considered. The gravity force is expressed as

$$F_G = \frac{4}{3}\pi a_P^3 \Delta\rho g \tag{3.12}$$

where $\Delta\rho = \rho_P - \rho_f$ is the density difference between a particle or droplet and the aqueous solution. The gravity force can be nondimensionalized with respect to the Brownian force, F_{Br}, ($F_{Br} = \frac{kT}{a_p}$). The ratio of these forces is referred to as the gravity number Gr, which is given by

$$\mathrm{Gr}=\frac{\text{Gravitaion force}}{\text{Browanian Force}}=\frac{4\pi}{3}\frac{\Delta\rho g\, a_p^4}{kT} = \frac{2}{9}\frac{\Delta\rho g\, a_p^3}{\mu_f\, D_\infty} \qquad (3.13)$$

3.7. Colloidal surface forces

When a colloidal particle or droplet approaches the collector surface within a separation distance less than 1 μm, its motion is affected by at least two types of colloidal forces that occur between the particle or droplet and the collector surface. These are van der Waals (VDW) interaction force and electrostatic double layer (EDL) interaction force. These two types of colloidal surface forces form the basis for the well known DLVO theory of colloidal stability developed independently by Derjaguin and Landau of USSR and Verwey and Overbeek of Netherlands [Masliyah, 1994]. Analytical expressions for DLVO interactions between a sphere and flat surface will be presented in this section.

3.7.1. van der Waals interaction

The van der Waals (VDW) forces, also known as dispersion forces, act between all molecules and atoms irrespective of their nature (similar to gravitation). These forces are quantum mechanical in origin and can be explained by quantum electrodynamics. For example, for a non-polar atom, the time average dipole moment is zero and yet at any instant there exists a finite dipole moment given by the instantaneous positions of the electrons around the nuclear protons. This instantaneous dipole generates an electric field that polarizes any nearby neutral atom, inducing a dipole moment in it. Thus, the resulting interaction between two dipoles gives rise to an instantaneous attractive force between two atoms and the time average of this force is finite [Israelachvili, 1992].

There are three major types of VDW forces [Israelachvili, 1992]:

1. Keesom interaction: permanent dipole – permanent dipole interaction.
2. Debye interaction: permanent dipole – induced dipole interaction.
3. London interaction: induced dipole – induced dipole interaction.

The main features of VDW forces can be summarized as follows [Israelachvili, 1992]:

1. They are long-range forces that can be effective from large distances such as 10nm down to interatomic spacing (0.2 nm).
2. They are always attractive between two identical bodies in a medium and may be attractive or repulsive for two different bodies in a medium.
3. VDW forces not only bring molecules together but also tend to align or orient them, though this orienting effect is usually weak.
4. VDW interactions between two bodies are affected by the presence of other nearby bodies (also known as non-additivity of an interaction).

The calculation of magnitude of dispersion attraction between particle or droplets has been attempted by two different approaches. One is based on a molecular model and is attributed to Hamaker [Hunter, 1981; Masliyah, 1994] and the other is based on electromagnetic properties as suggested by Lifshitz [Israelachvili, 1992].

In the molecular model, the attraction between particles or droplets is calculated by summing the attractive energies between all pairs of molecules in separate particles or droplets, ignoring multi-body perturbations [van de Ven, 1989; Masliyah, 1994]. Corrections are applied to take into account the effect of intervening material and retardation of dispersion forces due to the finite speed of light. This approach, though approximate, captures the essential physics and provides insight into van der Waals interactions.

The molar model, attributed to Lifshitz [Israelachvili, 1992] is based on quantum electrodynamics. In this model of particle – particle dispersion attractions, the lowering of the zero-point energy of a particle, due to the coordination of its instantaneous electric moments with those of a nearby particle, is calculated by quantum electrodynamics.

One can still use the formula developed by Hamaker for the calculation of van der Waals forces, which requires the knowledge of a material-dependent constant called the Hamaker constant. The Hamaker constant itself could be determined using the Lifshitz theory. Therefore, this treatment is a combination of both approaches. It is convenient to express van der Waals interactions for a heterogeneous system, i.e., media 1 and media 2 separated by media 3. Excellent reviews on this subject can be found elsewhere [Margenau and Kestner, 1971; Mahanty and Ninham, 1976; Israelachvili, 1992].

Using this approach, the Hamaker constant of a heterogeneous system (media 1 and media 2 separated by media 3), A_{132} can be written as [Gregory, 1981]

$$A_{132} = A_{12} + A_{33} - A_{13} - A_{23} \tag{3.14}$$

where A_{12}, A_{13} and A_{23} are the Hamaker constant of medium 1 and 2, medium 1 and 3 and medium 2 and 3, respectively in vacuum. A_{33} is the Hamaker constant medium, 3 in vacuum.

A useful approximation for calculating the Hamakar constant, A_{ij} of medium i and j is the geometric mean assumption [Masliyah, 1994]:

$$A_{ij} \approx \sqrt{A_{ii} A_{jj}} \qquad (3.15)$$

where A_{ii} is Hamaker constant of the different phases of the same material in vacuum. From Equation (3.14) and (3.15), we can write

$$A_{132} \approx (\sqrt{A_{11}} - \sqrt{A_{33}})(\sqrt{A_{22}} - \sqrt{A_{33}}) \qquad (3.16)$$

It is clear that the third medium can significantly reduce van der Waals interactions and lead to a repulsion force if phase 1 happens to be a gas for which the Hamaker constant is much less than that for a solid or a liquid [Visser, 1981; van Oss, 1990].

Considering a spherical particle or droplet of radius a_p within a small separation gap h (where $h \ll a_p$) from a flat surface, the van der Waals interaction potential can be expressed as [Mahanty and Ninham, 1976]

$$V_{VDW} = -\frac{A_{132}\, a_p}{6h} \qquad (3.17)$$

Equation (3.17) is based on the assumption that the speed of electromagnetic wave propagation is infinite. In reality, it takes a finite time for the propagation of the electromagnetic field through the separating media causing reduced correlation between the dipole oscillations in the interacting bodies i.e. media 1 and media 2. This results in weaker van der Waals interactions. This is also called the "retardation effect".

The retardation effect is accounted for by using a parameter λ (usually 100nm), which is the distance traveled by light during one rotation of a Bohr atom electron [Gregory, 1981; Israelachvili, 1992].

The van der Waals interaction between a sphere and flat surface is given by Suzuki et al. [1969]:

$$V_{VDW} = -\frac{A_{132}\,a_P}{6h}\frac{\lambda}{(\lambda + 11.116h)} \tag{3.18}$$

The relationship between force and energy is given by Masliyah [1994] as:

$$\text{Force} = -\frac{d(\text{energy})}{d(\text{dis tan ce})} = -\frac{d(V_{VDW})}{d\,h}$$

$$F_{VDW} = -\frac{dV_{VDW}}{d\,h} = -\frac{A_{132}\,a_P}{6h^2}\frac{\lambda(\lambda + 22.23h)}{(\lambda + 11.116h)^2} \tag{3.19}$$

Equation (3.19) can be nondimensionalized as

$$\overline{F}_{VDW} = \frac{F_{VDW}}{(kT/a_P)} = -Ad\frac{\overline{\lambda}(\overline{\lambda} + 22.232\overline{h})}{\overline{h}^2(\overline{\lambda} + 11.116\overline{h})^2} \tag{3.20}$$

where $Ad = \frac{A_{132}}{6kT}$, $\overline{\lambda} = \frac{\lambda}{a_P}$ and $\overline{h} = \frac{h}{a_P} = \frac{z - a_P}{a_P}$

Ad is referred to as the adhesion number, which is a measure of the strength of the van der Waals (VDW) interaction. $\overline{\lambda}$ is the dimensionless retardation wavelength and $\overline{h}$ is the dimensionless separation distance between a particle and a flat collector surface.

3.7.2. Electric double layer (EDL) interaction

Surfaces immersed in a polar medium such as water are usually charged [Israelachvili, 1992; Masliyah, 1994]. The origin of the charge could be due to several factors such as:

1. Ionization or dissociation of surface groups (e.g., the dissociation of a proton from surface groups).
2. Adsorption (binding) of ions from the solution onto the surface. Depending on the ionic conditions, air-water and hydrocarbon –water interfaces can become charged in this way.
3. Adsorption of ions from the solution onto oppositely charged surface sites.

Irrespective of the charging mechanism, the final surface charge is balanced by an equal and opposite charged region of counterions, some of which are bound to the surface, while others form an atmosphere of ions in rapid thermal motion close to the surface, known as the diffuse electric double layer (EDL) [Hunter, 1981; Israelachvili, 1992; Masliyah, 1994].

Stern [Hunter, 1981; Masliyah, 1994] proposed a model for EDL interactions in which, due to electrostatic attraction, some immobile counterions are located immediately adjacent to the charged surface to form a Stern layer, which is approximately one hydrated ion radius. This inner immobile boundary of the EDL is referred to as the Stern plane and the surface of Stern plane. The gap between the Stern plane and the charged surface is called the Stern layer which is shown in Figure 3-2. Outside the Stern layer is the diffuse mobile double layer, in which counterions are mobile and are distributed more broadly. The motion of ions in the mobile part of the EDL is balanced by the simultaneous influence of the electrostatic attraction and random diffusion due to thermal excitation. The inner mobile part of the EDL is located one to two radii from the charged surface and is also referred as the shear plane, where a no-slip fluid flow condition is assumed to apply.

The interaction between two approaching charged surfaces is governed by the overlap of the two diffuse layers. The relevant potential of interaction between approaching charged interfaces is the Stern potential, rather than the potential at the charged surface. There is no direct experimental method to determine the Stern potential but it can be adequately substituted (although this is still being debated) by electrokinetic potential or zeta-potential, ζ, which is the potential at the plane of shear as shown in Figure 3-2 [Hunter, 1981; Lyklema, 1993].

There are three major factors which effect EDL interactions between two charged surfaces: the magnitude of the effective surface potential (generally assumed to be zeta-potential ζ), the geometric configuration of the two surfaces and the extent of the diffuse layer. The extent of the diffuse layer is also known as the EDL thickness.

The extent of the diffuse layer or EDL thickness is quantified by the Debye-Huckel reciprocal length parameter κ, which is defined by Hunter [1981] as

$$\kappa = \left(\frac{e^2 \sum n_{io} z_i^2}{\varepsilon_o \, \varepsilon_r kT} \right)^{\frac{1}{2}} \qquad (3.21)$$

where

e = Charge of an electron ($e = 1.602 \times 10^{-19}$ C)

n_{io} = Bulk number concentration of type "i" ions.

ε_o = Permittivity in vacuum $\varepsilon_o = 8.854\times10^{-12}$ $\mathrm{CV^{-1}m^{-1}}$

ε_r = Dielectric constant (relative permittivity) of the solution for water, $\varepsilon_r \approx 80$

k = Boltzmann constant

Evidently, the EDL thickness is given by κ^{-1}. Equation (3.21) shows that the thickness of the EDL depends on solution ionic strength and its temperature.

Before calculating the EDL interaction between two charged surfaces, one needs to know the electrostatic potential distributions within the aqueous solution for a given geometry of charged surfaces. The surface potential distribution can be calculated by Gouy-Chapman theory [Hunter, 1981] through the use of the Poisson- Boltzmann (P-B) equation.

For a symmetric electrolyte, i.e. $n_o = n_{-o} = n_{+o}$ and $z_- = z_+ = z$, the Poisson-Boltzmann (P-B) equation is given by

$$\nabla^2 \varphi = \frac{2n_o z e}{\varepsilon_o \varepsilon_r}\sinh\left(\frac{ze\varphi}{\mathrm{kT}}\right) \qquad (3.22)$$

where, n_o is the ions number concentration in the bulk solution and z is the valence of ions and counterions. ∇^2 is the Laplacian operator and φ is the local potential.

Using the Debye- Huckel approximation [Masliyah, 1994], which is appropriate for low potentials ($\varphi \leq 0.025$V), we can write

$$\sinh\left(\frac{ze\varphi}{\mathrm{kT}}\right) \approx \frac{ze\varphi}{\mathrm{kT}} \quad \text{for } \frac{ze\varphi}{\mathrm{kT}} \ll 1 \qquad (3.23)$$

Equation (3.23) linearizes the P-B equation given by Equation (3.22). Hogg, Healy and Fuerstenau (HHF) [1966] obtained an analytical solution of the linearized P-B equation with constant potential boundary conditions for two unequal size spheres a_1 and a_2 with constant surface potential ψ_1 and ψ_2, using the Derjaguin approach:

$$V_{EDL} = \frac{2\pi\varepsilon_o\varepsilon_r a_1 a_2 \psi_1 \psi_2}{(a_1 + a_2)}\left[\ln\left\{\frac{1+\exp(-\kappa h)}{1-\exp(-\kappa h)}\right\} + \frac{(\psi_1^2 + \psi_2^2)}{2\psi_1\psi_2}\ln\{1-\exp(-2\kappa h)\}\right] \quad (3.24)$$

Equation (3.24) can be applied to particle-collector interaction by substituting, $a_1 = a_p$(radius of the particle), $a_2 \to \infty$ for the collector, $\psi_1 = \psi_p$ for particle and $\psi_2 = \psi_c$ for collector to yield

$$(V_{EDL})_{\substack{\text{particle}\\ \text{-collector}}} = 2\pi\varepsilon_o\varepsilon_r a_p \psi_p \psi_c \left[\ln\left\{\frac{1+\exp(-\kappa h)}{1-\exp(-\kappa h)}\right\} + \frac{(\psi_p^2 + \psi_c^2)}{2\psi_p\psi_c}\ln\{1-\exp(-2\kappa h)\}\right] \quad (3.25)$$

Assuming that the surface potential of a particle and the collector can be replaced by their respective zeta potentials, i.e., $\psi_p = \zeta_p$ and $\psi_c = \zeta_c$, we can write

$$(V_{EDL})_{\substack{\text{particle}\\ \text{-collector}}} = 2\pi\varepsilon_o \varepsilon_r a_p \zeta_p \zeta_c \left[\ln\left\{\frac{1+\exp(-\kappa h)}{1-\exp(-\kappa h)}\right\} + \frac{\left(\zeta_p^2 + \zeta_c^2\right)}{2\zeta_p\zeta_c}\ln\{1-\exp(-2\kappa h)\}\right] \quad (3.26)$$

The relationship between force and energy is given by Masliyah [1994] as:

$$\text{Force} = -\frac{d(\text{energy})}{d(\text{distance})} = -\frac{d(V_{EDL})}{dh}$$

The EDL force between a particle and the collector can be expressed as:

$$(F_{EDL})_{\substack{\text{particle}\\ \text{-collecor}}} = -\frac{d(V_{EDL})}{dh} = 4\pi\varepsilon_o\varepsilon_r \kappa a_p \zeta_p \zeta_c \left[\frac{\exp(-\kappa h)}{1+\exp(-\kappa h)} - \frac{\left(\zeta_p - \zeta_c\right)^2}{2\zeta_p\zeta_c}\frac{\exp(-2\kappa h)}{1-\exp(-2\kappa h)}\right] \quad (3.27)$$

The EDL force given by Equation (3.27) can be nondimensionalized using $\frac{kT}{a_p}$ and a dimensionless separation distance, defined as $\bar{h} = \frac{h}{a_p} = \frac{z - a_p}{a_p}$, to give

$$\bar{F}_{EDL} = \frac{F_{EDL}}{kT/a_p} = Dl\tau\left[\frac{\exp(-\tau\bar{h})}{1+\exp(-\tau\bar{h})} - Da\frac{\exp(-2\tau\bar{h})}{1-\exp(-2\tau\bar{h})}\right] \tag{3.28}$$

where Dl and Da are nondimensional EDL parameters. Dl is called the strength of EDL interaction and Da is called the asymmetry parameter. τ is the ratio of the particle radius, a_p to the EDL thickness κ^{-1}. These important dimensionless parameters are defined in Equations (3.29a) through (3.29c).

$$Dl = \frac{4\pi\varepsilon_o\varepsilon_r\kappa a_p\zeta_p\zeta_c}{kT} \tag{3.29a}$$

$$Da = \frac{\left(\zeta_p - \zeta_c\right)^2}{2\zeta_p\zeta_c} \tag{3.29b}$$

$$\tau = \kappa a_p \tag{3.29c}$$

3.8. Mass transport equation

Now it is possible to return to the mass transport equation and develop a solution procedure. Recall that the mass transport, Equation (3.3), is

$$\frac{1}{r}\frac{\partial}{\partial r}(r\, j_r) + \frac{\partial}{\partial z}(j_z) = 0 \tag{3.3}$$

where j_r and j_z are the components of the flux $\vec{j}$ in the radial and the axial directions, respectively. Recall also the Fokker-Planck equation, where the particles' mass flux can be written as

$$\vec{j} = \vec{u}\, c - \overline{\overline{D}} \bullet \nabla c + \frac{c}{kT} \overline{\overline{D}} \bullet \vec{F} \tag{3.4}$$

The flux components are given by

$$j_r = u_r\, c - D_\infty\, f_4 \frac{\partial c}{\partial r} + \frac{D_\infty\, f_4}{kT} F_r\, c \tag{3.30}$$

and

$$j_z = u_z\, c - D_\infty\, f_1 \frac{\partial c}{\partial z} + \frac{D_\infty\, f_1}{kT} F_z\, c \tag{3.31}$$

Since $u_r = v_r f_3 = \alpha\, r z f_3$ and $u_z = v_z\, f_1\, f_3 = -\alpha\, z^2\, f_1\, f_3$ from Equations (3.8) and (3.9), it is possible to write

$$j_r = \alpha\, r z f_3\, c - D_\infty\, f_4 \frac{\partial c}{\partial r} + \frac{D_\infty\, f_4}{kT} F_r\, c \tag{3.32}$$

$$j_z = -\alpha\, z^2\, f_1\, f_2\, c - D_\infty\, f_1 \frac{\partial c}{\partial z} + \frac{D_\infty\, f_1}{kT} F_z\, c \tag{3.33}$$

Near the stagnation point, the radial diffusion of particles can be neglected, i.e., $\frac{\partial c}{\partial r} = 0$.

As well, the radial components of the colloidal and gravity forces are zero, i.e., $F_r = 0$.

Equation (3.32) can now be written as

$$j_r = \alpha r z f_3 c \tag{3.34}$$

and Equation (3.33) becomes

$$j_z = -\alpha z^2 f_1 f_2 c - D_\infty f_1 \frac{\partial c}{\partial z} + \frac{D_\infty f_1}{kT} F_z c \tag{3.35}$$

Using the following dimensionless quantities:

$$\bar{c} = \frac{c}{c_o},\ \bar{r} = \frac{r}{a_p},\ \bar{z} = \frac{z}{a_p},\ \mathrm{Pe} = \frac{2\alpha a_p^3}{D_\infty},\ \bar{F}_z = \frac{F_z}{kT/a_p} \quad \text{and} \quad \bar{j}_i = \frac{j_i}{D_\infty C_o/a_p};\ (i = r, z)$$

one obtains

$$\bar{j}_r = \frac{1}{2} f_3 \mathrm{Pe}\,\bar{c}\,\bar{r}\,\bar{z} \tag{3.36}$$

$$\bar{j}_z = -\frac{1}{2} f_1 f_2 \mathrm{Pe}\,\bar{c}\,\bar{z}^2 - f_1 \frac{d\bar{c}}{d\bar{z}} + f_1 \bar{F}_z \bar{c} \tag{3.37}$$

The total force on the particle is given by expanding and non-dimensionalizing Equation (3.5).

$$\bar{F}_z = \bar{F}_G + \bar{F}_{VDW} + \bar{F}_{EDL}$$

Making use of Equations (3.13), (3.20) and (3.28), one obtains

$$\bar{F}_z = Gr - Ad \frac{\bar{\lambda}(\bar{\lambda} + 22.232\bar{h})}{(\bar{h})^2 (\bar{\lambda} + 11.116\bar{h})^2} + Dl\,\tau \left[\frac{\exp(-\tau\bar{h})}{1 + \exp(-\tau\bar{h})} - Da \frac{\exp(-2\tau\bar{h})}{1 - \exp(-2\tau\bar{h})} \right] \tag{3.38}$$

We can substitute expressions for $\bar{F}_z$ from Equation (3.38), j_r from Equation (3.36) and j_z from Equation (3.37) in the mass transport equation given by Equation (3.3) to obtain

$$\frac{1}{r}\frac{\partial}{\partial r}(\alpha r^2 z f_3 c)+\frac{\partial}{\partial z}(-\alpha z^2 f_1 f_2 c - D_\infty f_1 \frac{\partial c}{\partial z}+\frac{D_\infty f_1}{kT}F_z c)=0 \quad (3.39)$$

and

$$2\alpha z f_3 c - \frac{d}{dz}(\alpha z^2 f_1 f_2 c) - D_\infty f_1 \frac{d^2 c}{dz^2} + \frac{D_\infty f_1 F_z}{kT}\frac{dc}{dz} = 0 \quad (3.40)$$

After some mathematical manipulation, it is possible to write Equation (3.40) in dimensionless form, using dimensionless separation distance $\bar{h}$ as:

$$(1+\bar{h})Pef_3(\bar{h})\,\bar{c} = \frac{d}{d\bar{h}}\left\{ f_1(\bar{h})\left[\frac{d\bar{c}}{d\bar{h}}+\frac{1}{2}(1+\bar{h})^2 P_e\, f_2(\bar{h})\bar{c} - \bar{F}_z(\bar{h})\bar{c}\right]\right\} \quad (3.41)$$

where $\bar{h}=\frac{h}{a_p}=\frac{z-a_p}{a_p}$, $\bar{c}=\frac{c}{c_o}$, $Pe=\frac{2\alpha a_p^3}{D_\infty}$ and $\bar{F}_z=\frac{F_z}{kT/a_p}$.

3.9. Boundary conditions

Equation (3.41) is subject to following boundary conditions

$$\bar{c}=1 \quad \text{for} \quad \bar{h}\to\infty \quad (3.42a)$$

$$\bar{c}=0 \quad \text{for} \quad \bar{h}=\bar{\delta}=\frac{\delta}{a_p} \quad (3.42b)$$

From the boundary condition given by Equation (3.42a) it is quite clear that at a distance far from the collector, the particle concentration, c is equal to the bulk concentration, c_o. The second boundary condition, described by Equation (3.42b) states that at a certain distance, $\bar{\delta}$ from the collector surface, all particles are assumed to be irreversibly attached to the collector surface. This is referred to as the "perfect sink" condition. The "perfect sink" approximation is extensively used to model particle deposition [Preive and

Ruckenstein, 1974; Spielman, 1977; Elimelech, 1991]. In practice however, not all particles actually attach to the collector surface. Equation (3.41) is solved numerically using boundary conditions (3.42a) and (3.42b). The hypothetical distance δ is taken as the location of the primary energy minimum (PEM) typically located on the order of 1 nm from the collector surface [Israelachvili, 1992].

3.10. Numerical method

Equation (3.41) can be decomposed into two first order ordinary differential equations by introducing a new variable X, defined as the local dimensionless particle flux toward the collector surface:

$$X(\bar{h}) = f_1(\bar{h})\left[\frac{d\bar{c}}{d\bar{h}} + \frac{1}{2}(1+\bar{h})^2 Pe f_2(\bar{h})\bar{c} - \bar{F}_z(\bar{h})\bar{c}\right] \qquad (3.43)$$

Substituting Equation (3.43) in Equation (3.41), we can write Equation (3.41) as a set of two equations:

$$\frac{d\bar{c}}{d\bar{h}} = \frac{X(\bar{h})}{f_1(\bar{h})} - \frac{1}{2}(1+\bar{h})^2 Pe f_2(\bar{h})\bar{c} + \bar{F}_z(\bar{h})\bar{c} \qquad (3.44a)$$

and

$$\frac{dX(\bar{h})}{d\bar{h}} = (1+\bar{h}) Pe f_3(\bar{h})\,\bar{c} \qquad (3.44b)$$

The boundary conditions of Equation (3.42a) and (3.42b) are applicable to Equations (3.44) with the additional boundary condition

$$\text{at } \bar{h} = \bar{\delta} = \frac{\delta}{a_p}, \text{ together with } \bar{c} = 0 \;\; \rightarrow \;\; X(\bar{\delta}) = X_o$$

where X_o represents the dimensionless mass flux of particles to the collector surface. In other words, X_o is identical to the Sherwood number, Sh defined previously. Thus at

$$\bar{h} = \bar{\delta} = \frac{\delta}{a_p}, \text{together with } \bar{c} = 0 \quad \rightarrow \quad X(\bar{\delta}) = X_o = Sh .$$

The dimensionless mass flux of particles at the collector surface X_o is determined as described by Prieve and Lin [1980]. In this method, Equations (3.44a) and (3.44b) can be converted into an initial value problem by choosing a guess value of X_o at $\bar{h} = \bar{\delta} = \frac{\delta}{a_p}$ together with $\bar{c} = 0$ at the collector surface, i.e. all particles are assumed to be irreversibly attached to the collector surface when $\bar{h} = \bar{\delta}$.

Using the guess value of $X(\bar{\delta}) = (X_o)_{guess}$ we calculate by numerical integration the value of the dimensionless particle bulk concentration (i.e. $\bar{c}_o$ at an infinite distance, $\bar{h} = \bar{h}_\infty$) from Equations (3.44a) and (3.44b). We denote this value as $(\bar{c})_{calculated}$, which may not be unity as required by the boundary condition Equation (3.42a).

Since Equations (3.44a) and (3.44b) are linear, we can determine the actual value of the dimensionless mass flux at the collector surface, denoted by $(X_o)_{actual}$ from

$$\frac{(X_o)_{actual}}{(X_o)_{guess}} = \frac{(\bar{c})_{actual}}{(\bar{c})_{calculated}} \qquad (3.45)$$

Here, the unbounded bulk concentration of the particles in the solution is expressed by Equation (3.42a) is unity, i.e. $(\bar{c})_{actual} = 1$. Hence, in Equation (3.45), the only remaining unknown term is $(X_o)_{actual}$, the actual dimensionless mass flux at the collector surface. Equations (3.44a) and (3.44b) are stiff ordinary differential equations due to rapid changes of their coefficients over small separation distance. Consequently, a semi-implicit extrapolation method [Numerical Recipes, 1986] was used to perform numerical calculations.

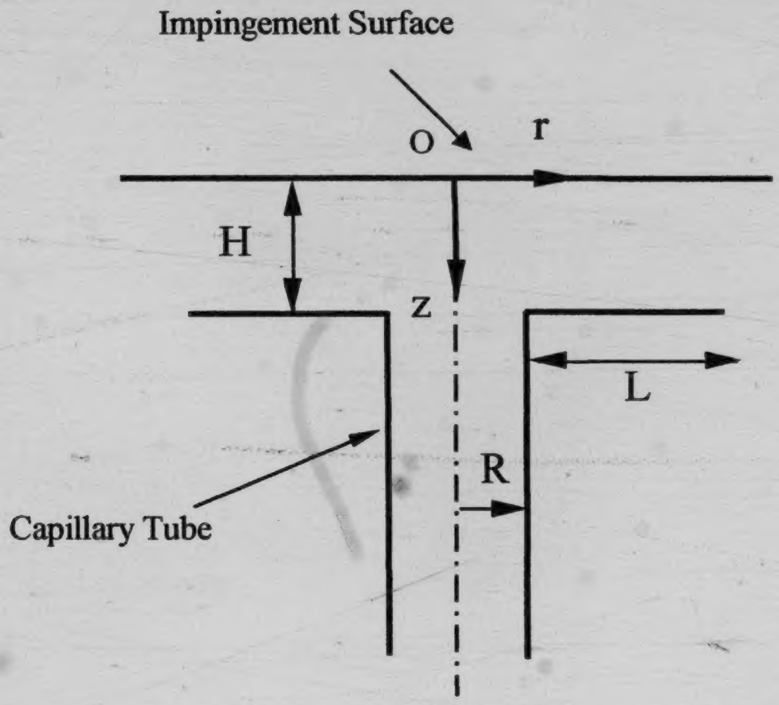
Impingement Surface
O
r
H
z
L
R
Capillary Tube

Figure 3-1. Geometry of impinging jet cell: R = 1.275 mm; H = 2.55 mm; L = 40 mm. Flow enters into the capillary tube of radius R and impinges and then impinges onto a collector surface I with a separation distance of H. The stagnation point O, located on the axis of symmetry and the impingement surface I, is the origin of the cylindrical coordinate system r and z.

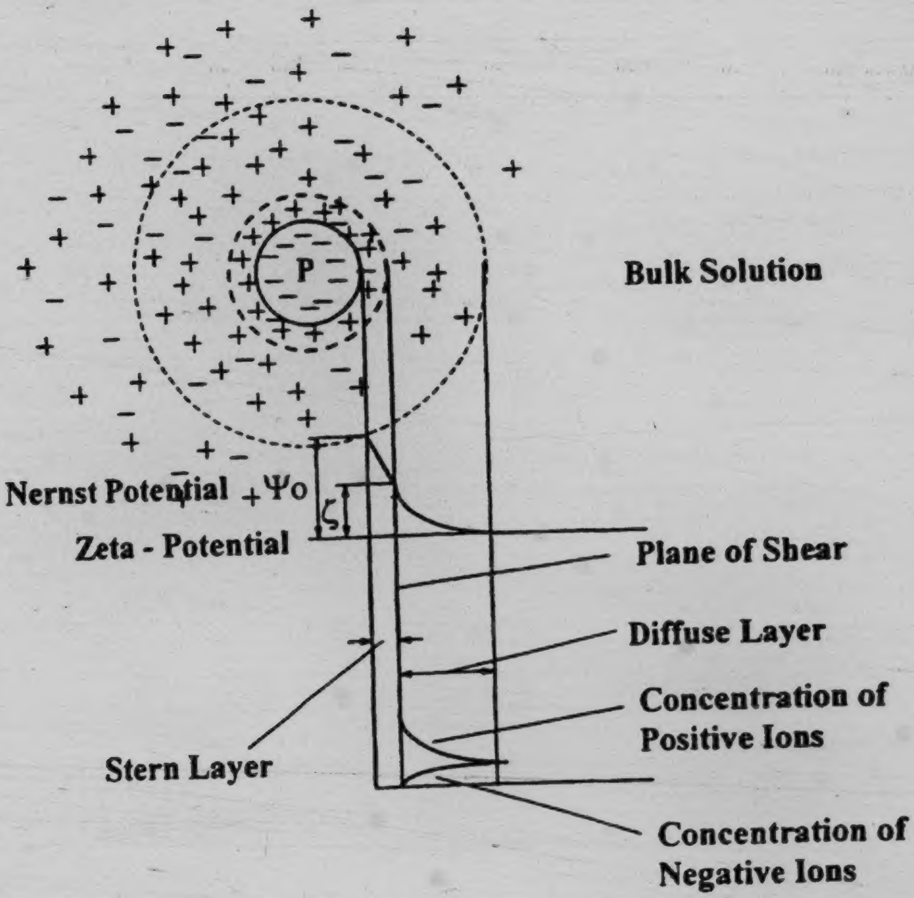
P
Bulk Solution
Nernst Potential +Ψo
ζ
Zeta - Potential
Plane of Shear
Diffuse Layer
Concentration of Positive Ions
Stern Layer
Concentration of Negative Ions

Figure 3-2. Schematic diagram representing charge distribution around a negatively charged particle [Hunter, 1981].

Chapter Four

Sensitivity analysis and validation

4.0. Introduction

Since the numerical model developed in Chapter 3 will be used to predict mass transfer rates of asphaltene-in-toluene droplets suspended in the water in the impinging jet system and then compared with those determined experimentally, it is important to test both the model and the experimental apparatus. Examination of the mass transport equation reveals that the mass transfer rate of colloidal particles or droplets depends on the size of the particle (a_p), flow rate (Re), gravitational force represented by Gr and colloidal interaction forces measured by adhesion number, Ad (VDW force) and Dl (EDL parameter). In this chapter, the sensitivity of the theoretical model is analyzed with changes in the particle size, adhesion number and EDL parameter. Since the size of asphaltene-in-toluene droplets is very small, the Gr is neglected for the sensitivity analysis. The sensitivity analysis of the present model will also be compared with a similar exercise done by Sanders [1997].

The validation of the model and experimental apparatus is done in two parts:

1. By choosing the experimental parameters of a previous researcher [Sanders, 1997], model simulations were performed to illustrate that the results of the present model are in reasonable agreement with those of Sanders' model [1977].
2. A set of experiments was performed, using a colloidal system of well defined, known properties (latex particles). The experimental mass transfer rates were then compared with those predicted by the model developed in Chapter 3 to verify the accuracy of

the predictions. Additionally, the results of the latex experiments from this study were also compared with those of Sanders [1997].

4.1. Effect of particle radius

A model system with the following parameters is selected for the sensitivity analysis:

1. The dimensionless separation gap, $\overline{H}_o = 2$ (which reflects the experimental setup).
2. EDL interaction, $Dl = 0$ (no energy barrier).
3. VDW interaction, $Ad = 0.1$.
4. Electrolyte concentration, $M_i = 0.01M$ (1: 1 electrolyte).
5. Gravitation parameter, $Gr = 0$ (small density difference).

Particle radii of 0.5μm, 1.0μm and 1.5μm are chosen to illustrate the effect of particle size on predicted mass transfer rates.

Figure 4-1 shows the predicted mass transfer rates (Sherwood number) determined for Reynolds numbers in the range of 100 to 1000 and for three different particle radii. The model predicts that the effect of particle size on mass transfer rate is quite strong. The mass transfer rate for the 1.0μm particles is nearly 4 times less than that for the 1.5μm particles, and about 7 to 8 times more than that for the 0.5μm particles. The results of this model for particle radius 0.5μm and 1.0μm are in good agreement with those in Sanders' [1997] model.

These results show that the model is very sensitive to the size of a colloidal particle or droplet. Therefore, the asphaltene-in-toluene droplets to be studied here must be characterized accurately in order to get good results from the model.

4.2. Effect of adhesion number

Recall that the adhesion number (Ad) is a measure of van der Waals (VDW) interactions and depends on the Hamaker constant. It is difficult to obtain representative values of the Hamaker constant, particularly for a non-idealized emulsion such as that under consideration in this study. Errors in estimating the Hamaker constant will have an adverse effect on the accuracy of the model predictions.

The model system described in Section 4.1 is again selected for this analysis, except that the particle radius is held constant at $a_p = 1.0$ μm. The variation of dimensionless mass transfer rate (Sherwood number) with different adhesion numbers is shown in Figure 4-2. Figure 4-2 shows that the theoretically predicted mass transfer rate by the model is comparatively insensitive to changes in the adhesion number. The 5 fold increase in the adhesion number increases the mass transfer rate only 1.2 times and a 10 fold increase in the adhesion number increases Sherwood number by 1.3 times. This indicates that the deposition using the chosen parameters is not very sensitive to adhesion number and any error in approximating Hamakar constant should not affect the predicted mass transfer rates. Comparing the present results with those of Sanders [1997], it is noticed that the agreement in the trend is good although absolute values of Sherwood numbers are different because the two analyses use different particle size.

4.3. Effect of electrostatic double layer (EDL) strength parameter Dl

The double layer strength parameter, Dl is directly dependent on the zeta potentials of the collector and the particle, i.e., it depends on electrostatic forces between the particle and the collector. The zeta potential itself is dependent upon the electrolyte type, electrolyte concentration and pH of the aqueous phase. Therefore, the mass transfer rates are expected to be dependent on these parameters. Two concentrations, 0.01M and 0.1M of 1:1 type electrolyte, were chosen to illustrate the effect of electrolyte concentration on mass transfer rates with respect to Dl (i.e. zeta potentials of the system). Particle radius ($a_p = 1.0$ μm) and adhesion number (Ad = 0.5) were kept constant.

Figures 4-3 and 4-4 show the dependence of Sherwood number on Dl for 0.1 M and 0.01 M of 1:1 electrolyte solutions for a Reynolds number of 200. Figures 4-3 and 4-4 show that the mass transfer rates (represented by the Sherwood number) are nearly constant until a critical value of Dl is reached (denoted as $Dl_{critical}$). As soon as the value of Dl exceeds $Dl_{critical}$, the mass transfer rate (Sh) decreases sharply.

In practical terms, for systems where $Dl \approx Dl_{critical}$, even a small degree of inaccuracy in zeta potential measurements may result in significant deviations between experimental observations and model predictions. Figures 4-3 and 4-4 also indicate that at higher electrolyte concentrations (0.1M), attachment is possible at much higher values of zeta potential than at the lower electrolyte concentration (0.01 M).

4.4. Numerical model validation and testing of experimental apparatus

Dabros et al. [1983] carried out pioneering studies with the latex particles deposition using an impinging jet system. Sanders [1997] successfully duplicated the theoretical predictions of Dabros et al. [1983] with his model. Sanders conducted deposition experiments with latex particles and found agreement of his experimental results with those of Dabros and van de Ven [1983]. In the present study, model simulations were performed using Sanders' latex particle parameters shown in Table 4-1.

Table 4-1: Characterization of Sanders' latex deposition experiments

Particle radius, a_p	0.416 μm
Adhesion number, Ad	0.2
EDL strength parameter, Dl	0
Strength of stagnation flow, $\overline{\alpha}$	$\overline{\alpha} = 0.52\,\mathrm{Re}^{0.5}$
Electrolyte Concentration (1:1 type), M_i	0.01M

Figure 4-5 shows the theoretical predictions of dimensionless mass transfer rate (expressed as Sherwood number) by the present study model (represented by the solid line) using Sanders' parameters tabulated in Table 4-1. Symbols represent results obtained by Sanders [1997] in his experimental work with latex particles. Figure 4-6 shows theoretical predictions of mass transfer rate for latex particle deposition by Sanders' model (represented by solid lines) and symbols represent results of Sanders' [1997] experimental work. The theoretical curve of Figure 4-5 fits the experimental results of Sanders in the same way as the theoretical curve of Figure 4-6 (only for Ad = 0.2). This comparison suggests that the model of the present study is reliable.

4.5. Deposition experiments using latex particles

In order to confirm the validity of the model and to test the impinging jet apparatus, a set of experiments was conducted with polystyrene latex particles (Surfactant Free, Sulfate White Polystyrene latex, Interfacial Dynamics Corporation, Portland, U.S.A). The mean diameter was 2.9 μm (± 0.07 μm).

A dilute latex suspension was prepared in Milli-Q water (pH = 5.8) with 0.01M NaCl. The particle concentration was checked using a Bright line hemacytometer (Hausser Scientific). Latex particle zeta potentials were measured using a Zetaphoremeter III (SEPHY-CAD Instrumentation, France). Zeta potentials were calculated from measured electrophoretic mobilities.

The microscopic glass slide was crushed into a powder and then an aqueous suspension of the powered glass was prepared at pH 5.8 and 0.01M [NaCl]. The zeta potential of the glass suspension was measured using Zetaphoremeter III (SEPHY-CAD Instrumentation, France). The collector surface was prepared as per the procedure described in Section 5.4.1. The experimental parameters are listed in Table 4-2.

Table 4-2: Characterization of latex deposition experiments.

Latex particle radius a_p	1.45 μm
Concentration of particles	6.2×10^6 Particles/ml
Electrolyte concentration	0.01M [NaCl]
Particle zeta potential, ζ_p	- 40 mV
Collector zeta potential, ζ_c	- 55 mV
Jet exit – collector, dimensionless separation, $\overline{H}_o$	2.0
Bulk pH	5.8

More than 30 deposition experiments were conducted using latex particles for a range of Reynolds numbers from 50 to 300. Figure 4-7 shows the stagnant region coating density (SRCD) curves with respect to Reynolds number for selected latex particle deposition experiments. The flux, J_o is calculated from the initial slopes of the SRCD curves (represented by solid lines) and then dimensionless mass transfer rates (expressed as Sherwood number) are calculated using Equation (2.2). Figure 4-8 shows mass transfer rates (expressed as Sherwood number) for the latex experiments. The solid line indicates the theoretically predicted Sherwood number and the symbols represent those determined experimentally. Figure 4-8 shows that there is good agreement between Sherwood numbers predicted by the model and those experimentally determined, which indicates that the present model has successfully predicted the mass transfer rates of latex particles in the deposition experiments using the impinging jet apparatus. It is important to note that the size of particles a_p, number concentration of latex particles in the bulk c_o, strength of stagnation flow $\overline{\alpha}$ and dimensionless separation distance between the exit of the impinging jet and the collector $\overline{H}_o$, are different from those of Dabros [1983] and Sanders [1997] but still the mass transfer rates are similar. Therefore, both the model and the experimental apparatus are verified. Hence, in this study, any disagreement found between theory and experimental results cannot be attributed to systematic errors associated with the model or impinging jet apparatus.

4.6. Conclusions

The sensitivity analysis shows that the theoretically predicted mass transfer rates are very sensitive to particle size, relatively insensitive to the adhesion number (i.e.

Hamaker constant) and affected by the hydrodynamic conditions for the EDL interactions where $Dl < Dl_{critical}$. Once critical value of Dl is reached, i.e., $Dl > Dl_{critical}$, the EDL interaction dominates all the other factors and theoretically predicted mass transfer rates decrease significantly. Therefore, accurate measurements of both particle and collector zeta potential will be very important for accurate predictions of droplet attachment rates.

The model developed in Chapter 3 and experimental apparatus setup is successfully validated for their application.

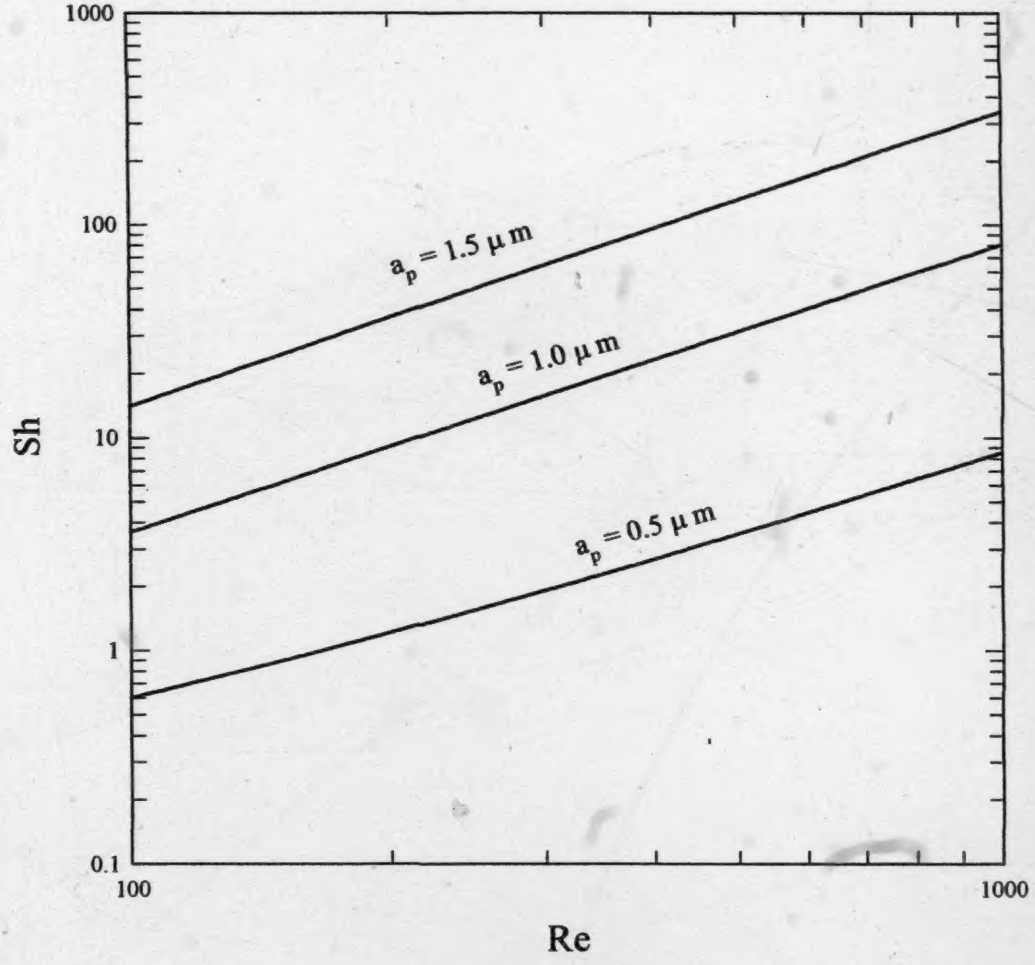

Figure 4-1. Predicted variation of Sherwood number with particle radius for a system described by Ad = 0.1, Dl = 0, Gr = 0, electrolyte concentration = 0.01M (1:1 type), $\overline{H}_o = 2$.

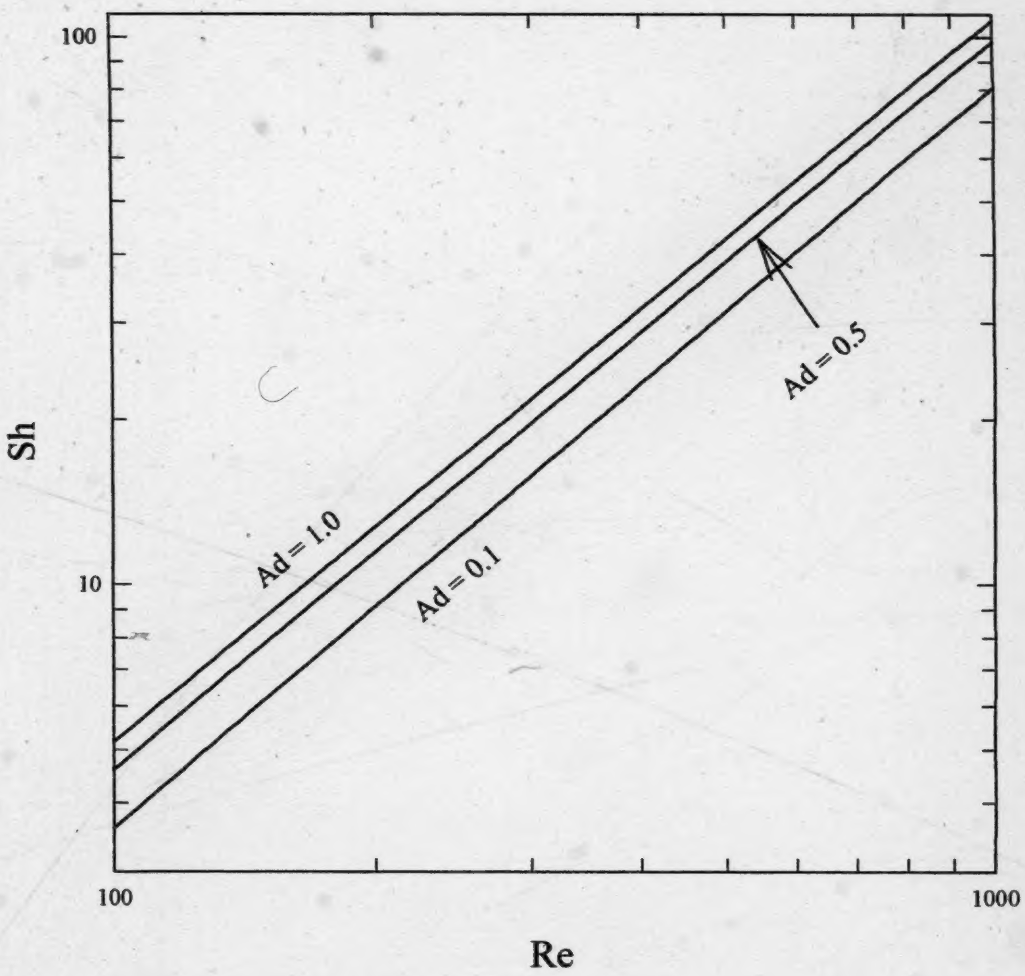

Figure 4-2. Predicted variation of Sherwood number with adhesion number for a system described by $a_p = 1.0$ μm, Dl = 0, electrolyte concentration = 0.01M (1:1 type), $\overline{H}_o = 2$, Gr = 0.

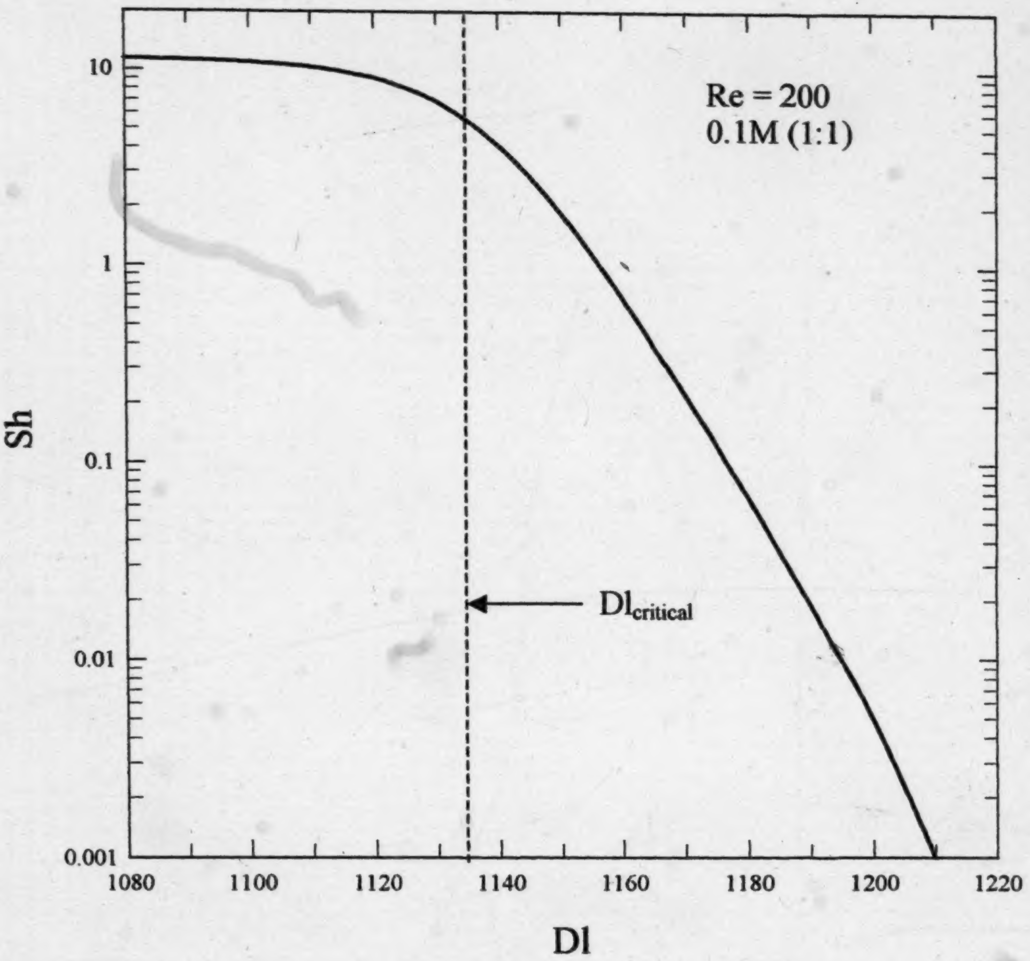

Figure 4-3. Predicted variation of Sherwood number with double layer strength parameter Dl for a system described by $a_p = 1.0\ \mu m$, Ad = 0.5, Gr = 0, Re = 200, $\overline{H}_o = 2$ and electrolyte concentration = 0.1M (1:1 type).

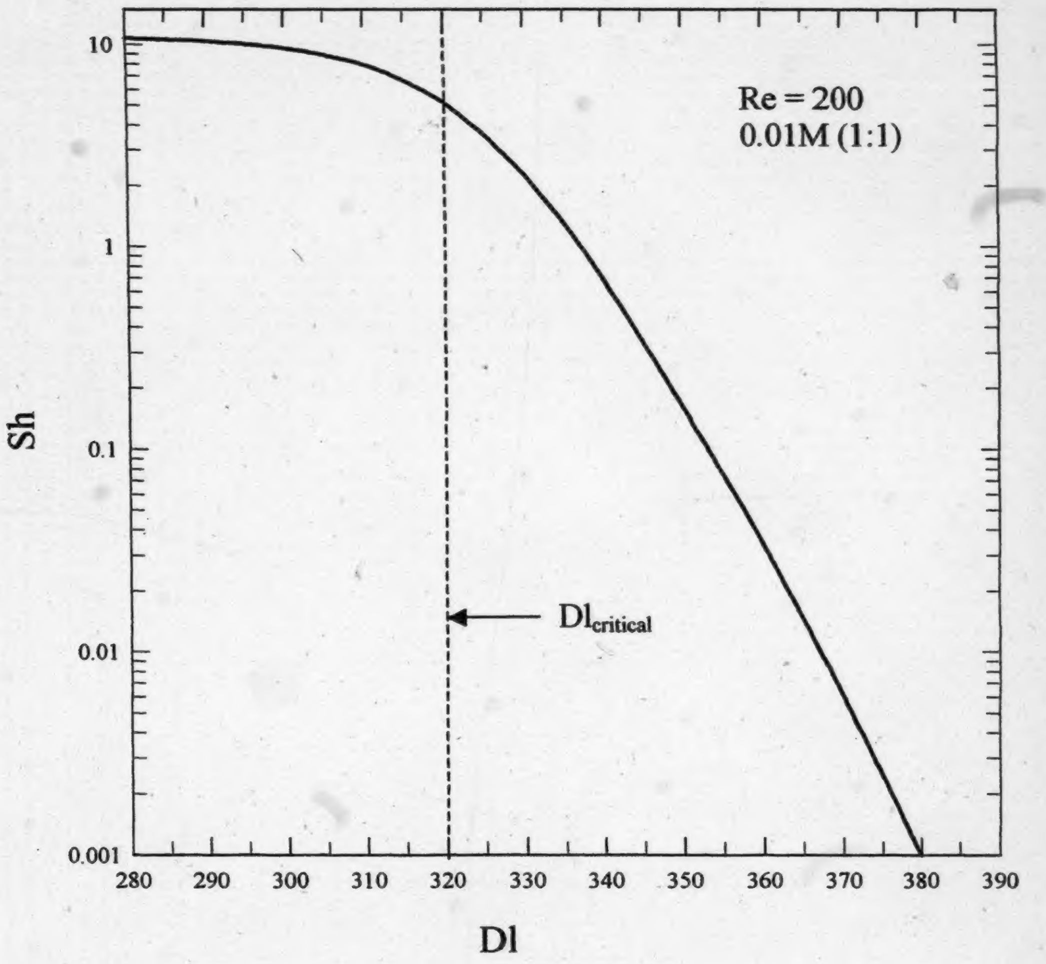

Figure 4-4. Predicted variation of Sherwood number with double layer strength parameter Dl for a system described by a_p = 1.0 μm, Ad = 0.5, $\overline{H}_o = 2$, Gr = 0, Re = 200 and electrolyte concentration = 0.01M (1:1 type).

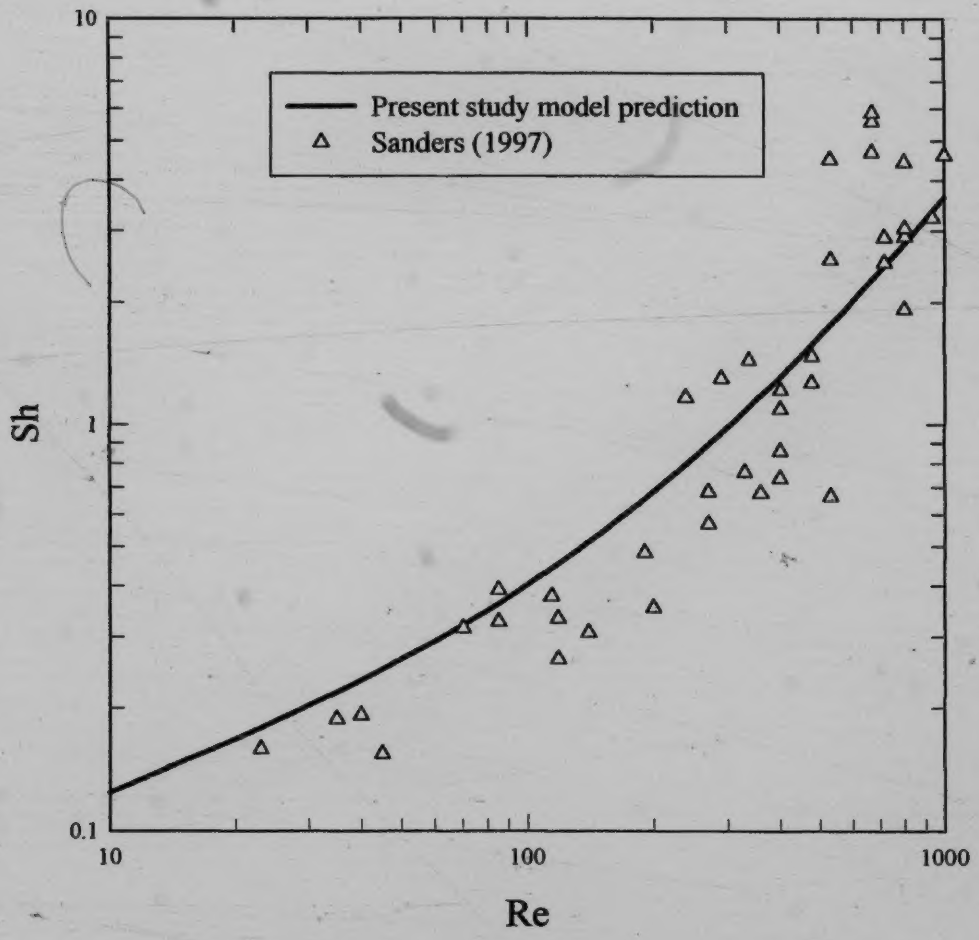

Figure 4-5. Simulation results (solid line) of the present study model for latex particle deposition experiments conducted by Sanders [1997]. Symbols represent Sanders' experimental results. Parameters used in the model: $a_p = 0.416$ μm; Ad = 0.2; [NaCl] = 0.01M; Dl = 0 and $\overline{\alpha} = 0.52\text{Re}^{0.5}$.

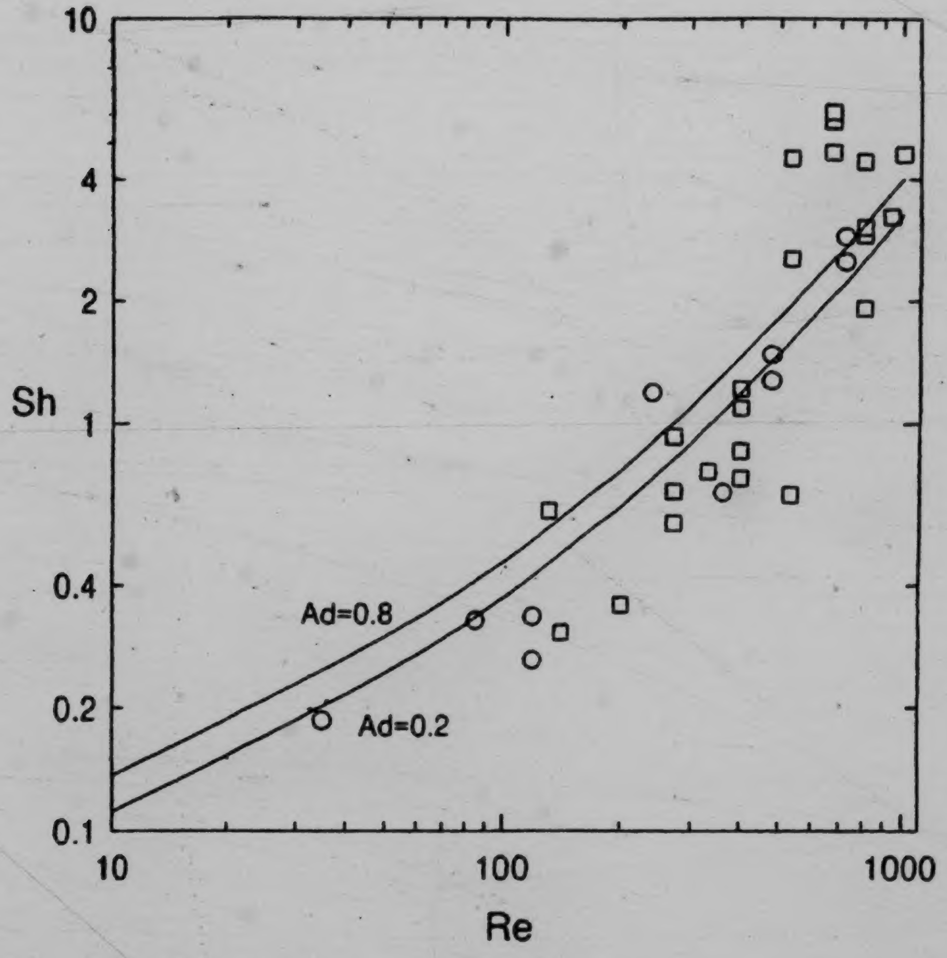

Figure 4-6. Sherwood number as a function of Reynolds number for the latex particle deposition experiments conducted by Sanders [1997]. Symbols represent experimental results and solid line represents predictions by Sanders' model using $a_p = 0.416$ μm, Ad = [0.2, 0.8], [NaCl] = 0.01M, Dl = 0 and $\overline{\alpha} = 0.52\mathrm{Re}^{0.5}$.

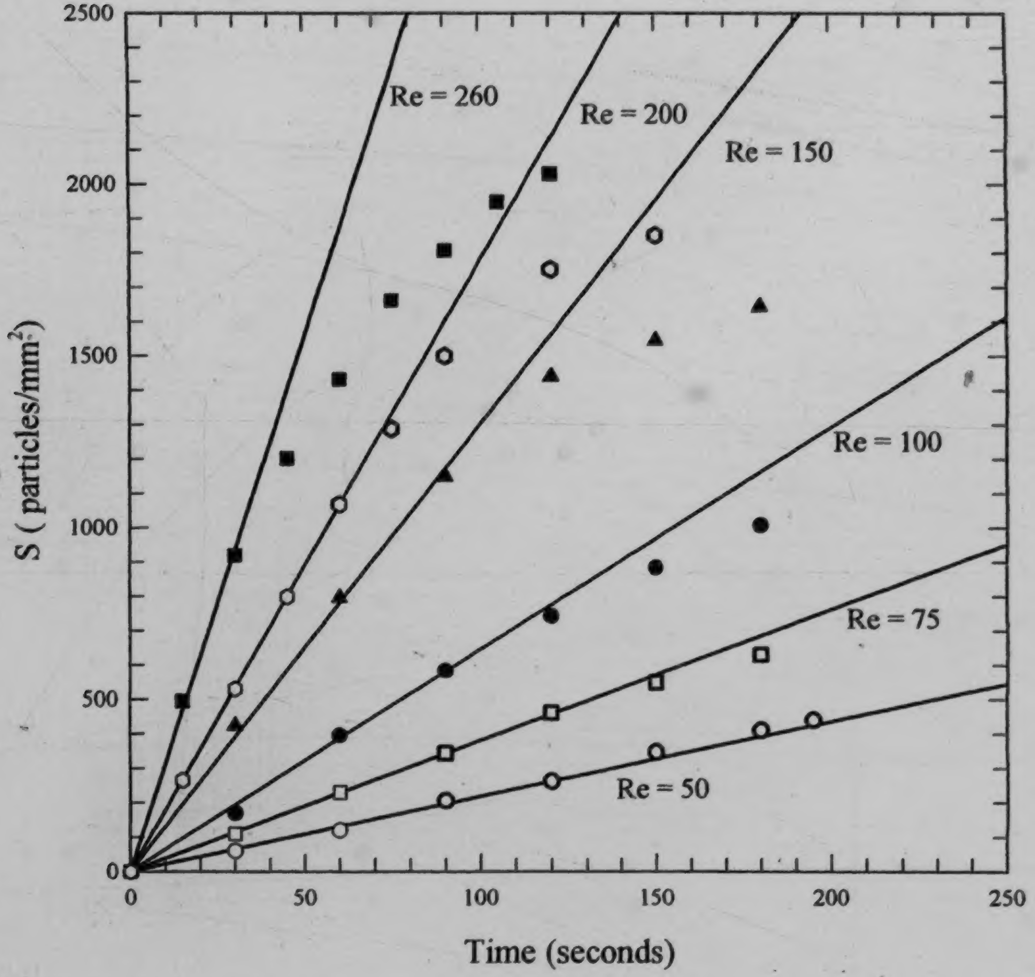

Figure 4-7. Stagnation Region Coating Density (SRCD) as a function of time for latex particle deposition experiment conducted in this study. $a_p = 1.45$ μm, $\overline{\alpha} = 5.3\mathrm{Re}^{0.5} - 8.13\,(\mathrm{Re} \geq 5)$, pH = 5.8, [NaCl] = 0.01M, and $\overline{\mathrm{H}}_{\mathrm{o}} = 2$.

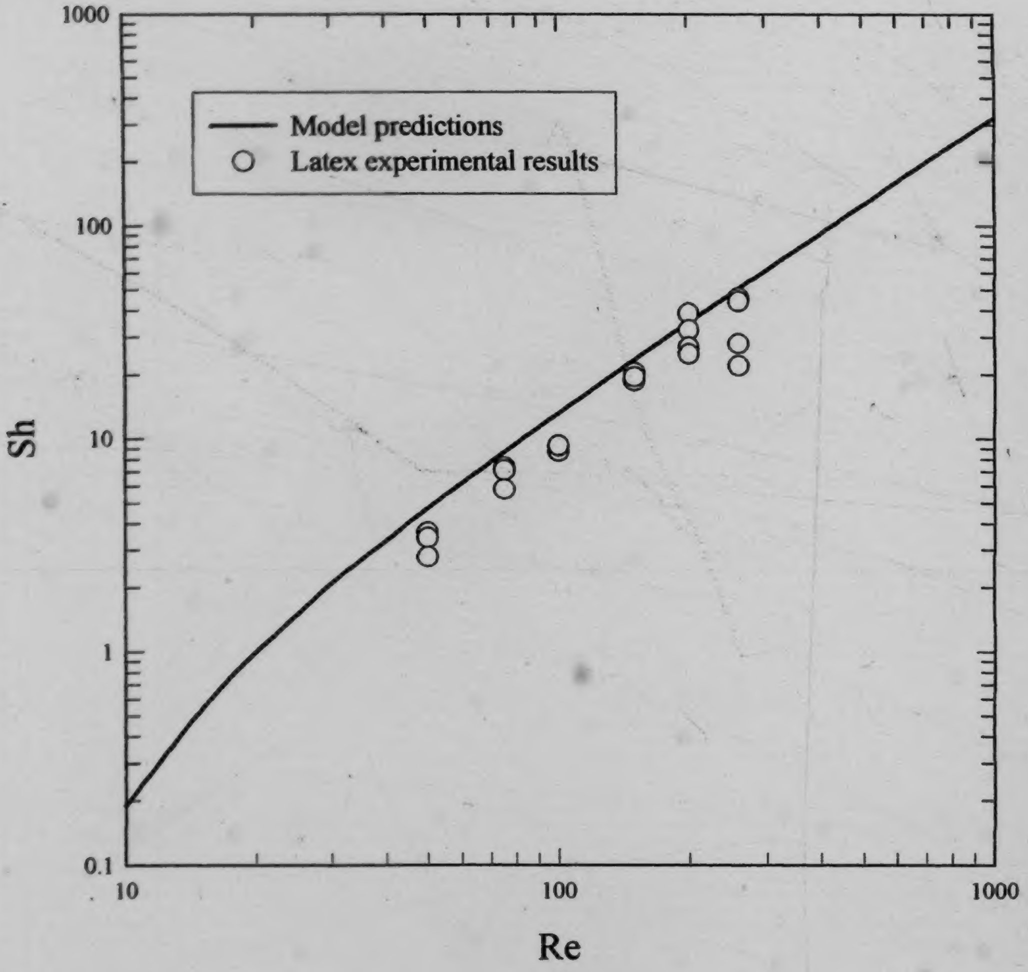

Figure 4-8. Sherwood number as a function of Reynolds number for the latex particle deposition experiments. Symbols represent experimental results and solid line indicates model predictions using $a_p = 1.45$ μm, Ad = 0.2, [NaCl] = 0.01M, Dl = 0, $\overline{H}_o = 2$ and $\overline{\alpha} = 5.3\mathrm{Re}^{0.5} - 8.13\ (\mathrm{Re} \geq 5)$.

Chapter Five

Experimental method

5.0. Introduction

The experimental procedures for the present study mainly consist of the following: 1. production of asphaltenes from the bitumen; 2. preparation of asphaltene emulsion and its characterization; 3. collector surface preparation and characterization; 4. performing impinging tests. The following methods were established to standardize the procedures and in all the experiments, the same established procedures were strictly followed.

5.1. Clean bitumen

First, coker feed bitumen obtained from Syncrude is dissolved in toluene at the ratio of 1:25 (by weight). This solution is placed on a mechanical shaker for four hours to prepare a homogeneous solution. Then the solution is centrifuged at 20,000 rpm (30,000g) for 30 minutes to separate solids (sand and clay) from the solution. The solids free bitumen solution in toluene is decanted and kept under slight vacuum (under a fume hood) until all the toluene is evaporated. The resulting purified bitumen is referred to as "clean bitumen".

5.2. Production of asphaltenes

The "clean bitumen" prepared in Section 5.1 is dissolved in n-heptane with the ratio of 1:20 (by weight) and placed on the shaker for four hours. This mixture is then kept at room temperature and pressure for four days to precipitate asphaltenes from the bitumen. The top portion of this mixture is decanted. The remaining mixture, containing precipitated asphaltenes is washed repeatedly with n-heptane. The washing process involves mixing the precipitated asphaltene with n-heptane in the ratio of 1:10 by weight and is placed on shaker for one hour.

This asphaltene-heptane mixture is then centrifuged to separate asphaltene aggregates from the mixture. The washing procedure is repeated five to six times until the heptane remains colorless. This procedure ensures that the asphaltenes are free from any bitumen leftover.

5.3. Preparation and characterization of asphaltene-in-toluene droplet suspension in water

5.3.1 Concentrated suspension

For each set of experiments, a new emulsion is prepared from the same batch of asphaltenes produced in the procedure outlined in Section 5.2. First, a concentrated solution of asphaltene is prepared in toluene. The aim is to prepare the solution as concentrated as possible. It was found that approximately 1g asphaltenes could be dissolved in 5 ml of toluene. Subsequently each new solution was prepared by dissolving

1 g of asphaltene in 5ml of toluene. This mixture is then placed on the shaker for two hours to ensure complete dissolution of the asphaltenes in the toluene.

This 5ml of concentrated asphaltene solution in toluene is emulsified by a hand-held homogenizer (Fisher Scientific) in 100 ml of distilled water (Milli-Q, Millipore) whose pH and salt concentration was pre-determined as was the requirement of the experiment and termed as "concentrated emulsion."

The concentrated emulsion shows two distinct phases. The upper layer consists of a concentrated water-in hydrocarbon emulsion and represents approximately 1/10th of the solution. The lower layer contains asphaltene-in-toluene droplets suspended in water. This is confirmed by observing samples of both emulsions under microscope. Only the lower layer is used to prepare the emulsion used in the experiments.

A number of interesting facts were noted regarding the properties of the concentrated emulsion. Normally, the concentrated emulsion is stable for approximately six hours. After six hours, the top portion of the emulsion developed a membrane with some associated yield stress. In the lower layer of this concentrated emulsion, the asphaltene particles started to aggregate and then deposit on the bottom of the container. After 24 hours, one can see three distinct phases in the emulsion: the upper portion, which forms a thick membrane; the middle portion, which is fairly transparent; and the bottom layer where asphaltene particles are deposited as a solid phase.

The emulsion remained steady for more than four hours which is sufficient for the required set of experiments. Therefore, a new concentrated emulsion is made before the start of every set of the experiments.

5.3.2. Dilute suspension

Each asphaltene emulsion used for the impinging jet experiments was prepared by extracting 20 ml from the lower layer of the concentrated emulsion. This concentrated emulsion was diluted by mixing with 750 ml of distilled water (Milli-Q, Millipore) whose pH and salt concentration was pre-determined as was the requirement of the experiment. This diluted emulsion is termed as " experimental emulsion" and used in impinging jet experiments. The zeta potential, concentration and size distribution studies of asphaltene-in-toluene droplets in the experimental emulsion were performed before each set of experiments. Figure 5-1 shows an image of the dilute suspension of asphaltene-in-toluene droplets in water.

5.3.3. Concentration and size distribution of asphaltene-in-toluene droplets

An optical hemacytometer (Bright line, Hausser Scientific) is used to determine the droplet concentration and size distribution. Concentration and size distribution measurements are conducted both before and after each experiment to ensure there is no appreciable change in the properties of the emulsion during the experiment.

A minimum of four different samples of the experimental emulsion were taken and eight sub samples of each were analyzed to determine concentration and size distribution of asphaltene droplets in order to provide statistically reliable data for each set of experiments. A typical result of concentration and size distribution study by the hemacytometer is shown in Figure 5-2. The average size of asphaltene-in-toluene droplets is calculated from the data of Figure 5-2, as shown below:

$$\text{Average size of the droplets} = \frac{5\times19 + 4\times55 + 3\times490 + 2\times34 + 1\times25}{620}$$

$$= \quad 3.0\ \mu\text{m}$$

5.4. Collector preparation and characterization

5.4.1. Hydrophilic (untreated) glass slides

Pre-cleaned microscopic slides super-frost, Fisher Scientific (size 50×75×1 mm) are used to prepare the collector surface for the experiment. The slides are first placed in an ultrasonic bath (Bransonic, USA) filled with DIUF water and 5% Ducan (detergent for cleaning glassware) for 30 minutes. These slides are then washed thoroughly with DIUF water and then immersed in a 12M-concentrated hydrochloric acid solution for four hours at 60°C. The slides are then removed from hydrochloric acid, washed thoroughly with DIUF water and dried in an oven at 60°C for an hour. All slides are cleaned using this procedure. Some are then used directly to perform the hydrophilic surface impinging jet experiments and others used to prepare hydrophobic surfaces. The cleaned slides are never stored more than two hours in water to minimize aging effect [Dabros et al., 1983].

Hydrophilic means water loving surface. These surfaces have molecules such as O-atoms as shown in Figure 5-3 [Arujo et al., 1995], which contain electronegative atoms capable of associating with H- bond networks in water [Israelachvili, 1992]. Hence, there is always an effective attraction between water and these surfaces [Israelachvili, 1992]. When water is exposed to these surfaces, it immediately forms an adsorbed monolayer on the surface. This phenomenon is also called as water wet. It is widely accepted to characterize glass surfaces by contact angle measurements. The contact angle is defined as the three phase (air-liquid-solid) contact angle measured through the water phase when a drop of water of diameter 1-2mm is placed on the surface using standard equipment and following a standard procedure. The contact angle on the hydrophilic surface is very small. Yang [2000] performed contact angle measurements on hydrophilic glass surfaces and found 7° to 9°. No contact angle measurements were performed in the study on hydrophilic glass surfaces as the same glass slides were used as were used by Yang [2000] in his experiments. In experiments, all slides were used once only and discarded after the experiments. No slides were re-used.

5.4.2. Hydrophobic (methylated) glass slides

The procedure followed here to alter surface wetting characteristics is well documented in the literature [Arujo, 1995; Sanders, 1997; Yang, 2000]. After treatment, a very thin hydrophobic film is uniformly coated on the surface. Araujo et.al. [1995], performed X-ray photoelectron spectroscopy on methylated glass slide surface and found that the surface is modified due to chemical adsorption of carbon groups after methylated treatment as shown in Figure 5-3.

The inability of these carbon groups to participate in H- bonding of water causes reorientation of the water molecules around carbon groups so that the surrounding water molecules can participate in H-bond formation more or less in the same way as in bulk water [Israelachvili, 1992]. Due to this reason when water is exposed to the hydrophobic surfaces, it rolls up into small lenses and subtends a large 3-phase (air-liquid-solid) contact angle measured through liquid phase [Israelachvili, 1992]. Hence, contact angle measurements are widely accepted to characterize the hydrophobicity of the surface.

The methylated glass surfaces were obtained by coating them with "organofunctional silanes" [Arujo, 1995; Sanders, 1997; Yang, 2000]. The salination procedure used here is same as used by Dabros [1983], Sanders [1997] and Yang [2000].

Clean slides prepared as described in Section 5.4.1 are immersed into 10% solution of dimethelydichlorosilane (Aldrich) in toluene by volume and are left to soaking overnight at room temperature. The slides are then washed with methanol (Fisher Scientific) and dried in air. These slides are stored in a closed jar.

Contact-angle tests are performed using by a goniometer (Rame-Hart Inc.) to confirm that these slides are hydrophobic. The detailed description of this procedure was provided by Zhou et al. [1998]. The contact angle of methylated (hydrophobised) glass slides was found between 105° to 108°. The results are in agreement with those of Zhou et al. [1998] and Yang [2000]. The results of the contact angle measurements confirm that the methylated glass surface is hydrophobic.

5.4.3. Bitumen coated slides

Application of asphaltene and bitumen coatings on glass slides was a challenge because after coating, the glass slide must have a reasonable light reflection and refraction properties to be used under the microscope. A thick coating would make the slide opaque while thin coating would result in non-uniform coating. Several methods were used with unsatisfactory results but finally Sanders' [1997] method with minor modification achieved a reasonably good coating.

The hydrophobic slides prepared as described in Section 5.4.2 are immersed in a 5% solution by weight of cleaned bitumen (prepared in section 5.1) in toluene for 30 minutes. The slides are then removed from the solution and dried in air. In this way, a thin film of bitumen is coated onto the hydrophobic slides. The slides were checked under microscope to confirm coating quality and uniformity.

5.4.4. Asphaltene coated slide

The hydrophobic slides prepared as described in Section 5.4.2 are immersed in 5% by weight of asphaltene (prepared in Section 5.2) in toluene for 30 minutes. The slides are then removed from the solution and dried in air. The microscopic slides are prepared before each set of experiments and used once only. The prepared slides are not kept for the next set of experiments and all the used slides are discarded at the end of the experiment.

5.5. Zeta potential measurements

Before the start of the experiment, two different samples were taken from the asphaltene-in-toluene droplet suspension in water and two readings of zeta potential from each sample were taken with a Zetaphoremeter-3 (SEPHY-CAD, France). The zeta potentials for hydrophobic and hydrophilic (clean glass) at experimental pH and electrolyte concentration were taken from the published values [Sanders, 1997; Somasundaran, 1998; Yang, 2000] from the literature.

The zeta potential of the asphaltene coated glass slides was taken equal to that of asphaltene-in-toluene droplets measured at the experimental conditions. The zeta potential was measured for the bitumen-in-water emulsion at the experimental pH and electrolyte concentration and these measured values were taken as the zeta potential of bitumen coated collector [Sanders, 1997].

5.6. Choice of Hamaker constant

Wu et al. [2000] measured the value of Hamaker constant experimentally for bitumen-water-bitumen system and deasphalted bitumen-water-deasphalted bitumen system. They found values of Hamaker constant for these systems to 3.2×10^{-21} J and 2.9×10^{-21} J respectively. From the above experimental values, it is clear that the value of Hamaker constant is similar for bitumen and deasphalted bitumen. Therefore, one can assume that the Hamaker constant for asphaltene-water-asphaltene system will be similar to that of a bitumen-water-bitumen system.

Takamura and Chow [1983] calculated the value of Hamaker constant for bitumen-water-glass system as 1.08×10^{-20} J. Once again, it is reasonable to assume an asphaltene-water-glass system is approximately equivalent to a bitumen-water-glass system for assigning a value for the Hamaker constant. Since the model has been shown to be quite insensitive to changes in adhesion number (Hamaker constant), this assumption is not expected to affect the accuracy of the predicted deposition rates.

5.7. List of experiments

Table 5.1 lists the deposition experiments of the asphaltene-in-toluene droplet suspension in water that were performed using different collectors.

Table 5-1: List of asphaltene-in-toluene deposition experiments

System	Collector	pH	NaCl concentration
1	Hydrophilic	9.5	0.01M
2	Hydrophilic	8.5	0.01M
3	Hydrophilic	3.5	0.01M
4	Hydrophilic	8.0	0.001M
6	Hydrophobic	9.5	0.01M
7	Hydrophobic	8.5	0.01M
8	Hydrophobic	3.5	0.01M
8	Hydrophobic	8.0	0.001M
10	Asphaltene coated	9.5	0.01M
11	Asphaltene coated	3.5	0.01M
12	Bitumen coated	9.5	0.01M
13	Bitumen coated	3.5	0.01M

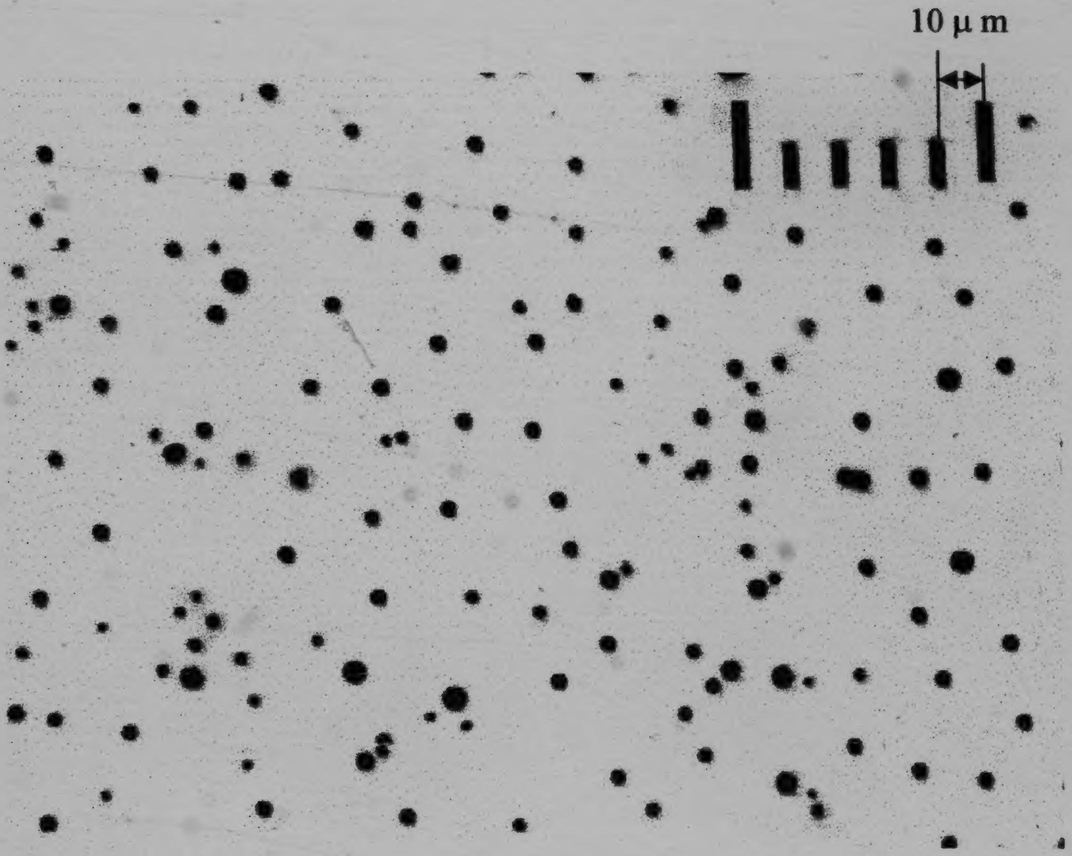

Figure 5-1. Image of asphaltene-in-toluene droplets obtained with 50X objective.

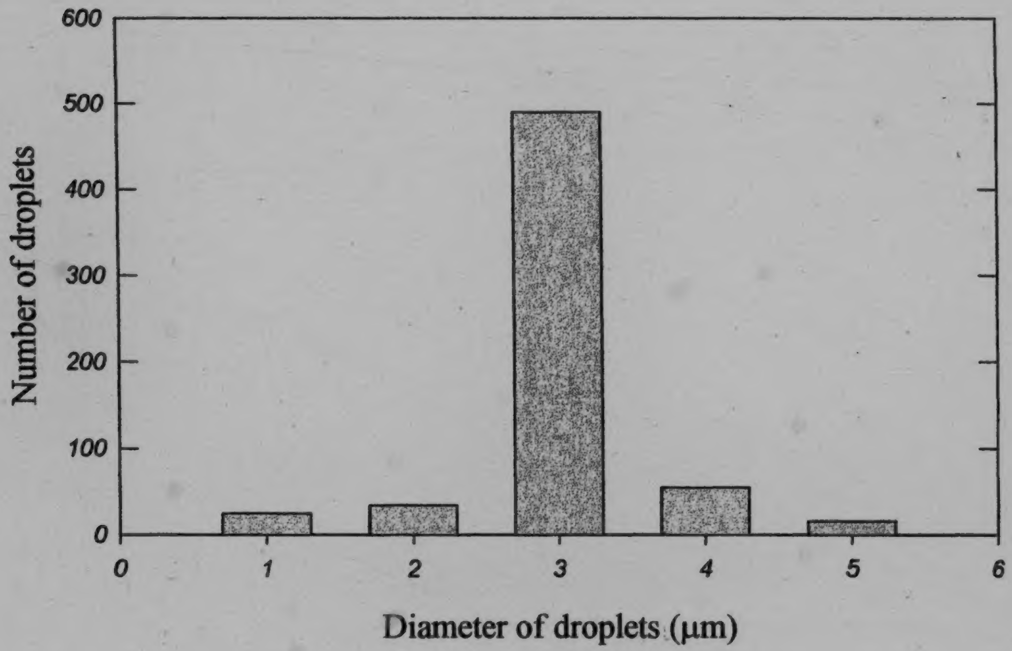

Figure 5-2. A typical hemacytometer result of size distribution and concentration measurements for asphaltene-in-toluene droplet suspension in water.

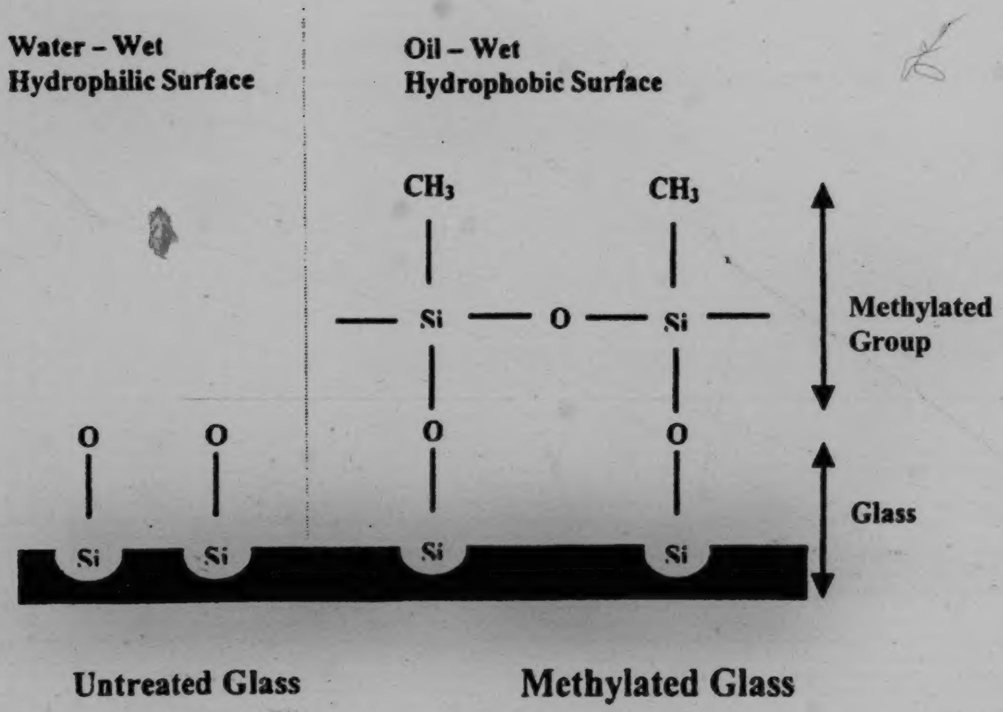
Water – Wet
Hydrophilic Surface
Oil – Wet
Hydrophobic Surface
CH3
CH3
Si
O
Si
Methylated
Group
O
O
O
O
Glass
Si
Si
Si
Si
Untreated Glass
Methylated Glass

Figure 5-3. Schematic diagram of chemical structures for untreated and methylated glass surfaces, proposed by Araujo et al. [1995].

Chapter Six

Deposition of asphaltene-in-toluene droplet suspension in water on hydrophilic collectors

6.0. Introduction

The aim of this set of experiments is to investigate the experimental conditions (i.e. values zeta potentials, electrolyte concentration and pH) required for attachment of asphaltene-in-toluene droplets on hydrophilic collectors. As well, the experiments were conducted to compare the deposition results with the theoretical model that is based on the DLVO theory.

There were four sets of experiments conducted to study the deposition of asphaltene-in-toluene droplet suspension in water on hydrophilic collectors:

1. pH = 9.5 and 0.01M [NaCl] at different Re (Set # 1).
2. pH = 8.5 and 0.01M [NaCl] at different Re (Set # 2).
3. pH = 3.5 and 0.01M [NaCl] at different Re (Set # 3).
4. pH = 8.0 and 0.001M [NaCl] at different Re (Set # 4).

6.1. Analysis of the deposition experiments with hydrophilic collectors

A new emulsion was prepared in advance of each set of experiments. In all experiments the same batch of asphaltenes was used which was produced in bulk one time as per the procedure described in Section 5.3.1 and 5.3.2 and characterized as per the procedure described in Section 5.3.3. Table 6-1 lists the experimental parameters for the deposition experiments conducted for the asphaltene-in-toluene droplet suspension in water on a hydrophilic (untreated) glass collector.

Table 6-1: Experimental conditions for asphaltene-in-toluene droplet deposition onto a hydrophilic (untreated) glass collector: $a_p = 1.5$ μm.

Set #	Bulk pH	[NaCl] (mol/L)	Droplet zeta potential, ζ_p, (mV)	Collector zeta Potential, ζ_c (mV)	Bulk droplet concentration, c_o droplets/ml
1	9.5	0.01	-75	-71	6.2×10^6
2	8.5	0.01	-55	-65	7.1×10^6
3	3.5	0.01	-20	-45	2.1×10^6
4	8.0	0.001	-60	-75	8.1×10^6

For Set # 1 and Set # 2, 20 experiments in each set were conducted for a range of Reynolds numbers from 46 to 800. No droplet attachment was observed at these experimental conditions. These experiments were repeated to ensure that no deposition occurred under these conditions and to check the reproducibility of the deposition results. When the experimental parameters of Set # 1 and Set # 2 were used in the model, it was predicted that no attachment would occur at these experimental conditions. These results can be explained by analyzing the zeta potentials of asphaltene and the collectors and the corresponding Dl values: $Dl_{set\,\#\,1} = 18\,250$ and $Dl_{set\,\#\,2} = 11\,600$. By referring back to Figure 4-5 one can observe that $Dl > Dl_{critical}$ ($Dl_{critical} = 420$). Hence, no attachment is possible according to DLVO theory.

For the experiments described as Set # 3, asphaltene droplet attachment was observed. Figure 6-1 shows the stagnation region coating density (SRCD) curves with respect to time (in seconds) for different Reynolds numbers. The SRCD curves show that the rate of particle attachment is constant initially and levels off as the experiment progresses. The leveling off in the deposition rate is called the blocking effect [Dabros et al., 1987] and is due to the repulsive interaction force between the particles already attached in the stagnation region of the impinging jet surface and new particles flowing toward the stagnation region. This phenomenon is more prominent at higher Reynolds numbers when the coating densities are much higher. The initial slopes of the SRCD lines (shown by solid lines in Figure 6-1) were used to evaluate the flux, J_o to the collector surface as per Equation (2.1).

Once J_o is calculated for a particular Reynolds number, the dimensionless mass transfer rate to the collector surface (expressed as Sherwood number, Sh) is calculated using Equation (2.2). Figure 6-2 shows the variation of Sherwood number with respect to changes in flow rate for Set # 3. Symbols represent experimentally determined Sherwood numbers for Set # 3. No deposition was predicted by the model based on the DLVO theory using experimental parameters of Set # 3 (Table 6-1). The solid line in Figure 6-2 represents model predictions using Dl = 0 i.e. when the electrostatic double layer (EDL) interactions are ignored. One can observe that there is reasonable agreement between Sherwood number predicted by the model (when EDL interactions are ignored, i.e. Dl = 0) and those experimentally determined. This indicates that the model can still be used to predict deposition as long as electrostatic double layer forces are neglected.

When experiments in Set # 4 were performed, droplet deposition was observed. Figure 6-3 shows Sherwood numbers for Set # 4 over a range of Reynolds numbers. For these experimental conditions, however, no attachment was predicted by the model.

Again, when Dl is set to zero, reasonable agreement between experimental data and theory is present.

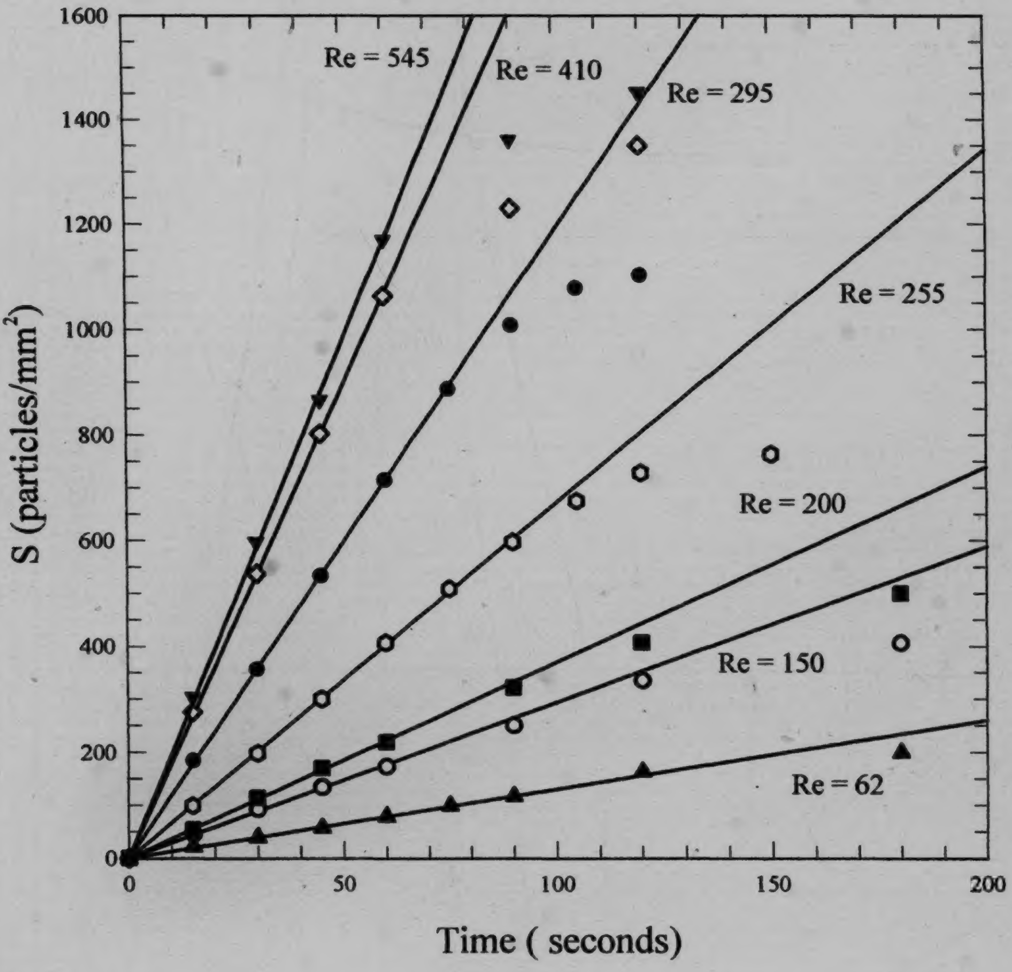

Figure 6-1. Stagnation Region Coating Density (SRCD) as a function of time for asphaltene-in-toluene droplet deposition experiments onto hydrophilic (untreated) glass surfaces (Set # 3 in Table 6-1): pH = 3.5, [NaCl] = 0.01M, ζ_p = - 20 mV, ζ_c = - 45 mV, Ad = 0.412.

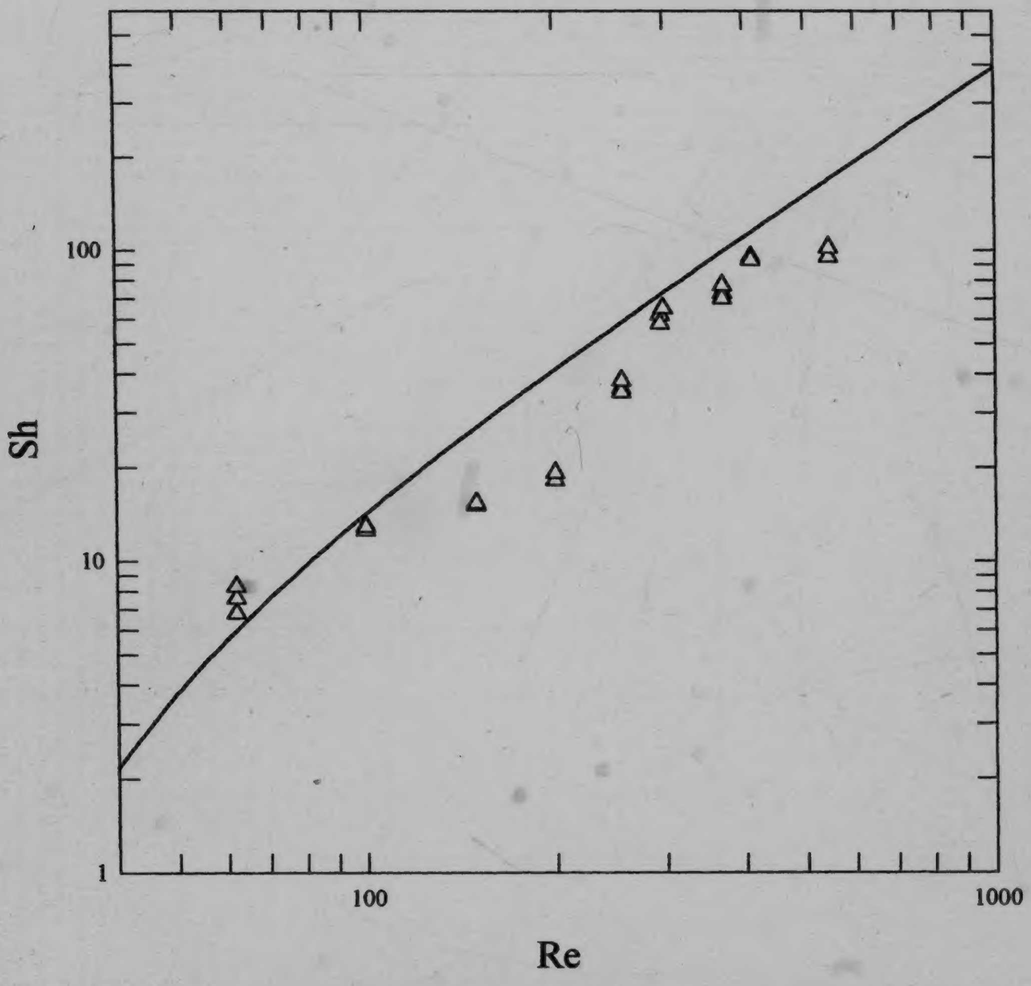

Figure 6-2. Dimensionless mass transfer rate (expressed as Sherwood number) as a function of Reynolds number for asphaltene-in-toluene droplet deposition onto hydrophilic (untreated) glass surfaces (Set # 3 in Table 6-1): pH = 3.5, $a_p = 1.5$ μm, Ad = 0.412, $\zeta_p = -20$ mV, $\zeta_c = -45$ mV, [NaCl] = 0.01M and $\overline{\alpha} = 5.3\,\mathrm{Re}^{0.5} - 8.13\ (\mathrm{Re} \geq 5)$. Symbols represent experimental results and solid line indicates model predictions using Dl = 0.

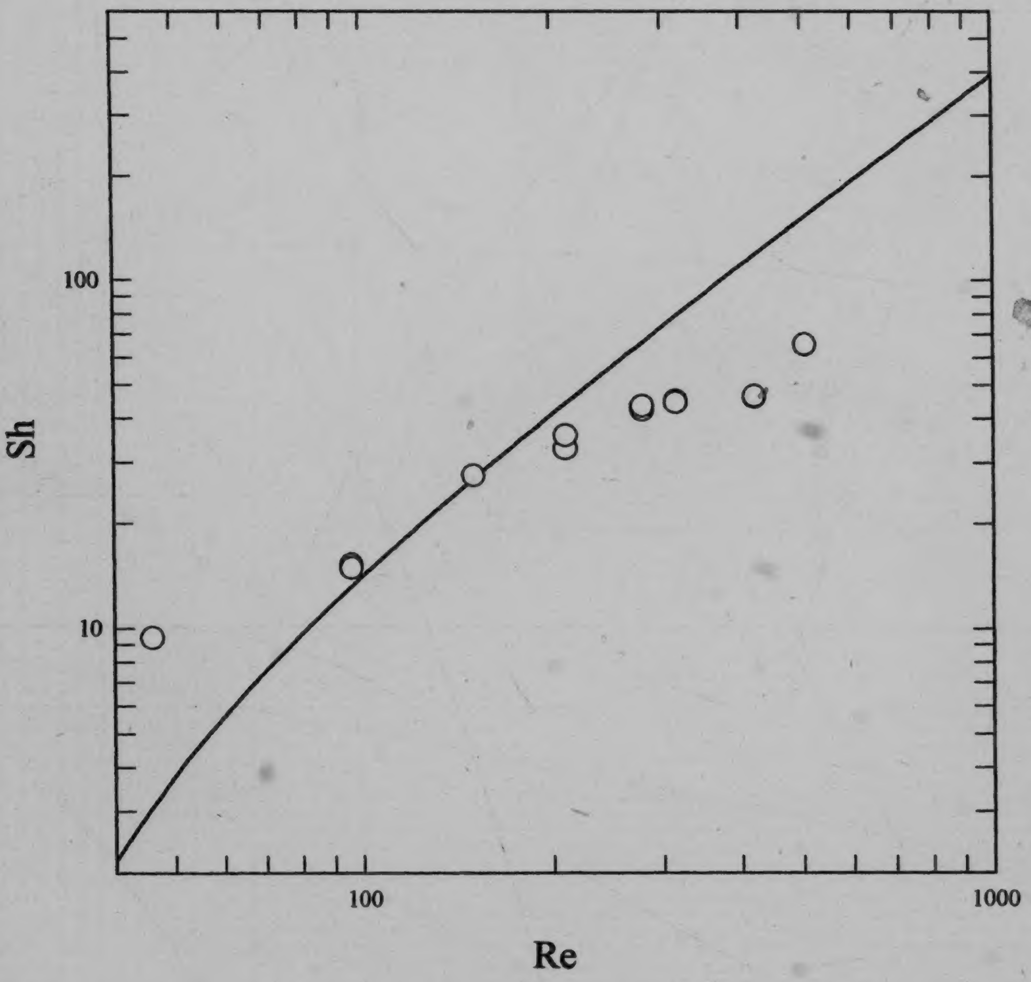

Figure 6-3. Dimensionless mass transfer rate (expressed as Sherwood number) as a function of Reynolds number for asphaltene-in-toluene droplet deposition onto hydrophilic (untreated) glass surfaces (Set # 4 in Table 6-1): pH = 8.0, [NaCl] = 0.001M, ζ_p = - 60 mV, ζ_c = - 75 mV, Ad = 0.412. Symbols represent experimental results and solid line indicates model predictions using Dl = 0.

Chapter Seven

Deposition of asphaltene-in-toluene droplet suspension in water on hydrophobic collectors

7.0. Introduction

In this set of experiments, the collector surface is altered from being hydrophilic to hydrophobic using a chemical treatment [Araujo et al., 1995; Sanders, 1997; Yang, 2000]. The procedure for the surface modification was described in Sections 5.4.1 and 5.4.2. The purpose of these experiments is to obtain deposition results for asphaltene-in-toluene droplets using a hydrophobic collector.

The interaction between two hydrophobic surfaces placed in water is usually strongly attractive [Israelachvili, 1992] and is often stronger than their attraction in free space. This strong attractive interaction force in water cannot be accounted for by continuum theories of van der Waals forces, which actually predict reduced interaction between such surfaces in water. Israelachvili and Pashley [1982] measured the hydrophobic force between two macroscopic curved hydrophobic surfaces in water. They found that in the range 0 – 10 nm the force decayed exponentially with a decay length of about 1 nm.

Hydrophilic (hydration) and hydrophobic interactions are dependent upon each other, since both ultimately rely on the structure of the water H-bonds adopted around surfaces. When both hydrophilic and hydrophobic groups are present on a surface the net interaction between two such surfaces is not the sum of the separate components [Israelachvili, 1992].

There is no satisfactory theory available for the origin of hydrophobic interactions. There are many different opinions expressed in the literature, some of which are given below:

1. Hydrophobic interaction mainly is an entropic phenomenon, arising from the rearrangement and reorientation of the H-bond configurations of water molecules in the overlapping solvation zones as two hydrophobic species come together [Israelachvili, 1984; Claesson, 1986] and has a range much longer than that of any typical bond [Joesten and Schaad, 1974; Israelachvili, 1992].
2. It arises due to a phase change at the interfacial layer between two hydrophobic bodies [Christenson, 1988; Claesson et al., 1988].
3. They are due to polarization of water molecules near a hydrophobic surface [Rabinovich et al., 1988].

An excellent review on this subject is given by Israelachvili [1992].

The DLVO theory does not take into consideration the additional attractive force between hydrophobic bodies in the water. The deposition experiments conducted with hydrophobic surfaces are same as those described in Chapter 6, only the collector surface has been altered by a chemical treatment from hydrophilic to hydrophobic. There were four sets of experiments conducted to study the deposition of asphaltene-in-toluene droplet suspension in water on hydrophobic collectors:

1. pH = 9.5 and 0.01M [NaCl] at different Re (Set # 1).
2. pH = 8.5 and 0.01M [NaCl] at different Re (Set # 2).
3. pH = 3.5 and 0.01M [NaCl] at different Re (Set # 3).
4. pH = 8.0 and 0.01M [NaCl] at different Re (Set # 4).

7.1. Collector surface preparation and characterization

Hydrophobic glass slide surfaces were prepared from the same microscopic glass slides (50×75×1 mm, Fisher Scientific) as used in the previous experiment by methylation or silanation treatment process [Araujo et al., 1995; Sanders, 1997; Yang, 2000] as described in Sections 5.4.1 and 5.4.2. Contact angle measurements were done by a goniometer (Rame-Hart Inc.) through the water phase and found to be 105° to 108° indicating that the surface is hydrophobic. The zeta potential measurements of the methylated glass slides were taken directly from the literature [Sanders, 1997; Somasundaran et al., 1998; Yang, 2000].

7.2. Analysis of the deposition experiments

Once the hydrophobic glass slides were prepared, the asphaltene-in-toluene droplet suspension in water was prepared from the batch source of asphaltenes used in previous experiments following the procedures described in Sections 5.3.1 and 5.3.2. When the experimental emulsion was ready, size distribution and concentration studies were performed using the Bright line hemacytometer as per the procedure described in Section5.3.3 and recorded for analysis. The zeta potential measurements of asphaltene-in-toluene droplets were performed with a Zetaphoremeter-3 (SEPHY-CAD, France). The zeta potential of methylated glass was taken directly from the literature [Sanders, 1997; Somasundaran et al., 1998; Yang, 2000]. The experimental conditions can be characterized as shown in Table 7-1.

Table 7-1: Experimental conditions for asphaltene-in-toluene droplet deposition onto a methylated (hydrophobic) glass collector: $a_p = 1.5$ μm.

Set #	Bulk pH	[NaCl] (mol/L)	Droplet zeta potential, ζ_p (mV)	Collector zeta Potential, ζ_c (mV)	Bulk droplet concentration, c_o (droplets/ml)
1	9.5	0.01	-75	-45	6.2×10^6
2	8.5	0.01	-55	-30	7.1×10^6
3	3.5	0.01	-20	-10	2.1×10^6
4	8.0	0.001	-60	-40	8.1×10^6

For Set # 1, experiments were conducted for a range of Reynolds numbers from 46 to 600. No droplet attachment was observed at these experimental conditions. These experiments were repeated to ensure that no attachment occurred under these conditions. When experimental parameters of Set # 1 were used in the theoretical model, no attachment was predicted by the model.

A new set of hydrophobic glass slides was prepared for the experiments of Set # 2. When the deposition experiments were conducted under these conditions, deposition was observed. Figure 7-1 shows SRCD curves for experiments of Set # 2. The initial slopes of the SRCD lines (shown by solid lines in Figure 7-1) were used to evaluate the flux, J_o to the collector surface as per Equation (2.1). Once J_o is known, the dimensionless mass transfer rate to the collector surface (expressed as Sherwood number, Sh) was calculated using Equation (2.2). Figure 7-2 shows the variation of Sherwood number with respect to changes in the flow rate in the system for Set # 2 (Table 7-1). No deposition was predicted by the model for the experimental conditions of Set # 2 (Table 7-1). The solid line of Figure 7-2 represents theoretically predicted Sherwood numbers using Dl = 0. Symbols represent experimentally determined Sherwood numbers for Set # 2 (Table 7-1).

When experiments were conducted for Set # 3 (pH = 3.5 and 0.01M [NaCl]), deposition of asphaltene–in-toluene droplets was observed. Figure 7-3 shows SRCD curves for this set of deposition experiments. Again, the flux, J_o, is calculated from the initial slope of the SRCD curves. The dimensionless mass transfer rates were calculated from the values of J_o, using Equation (2.2).

Figure 7-4 shows the variation of Sherwood number with Reynolds number. Symbols represent experimentally determined Sherwood numbers for Set # 3. No deposition is predicted by the model based on the DLVO theory for the experimental conditions of Set # 3 (Table 7-1). Again, when electrostatic double layer (EDL) interactions are ignored (i.e. Dl is set to zero in the model) the predicted mass transfer rates (represented by the solid line in Figure 7-4) are in good agreement with those experimentally determined. This suggests that the model could still be used to predict the mass transfer rates of asphaltene-in-toluene droplets at the experimental conditions described in Set # 3 of Table 7-1, provided that electrostatic forces are neglected.

When Set # 4 (Table 7-1) experiments (pH = 8.0 and 0.001M [NaCl]) were conducted, deposition was observed. Figure 7-5 shows variation of experimentally determined Sherwood number (represented by the symbols) with respect to changes in Reynolds number. When the experimental parameters of Set # 4 in the Table 7-1 were used in the theoretical model, no deposition was predicted. Again when EDL interactions were ignored by setting Dl = 0 in the model, the mass transfer rates predicted by the model (represented by the solid line in Figure 7-5) are in reasonable agreement with those determined experimentally (represented by the symbols in Figure 7-5). Sanders [1997] also noted a similar observation for the deposition of bitumen-in-water emulsions at 0.005 M NaCl in impinging jet experiments.

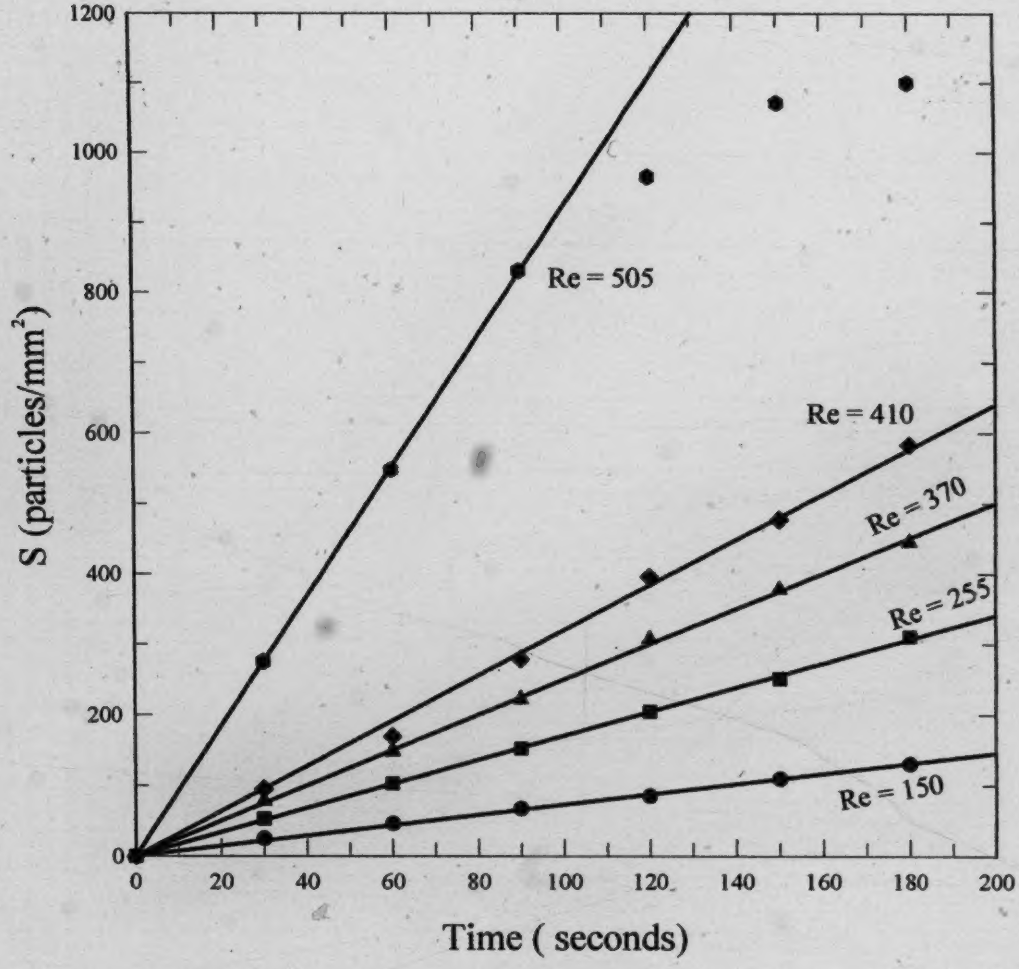

Figure 7-1. Stagnation Region Coating Density (SRCD) as a function of time for asphaltene-in-toluene droplet deposition experiments onto hydrophobic (methylated) glass surfaces (Set # 2 in Table 7-1): a_p = 1.5 μ m, pH = 8.5, [NaCl] = 0.01M, ζ_p = - 55 mV, ζ_c = - 30 mV, Ad = 0.412.

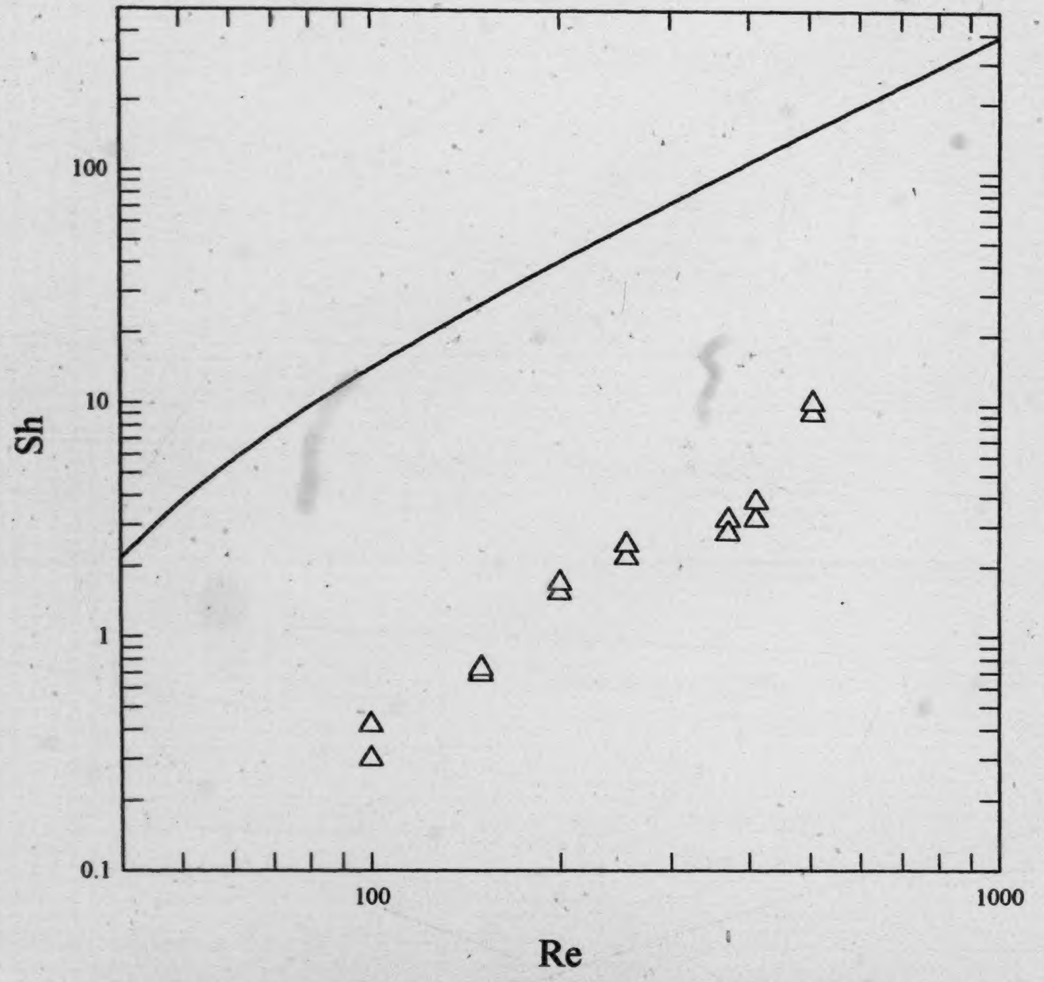

Figure 7-2. Dimensionless mass transfer rate (expressed as Sherwood number) as a function of Reynolds number for asphaltene-in-toluene droplet deposition onto hydrophobic (methylated) glass surfaces (Set # 2 in Table 7-1): pH = 8.5, [NaCl] = 0.01M, a_p = 1.5 μm, Ad = 0.412, ζ_p = - 55 mV, ζ_c = - 30 mV, and $\overline{\alpha} = 5.3\mathrm{Re}^{0.5} - 8.13\ (\mathrm{Re} \geq 5)$. Symbols represent experimental results and solid line indicates model predictions using Dl = 0.

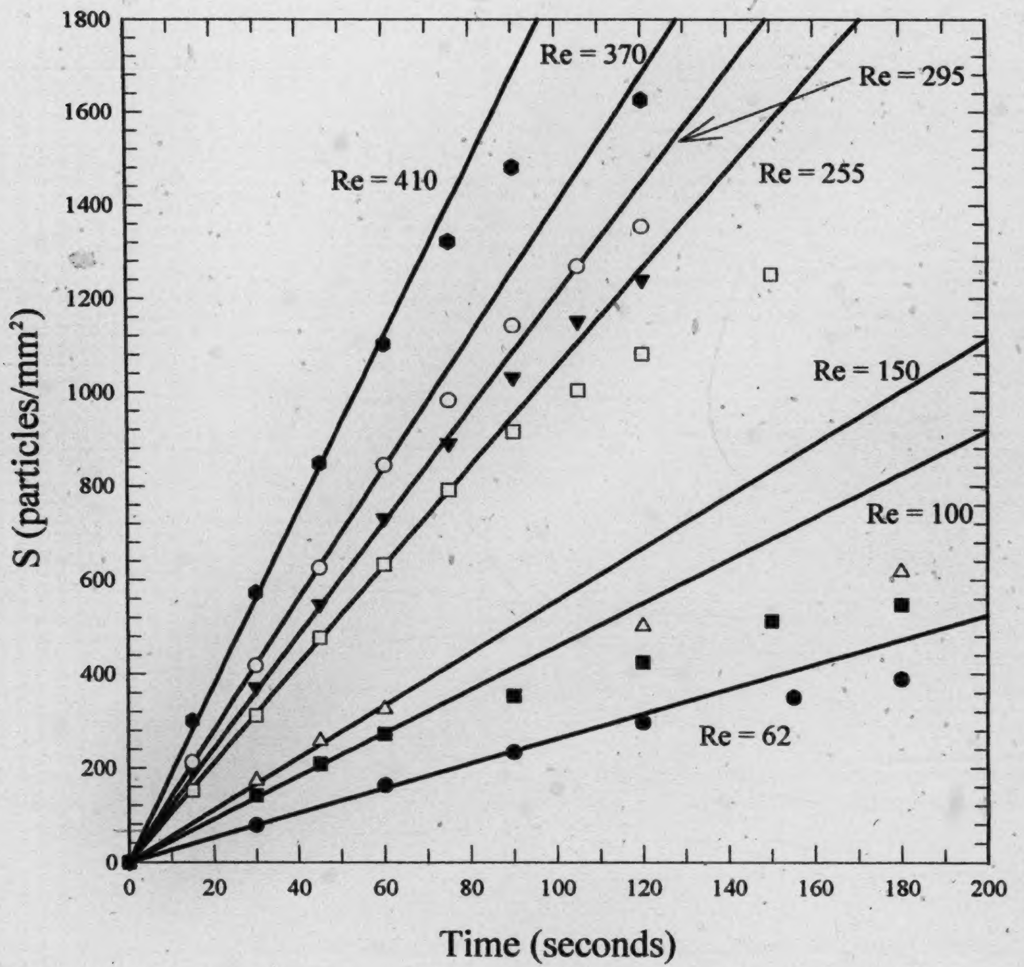

Figure 7-3. Stagnation Region Coating Density (SRCD) as a function of time for asphaltene-in-toluene droplet deposition experiments onto hydrophobic (methylated) glass surfaces (Set # 3 in Table 7-1): pH = 3.5, [NaCl] = 0.01M, ζ_p = - 20 mV, ζ_c = - 10 mV, Ad = 0.412.

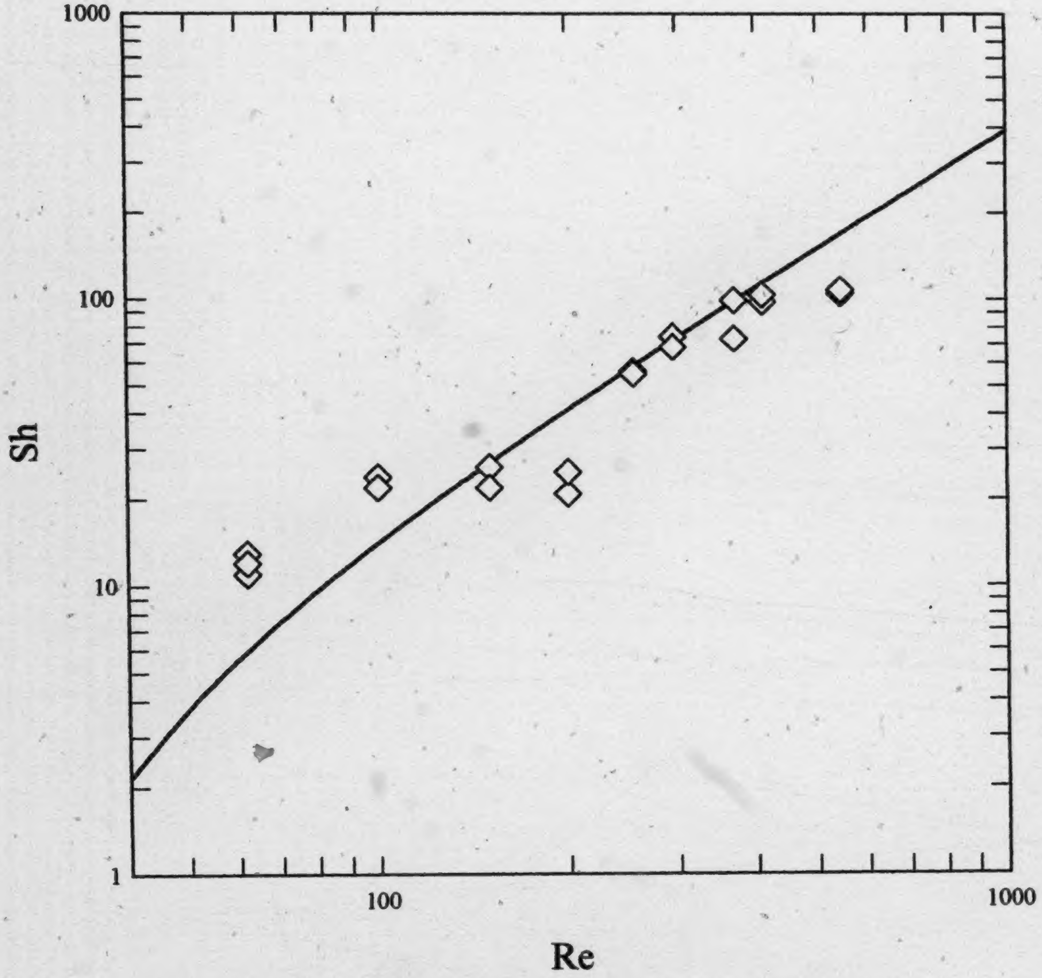

Figure 7-4. Dimensionless mass transfer rate (expressed as Sherwood number) as a function of Reynolds number for asphaltene-in-toluene droplet deposition onto hydrophobic (methylated) glass surfaces (Set # 3 in Table 7-1): pH = 3.5, [NaCl] = 0.01M, a_p = 1.5 μm, Ad = 0.412, ζ_p = - 20 mV, ζ_c = - 10 mV, [NaCl] = 0.01M and $\overline{\alpha} = 5.3\mathrm{Re}^{0.5} - 8.13\ (\mathrm{Re} \geq 5)$. Symbols represent experimental results and solid line indicates model predictions using Dl = 0.

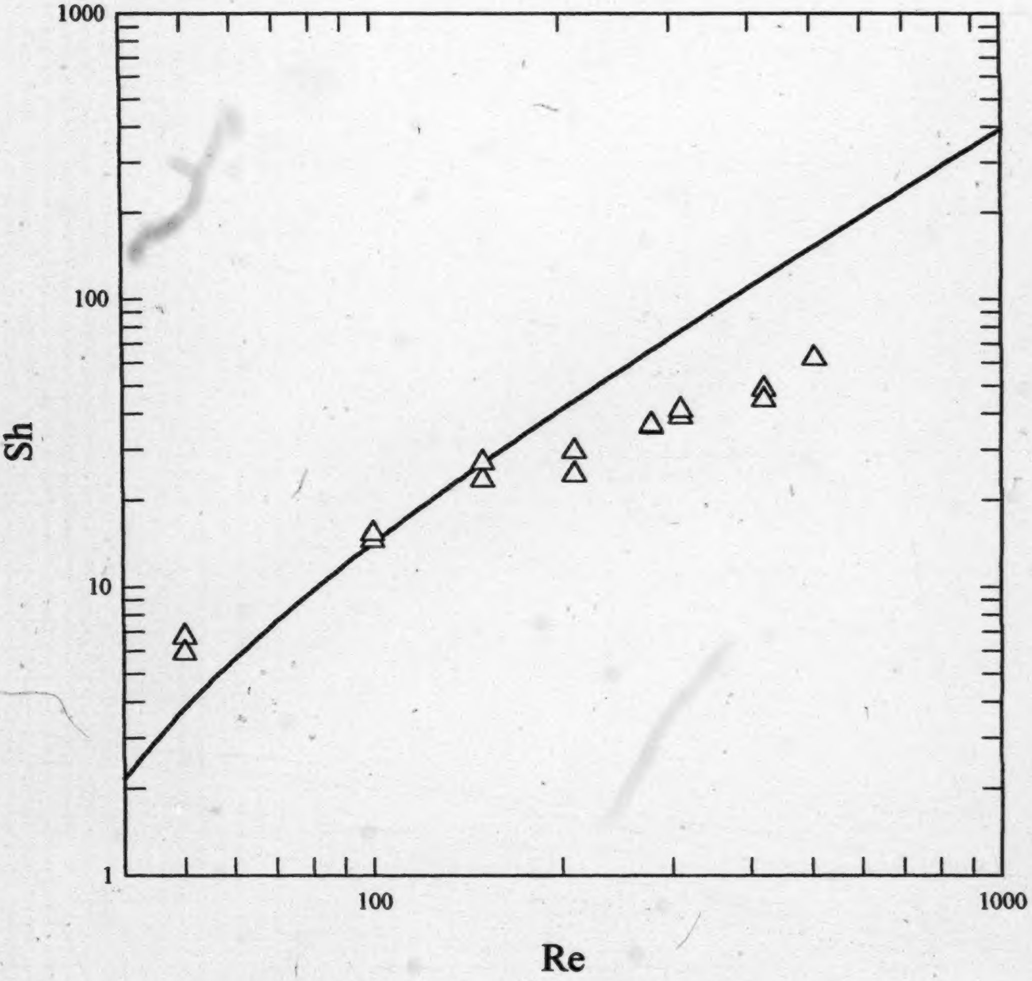

Figure 7-5. Dimensionless mass transfer rate (expressed as Sherwood number) as a function of Reynolds number for asphaltene-in-toluene droplet deposition onto hydrophobic (methylated) glass surfaces (Set # 4 in Table 7-1): pH = 8.0, [NaCl] = 0.001M [NaCl], ζ_p = - 60 mV, ζ_c = - 40 mV, Ad = 0.412. Symbols represent experimental results and solid line indicates model predictions using Dl = 0.

Chapter Eight

Deposition of asphaltene-in-toluene droplet suspension in water on coated collectors

8.0. Introduction

The aim of the present study is to quantify the interactions of an asphaltene-in-toluene droplet suspension in water with bitumen and asphaltenes. This study can assist in understanding asphaltene-asphaltene agglomeration in the Albian Sands' froth treatment process. Many questions arise, e.g., how will precipitated asphaltenes interact with other asphaltenes and with bitumen? In order to provide some experimental results for this problem, collector surfaces were coated with asphaltene or with bitumen to evaluate asphaltene-asphaltene and asphaltene- bitumen interactions.

There were four sets of experiments conducted in this category.

1. Deposition of asphaltene-in-toluene droplets suspended in water onto an asphaltene coated glass slide at pH = 9.5 and 0.01M [NaCl] at different Re (Set # 1).
2. Deposition of asphaltene-in-toluene droplets suspended in water onto an asphaltene coated glass slide at pH = 3.5 and 0.01M [NaCl] at different Re (Set # 2).
3. Deposition of asphaltene-in-toluene droplets suspended in water onto a bitumen coated glass slide at pH = 9.5 and 0.01M [NaCl] at different Re (Set # 3).
4. Deposition of asphaltene-in-toluene droplets suspended in water onto a bitumen coated glass slide at pH =3.5 and 0.01M [NaCl] at different Re (Set # 4).

8.1. Preparations

Bitumen and asphaltene coated collectors were prepared using methylated glass slides. The methylated glass slides were coated with bitumen or asphaltenes as per the procedure described in Sections 5.4.3 and 5.4.4. All the slides were used once only and discarded after each set of experiments.

Once the asphaltene and the bitumen coated collectors were ready for use, an asphaltene-in-toluene droplet suspension in water was prepared according to the procedures described in Sections 5.3.1 and 5.3.2. Concentration and droplet size distribution studies were performed before and after each set of experiments as per the procedure described in Section 5.3.3. The zeta potential measurements for the asphaltene-in-toluene droplet suspension in water were performed by Zetaphoremeter-3 (SEPHY-CAD, France). The zeta potential of each asphaltene-coated collector is assumed to be identical to asphaltene-in-toluene droplet suspension in water measured for the deposition experiments. The zeta potential of each bitumen-coated collector is taken from the measurement of zeta potential performed for the bitumen-in-water emulsion at the experiential pH and electrolyte concentration.

8.2. Analysis of the experiments with asphaltene coated collector

Experiments were performed with asphaltene coated collectors at pH = 9.5 and pH = 3.5, both at 0.01M [NaCl]. The properties of asphaltene-in-toluene suspension in water and the collectors are tabulated in Table 8-1.

Table 8-1: Experimental conditions for asphaltene coated collectors deposition experiments; average droplet size $= 1.5\mu m$.

Set #	Bulk pH	[NaCl] (mol/L)	Droplet zeta potential, ζ_p (mV)	Collector zeta Potential, ζ_c (mV)	Bulk droplet concentration, c_o droplets/ml
1	9.5	0.01	-75	-75	6.1×10^6
2	3.5	0.01	-20	-20	3.1×10^6

For Set # 1, experiments were conducted for a range of Reynolds numbers from 46 to 600. No droplet deposition was observed at these experimental conditions. The experiments were repeated to ensure that no attachment occurred under these conditions. When model simulations were conducted using the experimental parameters of Set # 1 from Table 8-1, the model predicted that no attachment would occur.

In the experiments of Set # 2, asphaltene-in-toluene droplet deposition was observed. Figure 8-1 shows stagnation region coating density (SRCD) curves at different flow rates. The initial slopes of SRCD curves (represented by solid lines of Figure 8-1) were used to calculate the flux, J_o to the collector. Once J_o is calculated, the dimensionless mass transfer rates (Sherwood numbers) were calculated using Equation (2.2). No deposition was predicted by the model for the experimental conditions described in Set # 2 (Table 8-1). The solid line in Figure 8-2 represents the mass transfer rates predicted by the model for $Dl = 0$ (i.e. EDL interactions are ignored) and the symbols in Figure 8-2 represent the mass transfer rates determined experimentally. One can observe that there is good agreement between the predicted Sherwood numbers (for $Dl = 0$) and those determined experimentally for Set # 2. This indicates that the model could still be used to predict the deposition of asphaltene-in-toluene droplets on an asphaltene coated glass slide at the test conditions described for Set # 2 (Table 8-1), provided that electrostatic interactions are neglected.

8.3. Analysis of the experiments with the bitumen coated collectors

Bitumen coated collectors were prepared from methylated glass slides as per the procedures in Section 5.4.3. The experimental electrolyte solution containing suspended asphaltene-in-toluene droplets was prepared as per the procedures described in Section 5.3.1 and 5.3.2. The characterization of the emulsion was done as per the procedure of Section 5.3.3. The zeta potentials of asphaltene-in toluene droplets suspended in water were measured using the Zetaphoremeter-3 (SEPHY-CAD, France) prior to conducting deposition experiments. The zeta potentials of the bitumen coated collectors were taken from the measurements of bitumen-in-water emulsion conducted at experimental pH and electrolyte concentration [Sanders, 1997]. The experimental conditions are tabulated in Table 8-2.

Table 8-2: Experimental conditions for bitumen coated collectors deposition experiments; average droplet size of asphaltene = 1.5μm.

Set #	Bulk pH	[NaCl] (mol/L)	Droplet zeta potential,ζ_p (mV)	Collector zeta Potential,ζ_c (mV)	Bulk droplet concentration, c_o droplets/ml
3	9.5	0.01	-75	-80	6.1×10^6
4	3.5	0.01	-20	-25	3.1×10^6

No deposition of asphaltene-in-toluene droplets was observed on the bitumen coated collectors in the experiments conducted for the conditions of Set # 3 in Table 8-2 for a range of Reynolds numbers from 46 to 600. Deposition experiments were repeated to ensure that no attachment occurred under these conditions. When the model simulation was conducted for the experimental parameters of Set # 3 from Table 8-2, the model predicted that no attachment would occur.

Deposition of asphaltene-in-toluene droplets was observed in the deposition experiments denoted as Set # 4. Figure 8-3 shows the SRCD curves for the deposition of asphaltene-in-toluene droplet suspension in water on bitumen-coated collectors for a range of flow rates. Experimental Sherwood numbers were calculated from the slopes of the SRCD curves in Figure 8-3 and Equation (2.2). No deposition was predicted by the model based on the DLVO theory for the experimental conditions described in Set # 4 of Table 8-2. Again when EDL interactions were ignored in the model by setting Dl = 0 for the test conditions of Set # 4 (Table 8-2), the predicted mass transfer rates (represented by the solid line in the Figure 8-4) were found to be in reasonable agreement with those experimentally determined (represented by the symbols in Figure 8-4). This indicates that although the deposition of asphaltene-in-toluene droplets on the bitumen collector does not follow the DLVO theory, the model can still be used to predict the mass transfer rates at the experimental conditions described in Set # 4 of Table 8-2 as long as the contribution of the electrostatic double layer interactions is ignored.

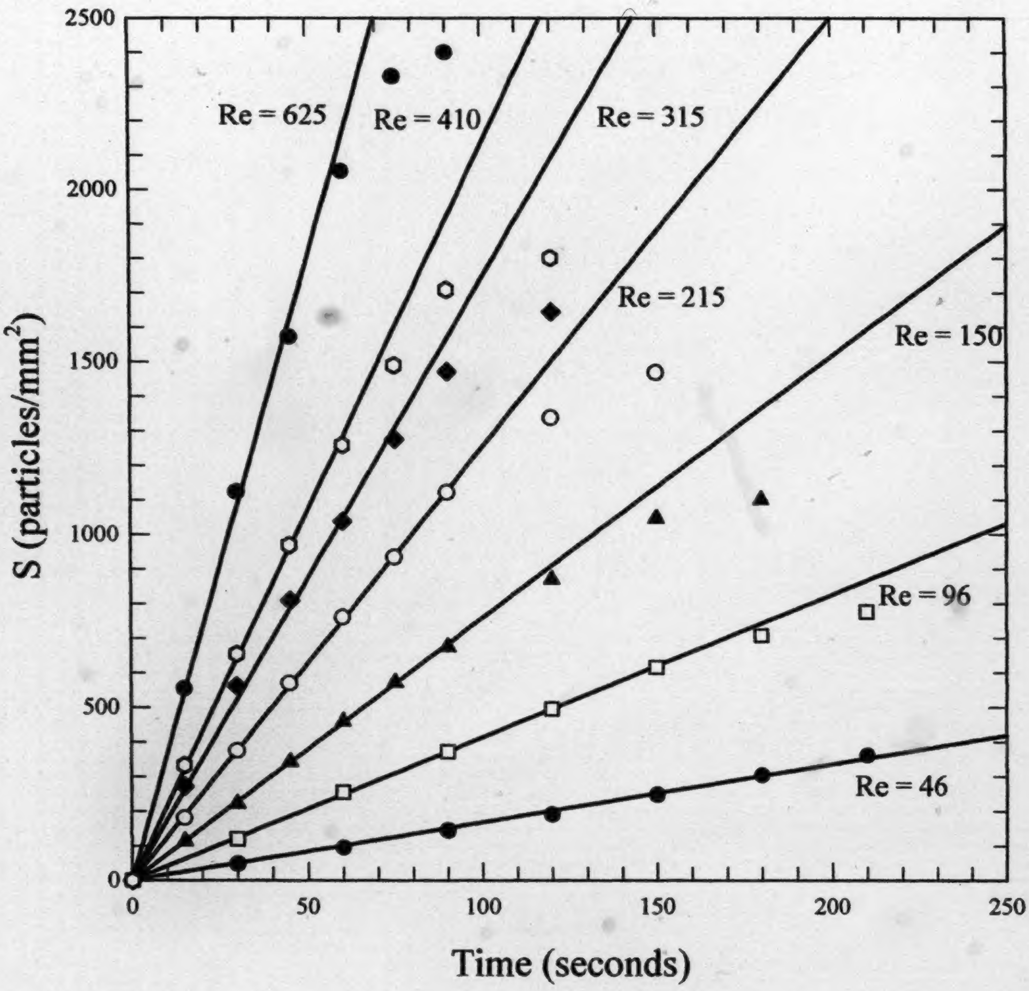

Figure 8-1. Stagnation Region Coating Density (SRCD) as a function of time for asphaltene-in-toluene droplet deposition experiments onto asphaltene coated collector surfaces (Set # 2 in Table 8-1): pH = 3.5, [NaCl] = 0.01M, ζ_p = - 20 mV, ζ_c = - 20 mV, Ad = 0.132.

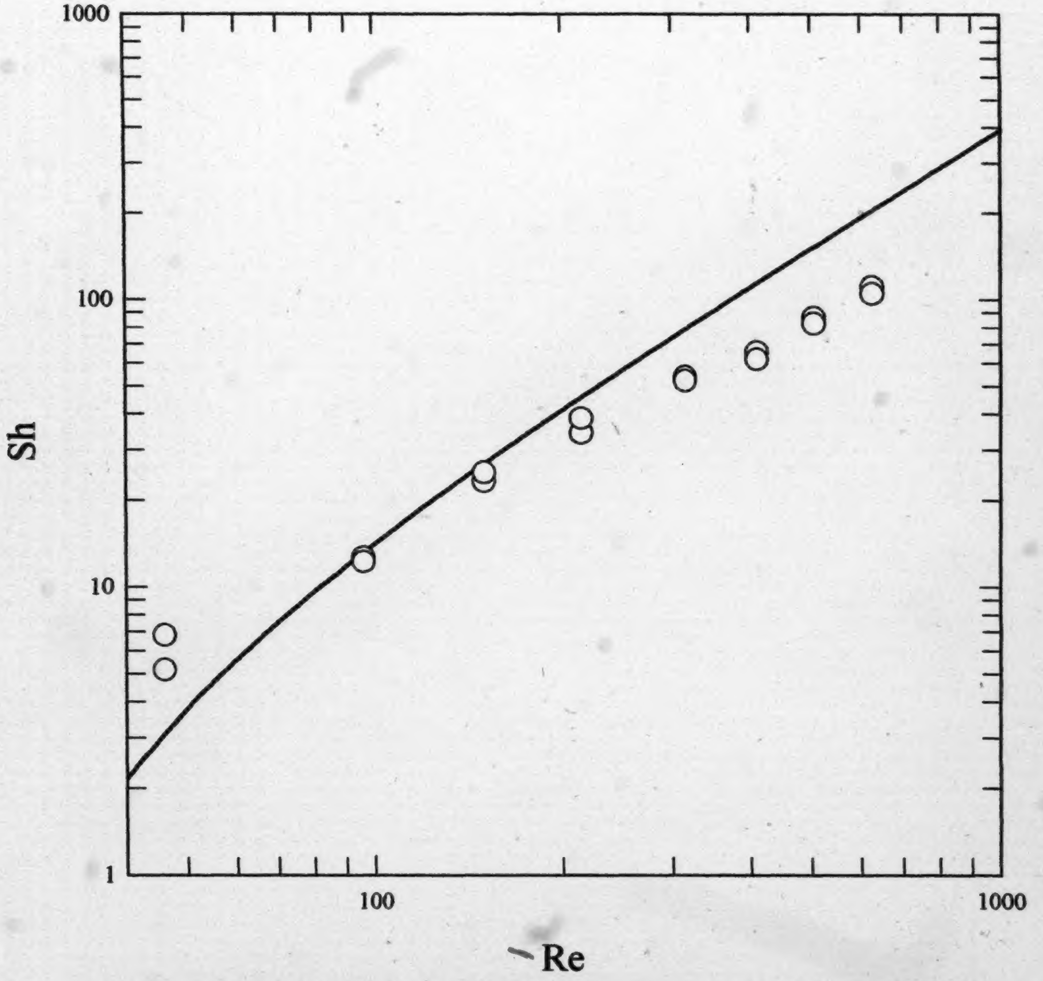

Figure 8-2. Dimensionless mass transfer rate (expressed as Sherwood number) as a function of Reynolds number for asphaltene-in-toluene droplet deposition onto asphaltene coated glass collectors (Set # 2 in Table 8-1): pH = 3.5, [NaCl] = 0.01M, a_p = 1.5 μm, Ad = 0.132, ζ_p = -20 mV, ζ_c = - 10 mV and $\overline{\alpha} = 5.3\mathrm{Re}^{0.5} - 8.13\ (\mathrm{Re} \geq 5)$. Symbols represent experimental results and solid line indicates model predictions using Dl = 0.

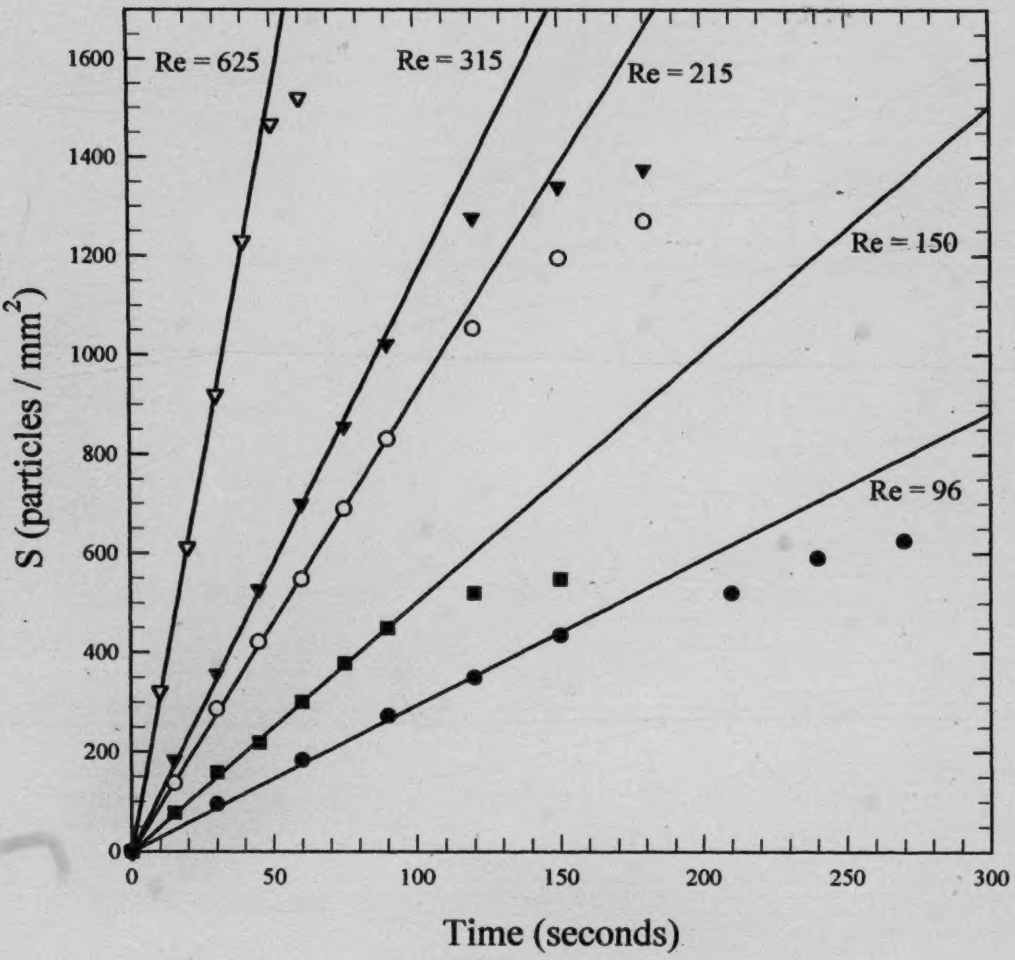

Figure 8-3. Stagnation Region Coating Density (SRCD) as a function of time for asphaltene-in-toluene droplet deposition experiments onto bitumen coated collectors (Set # 4 in Table 8-2): pH = 3.5, [NaCl] = 0.01M, ζ_p = - 20 mV, ζ_c = - 25 mV, Ad = 0.132.

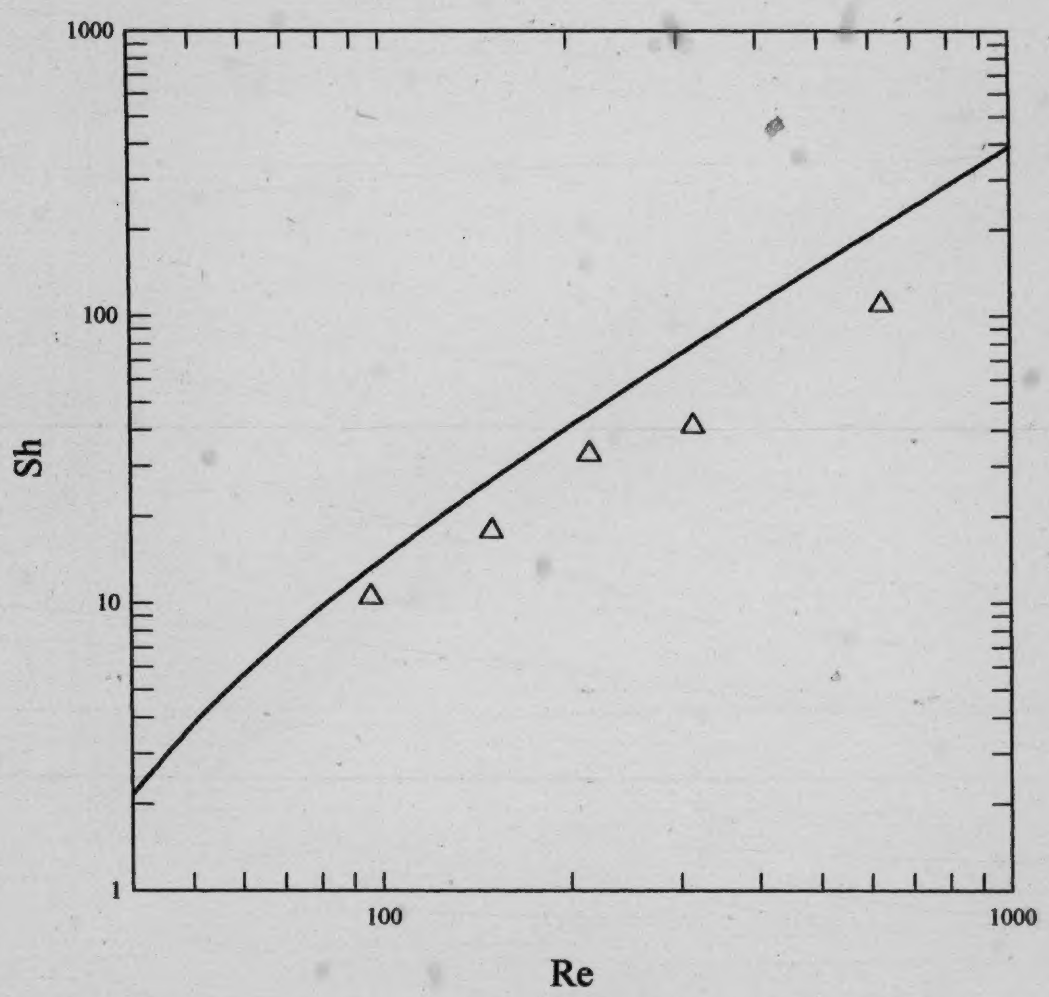

Figure 8-4. Dimensionless mass transfer rate (expressed as Sherwood number) as a function of Reynolds number of asphaltene-in-toluene droplet deposition onto bitumen coated glass collectors (Set # 4 in Table 8-2): pH = 3.5, a_p = 1.5 μm, Ad = 0.132, ζ_p = - 20 mV, $\overline{\alpha} = 5.3\mathrm{Re}^{0.5} - 8.13\,(\mathrm{Re} \geq 5)$ ζ_c = - 25 mV, and [NaCl] = 0.01M. Symbols represent experimental results and solid line indicates model predictions using Dl = 0.

Chapter Nine

Summary, Conclusions and Recommendations

This chapter contains recommendations for future work as well as a summary of the thesis results and conclusions. It also presents an overview of the contributions made by this study. A brief discussion of non-DLVO behavior has been included to explain the discrepancy found in the deposition experiments of asphaltene-in-toluene droplets on hydrophilic, hydrophobic and coated glass surfaces.

9.0. Discrepancy between experimental results and theoretical predictions (non – DLVO behavior)

It has been shown that the theoretical predictions of the model agree reasonably well with the experimental results for the range of Reynolds number (40 to 700) only when Dl is set zero, i.e. no electrostatic force is present.

In the literature, many researchers [Czarnecki, 1986; Tobiason, 1989; Elimelech and O'Melia, 1990; Sanders, 1997; Yang, 2000] have reported significant deposition when deposition conditions were unfavorable as per classical DLVO theory. At unfavorable conditions, significant deposition is observed while models based on DLVO theory predict none. The models predict an abrupt decrease in deposition to zero at a critical repulsive force while experimental results illustrate a gradual decrease in the deposition [Tobiason, 1989; Elimelech and O'Melia, 1990; Sanders, 1997; Yang, 2000]. The source of this discrepancy is not clear. The hypotheses that have been proposed to explain the failures of the models are all related to the assumptions of ideality associated with the DLVO theory: ideal, homogeneous particles and collectors and equilibrium surface interactions. The hypotheses include the effect of surface roughness, heterogeneity of the surface of individual particles and collectors (non uniform distribution of the surface potential on the particle or droplets and discrete surface charge), heterogeneity among particles and collectors and dynamic aspects of EDL interactions. A quantitative analysis of these effects is complex theoretically and difficult experimentally. A brief discussion of the effect of the factors listed above on the model predictions for the system studied in this work is presented below.

A non uniform surface charge density can arise due to the finite size of ions and /or other charged complexes on the interacting surfaces. Electrophoretic mobility measurements of various colloidal particles [Rajagopalan, 1982] indicate wide distribution of mobility values. This indicates that individual particles in a suspension possess different values of surface potentials. Tobiason [1989] and Elimelech et al. [1990] used surface potentials that are normally distributed variables with mean and standard deviation based on measured or estimated values. Kuin [1990] used two-dimensional Fourier series to describe the surface potential distribution on the interacting surfaces. Following these approaches, analyses for particle deposition flux indicate that the interaction energy barrier is significantly reduced leading to improved model predictions. If heterogeneity of surface charge exists on the studied system, the above listed approaches could be incorporated in the model to improve predictions.

Another type of heterogeneity is the surface roughness of a particle and /or collector. The effect of roughness on deposition is well recognized in literature [Czarnecki, 1986; Tobiason, 1989; Bhattacharjee et al., 1998 and Walz, 1998] and depends on the size of the surface irregularities compared to representative scaling factors such as particle size or diffuse layer thickness. Czarnecki [1986] modeled rough particles that have solid smooth cores on which a number of small spheres of randomly varying sizes are present. Bhattacharjee et al. [1998] modeled surface roughness as hemispherical or conical shape protrusion and depression (called asperities) on the surface. These asperities are randomly distributed as sinusoidal waves on the surface. In all the above models, the analysis indicates that the interaction energy is substantially reduced even for very small asperities (compared to the particle radius). Both the repulsive DLVO interaction energy barrier and the primary energy minimum of the rough surfaces are considerably lower or even negligible in comparison to those of smooth surfaces. Hence, deposition of particle with rough surface could occur on rough collector even when DLVO theory predicts none.

The DLVO theory assumes that the interaction energy at a given distance (and energy barrier height) remains constant during particle-collector encounter (i.e., it does not depend on time). However, in a real system, the barrier height is subjected to fluctuations [Czarnecki, 1986]. These fluctuations are caused by the translation and rotation of a particle relative to the collector surface when the surfaces are rough and /or have discrete charge surface sites. If the time duration of the fluctuation in the interaction energy is comparable to or longer than the time required by the particle to cross the energy barrier, the deposition is determined by the minimum energy barrier rather than its maximum or mean values. Under such conditions, deposition may occur in the system where none is predicted by the classical DLVO theory.

Studies of interfacial electrodynamics [Dukhin et al., 1987] indicate that the dynamics of interacting double layers in the model should be considered. However, no theory exists that treats rigorously the dynamics of interacting EDL's. In a complete theory of dynamic EDL interaction, the repulsion should be a function of not only distance of separation but also of the velocity at which surfaces approach each other and of the various fluxes of ions at the interface during interaction [Elimelech and O' Melia, 1990]. These fluxes disturb the nature of the double layer and may have significant effect on the rate of deposition. However, it is difficult to link this effect to the current experiments due to a lack of sufficient data.

9.1. Summary

The impinging jet technique provided an effective means to study asphaltene interactions with hydrophilic, hydrophobic, asphaltene-coated and bitumen-coated surfaces. The results indicate that asphaltene-in-toluene droplet deposition does not follow DLVO theory in the cases considered. However, the theoretical model based on DLVO theory can predict the deposition reasonably when the electrical repulsive force is neglected.

9.2. Conclusions

1. The impinging jet technique is a useful method to conduct deposition experiments for asphaltene-in-toluene droplet suspensions in water.
2. The classical DLVO theory cannot predict, to a large extent, the deposition of asphaltene-in-toluene droplets suspended in water on collectors having different surface properties. However, reasonable prediction is obtained when Dl = 0 (i.e. when EDL interactions are ignored).

9.3. Recommendations for future work

1. The interacting surfaces need to be more completely characterized. In this study, only zeta potentials are used to characterize the collector surface. The role of surface heterogeneities should also be considered.
2. Further studies should be conducted with different electrolytes, progressively moving toward the use of actual process water.
3. The role of surfactants should also be investigated because they can alter van der Waals and EDL interactions.
4. The role of fines [Illite, Kaolinite and Montmorillite] should also be investigated using deposition experiments, as they are present in plant process water.
5. The surface roughness of the collector should be included in the transport equation and experiments should be conducted with a different degree of surface roughness to compare their conformity with the modified model.
6. A software package should be employed to automate the particle counting process. This will make the analysis of experiments more efficient.
7. More accurate and efficient methods of determining particle concentration and size distribution should be utilized.

9.4. Contributions of this study

1. The impinging jet technique is successfully used to study the deposition of asphaltene-in-toluene droplets suspended in the water.
2. As asphaltene is a solid, anistropic material, its inclusion in toluene to provide uniform and reproducible characteristics was a major achievement of this study.
3. The results of this study give some insight into asphaltene-asphaltene agglomeration such as that which will occur in the Albian Sands' froth treatment process.

References

Adamczyk, Z., Siwek, B., Warszynski, P. and Musial, E., *J. Colloid and Interface Sci.* **242**, 14 (2001).

Adamczyk, Z., Szyk, L. and Warszynski, P., *J. Colloid and Interface Sci.* **209**, 350 (1999).

Adamczyk, Z., Siwek, B., Zembala, M. and Belouschek, P., *Adv. Colloid Interface Sci.* **48**, 151 (1994).

Adamczyk, Z., Siwek, B., Zembala, M. and Warszynski, P., *J. Colloid and Interface Sci.* **140**, 123 (1990).

Adamczyk, Z., Siwek, B., Zembala, M. and Warszynski, P., *J. Colloid and Interface Sci.* **130**, 578 (1989).

Adamczyk, Z., Zembala, M., Siwek, B. and Czarnecki, J., *J. Colloid and Interface Sci.* **110**, 188 (1986).

Adamczyk, Z., Czarnecki, J. and Warszynski, P., *J. Colloid and Interface Sci.* **106**, 299 (1985).

Adamczyk, Z., Dabros, T., Czarnecki, J. and van de Ven, T.G.M., *Adv. Colloid Interface Sci.* **19**, 183 (1983).

Adamczyk, Z. and van de Ven, T.G.M., *J. Colloid and Interface Sci.* **84**, 497 (1981).

Adamczyk, Z. and van de Ven, T.G.M., *J. Colloid and Interface Sci.* **80**, 340 (1981).

Alargova, R. G., Petkov, J.T., Denkov, N.D. and Ivanov, I.B., *Colloids Surf.* **134**, 331 (1998).

Araujo, Y.C., Toledo, P.G., Leon, V. and Gonzalez, H.Y., *J. Colloid and Interface Sci.* **176**, 485 (1995).

Bhattacharjee, S., Chun-Han Ko and Elimelech, M., *Langmuir.* **14**, 3365 (1998).

Bird, B., Stewart, W. and Lightfoot, E., *"Transport Phenomena"* John Wiley and Sons Toronto (1960).

Boluk, M.Y. and van de Ven, T.G.M., *Colloids Surf.* **36**,157 (1990).

Boluk, M.Y. and van de Ven, T.G.M. *PhysicoChem. Hydrodyn.* **11,** 113 (1989).

Bowen, B.D., Levine, S. and Epstein, N., *J. Colloid and Interface Sci.* **54**, 375 (1976).

Bowen, B.D. and Epstein, N., *J. Colloid and Interface Sci.* **72**, 81 (1979).

Brenner, H., *Chem. Eng. Sci.* **16**, 242 (1961).

Chirstenson, H.K., *J. Dispersion Sci. Technol.* **9**, 1 (1988).

Chow, R.S. and Takamura, K., *J. Colloid and Interface Sci.***125**, 226 (1988).

Claesson, P.M. and Christenson, H.K., *J. Phys. Chem.* **92**,1650 (1988).

Claesson, P.M., *Prog. Colloid Polymer Sci.* **74**, 48 (1987).

Claesson, P.M., Blom, C.E., Herder, P.C. and Ninham, B.W., *J. Colloid and Interface Sci.* **114**, 234 (1986).

Clark, K.A.; Pasternack, D.S., Report No.5, Research Council of Alberta, 1949.

Czarnecki, J., *Adv. Colloid Interface Sci.* **24**, 283 (1986).

Czarnecki, J., *J. Colloid and Interface Sci.* **98**, 590 (1984).

Czarnecki, J. and Dabros, T., *J. Colloid and Interface Sci.* **78**, 25 (1980).

Dabros, T., Dai, Q., Hamaza, H. and Czarnecki, J., *Proc. 1st UBC–McGill Bi-annual Int. Symp., "Fundamentals of Mineral Processing"*. Vancouver BC, Aug. 20-24 (1995), pp. 413-424.

Dabros, T. and van de Ven, T.G.M., *PhysicoChem. Hydrodyn.* **8**, 161 (1987).

Dabros, T. and van de Ven, T.G.M., *Colloid Polymer Sci.* **261**, 694 (1983a).

Dabros, T. and van de Ven, T.G.M., *J. Colloid and Interface Sci.* **93**, 576 (1983b).

Dabros, T. and Adamczyk, Z., *Chem. Eng. Sci.* **34**, 1041 (1979).

Deshpande, M.D. and Vaishnav, R.N., *J. Fluid Mech.* **114**, 213 (1982).

Dijt, J.C., Stuwart, M.A., Hofman, J.E. and Fleer, G.J., *Colloids Surf.* **51**,141 (1990).

Duhkin, S.S. and Derjaguin, B.V., in *"Surface and Colloid Science."* (Matijevic, E., Ed.), *Electrokinetic Phenomena*, Wiley Interscience, New York, Vol. 7 (1974).

Elimelech, M., *J. Colloid and Interface Sci.* **164**, 10 (1994).

Elimelech, M., *J. Colloid and Interface Sci.* **146**, 337 (1991).

Elimelech, M. and O'Melia, C.R., *Langmuir.* **6**, 1153 (1990).

Epstein, N. and Masliyah, J.H., *Chem. Eng. J.* **3**, 169 (1972).

Faibish, R.S., Elimelech, M. and Cohen, Y., *J. Colloid and Interface Sci.* **204**, 77 (1998).

Goldman, A.J., Cox, R.G. and Brenner, H., *Chem. Eng. Sci.* **22**, 621 (1967a); 637 (1967b).

Goldman, A.J., Cox, R.G. and Brenner, H., *Chem. Eng. Sci.* **21,** 1151 (1966).

Goren, S.L. and O'Neill, M.E., *Chem. Eng. Sci.* **26**, 325 (1971).

Goren, S.L., *J. Fluid Mech.* **41**, 619 (1970).

Gosman, A. D., Pun, W.M., Runchal, A.K., Spalding, D.B. and Wolfshtein, M., *"Heat and Mass Transfer in Recirculating Flows"*, Academic Press, London (1969).

Gregory, J., *Critical Rev. Environ. Control.* **19**, 185 (1991).

Gregory, J., *J. Colloid and Interface Sci.* **83**,138 (1981).

Gregory, J. and Wishart, A.J., *Colloids Surf.* **1**, 313 (1980).

Healy, T.W. and White, L.R., *Adv. Colloid Interface Sci.* **9**, 303 (1978).

Hiemenz, P. C. and Rajagopalan, R., *"Principles of Colloid and Surface Chemistry"*, 3rd edition, Marcel Dekker Inc., New York (1977).

Hogg. R., Healy, T.W. and Fuerstenau, D.W., *Trans. Faraday Soc.* **62**, 1638 (1966).

Hong, S., Faibish, R.S. and Elimelech, M., *J. Colloid and Interface Sci.* **196**, 267 (1997).

Huisman, I.H., Tragardh. G. and Tragardh, C., *Chem. Eng. Sci.* **54**, 281 (1999).

Hung, C. C. and Tien, C., *Desalination* **18**, 173 (1976).

Hunter, R. J., *" Zeta Potential in Colloid Science: Principal and Application"*, Academic Press London (1981).

Israelachvili, J. N., *"Intermolecular and Surface Forces"*, 2nd edition, Academic Press, London (1992).

Israelachvili, J.N., *J. Colloid and Interface Sci.* **98**, 500 (1984).

Israelachvili, J.N., *Adv. Colloid Interface Sci.* **16**, 31 (1982).

Israelachvili, J. N. and Pashley, R. M., *Nature* **300**, 341 (1982b).

Israelachvili, J.N., *Faraday Discuss. Chem. Soc.* **65**, 20 (1978).

Israelachvili, J. N., *Q. Rev. Biophys.* **6**, 341 (1974).

Israelachvili, J.N. and Tabor, D., *Prog. Surf. Membr. Sci.* **7**, 1 (1973).

Israelachvili, J.N. and Tabor, D., *Proc. R. Soc. Lond.* A **331**, 19 (1972).

Joesten, N. and Schaad, L. J., "*Hydrogen Bonding*", Dekkar, New York (1974).

Kallay, N. and Matijevic, E., *Adv. Colloid Interface Sci.* **27**, 1 (1987).

Kilpatrick, Peter K., McLean, Joseph D., Spiecker, M. and Sullivan, P., *"Structures and Dynamics of Asphaltenes"* (Mullin and Sheu, Eds.), Plenum Press, New York (1998), pp. 377 - 422.

Kostoglou, M. and Karabelsas, A. J., *J. Colloid and Interface Sci.* **151**, 534 (1992).

Lakkapragara, S. and Walz, J.Y., *J. Colloid and Interface Sci.* **196**, 177 (1997).

Lakkapragara, S. and Walz, J.Y., *J. Colloid and Interface Sci.* **183**, 199 (1996).

Larsen, A.E. and Grier, D.G., *Nature* **385**, 230 (1997).

Leal, L. G., *"Laminar Flow and Convective Transport Processes"*, Butterworth-Heinemann, Boston (1992).

Levich, V.G., *"Physicochemical Hydrodynamics"*, Prentice-Hall, Englewood Cliffs, New Jersey (1962).

Li, Y. and Park, C.W., *J. Colloid and Interface Sci.* **185**, 49 (1997).

Lin, F.Y.H. and Li, D., *Chem. Eng. Sci.* **50**, 2633 (1995).

Luthi, Y. and Ricka, J., *J. Colloid and Interface Sci.* **206**, 302 (1998).

Lyklema, J., *"Fundamentals of Interface and Colloid Science"*, Academic Press, Toronto, (1993).

Mahanty, J. and Ninham, B.W., *"Dispersion Forces"*, Academic Press, London (1976).

Margenau, H and Kestner, N. R., *"Theory of Intermolecular Forces"*, Pergamon Oxford (1971).

Marshall, J.K. and Kitchener, J.A., *J. Colloid and Interface Sci.* **22**, 342 (1966).

Masliyah, J. H., *"Electrokinetic Transport Phenomena"*, Alberta Oil Sand Technology and Research Authority (AOSTRA), Technical Publication Series No. 12, AOSTRA, Edmonton, Alberta (1994).

McDowell-Boyer, L. M., Hunt, J. R. and Sitar, N., *Water Resour. Res.* **22**, 1901 (1986).

Meinders, J.M., van der Mei, H.C. and Busscher, H.J., *J. Colloid and Interface Sci.* **176**, 329 (1995).

Moelwyn-Hughes, E.A., *"Physical Chemistry"*, 2nd edition, Pergamon, Oxford (1961).

Ninham, B. W. and Persegian, V. A., *Biophys. J.* **10**, 646 (1970).

"Numerical Recipes." 2nd edition, Cambridge University Press (1986).

Patanker, S. V., *"Numerical Heat Transfer and Fluid Flow"*, McGraw-Hill, New York (1980).

Polat, S., Huang, B., Mujumdar, A.S. and Douglas, W.J.M., *"Numerical Flow and Heat Transfer under Impinging Jets-a Review", Ann. Rev. Num. Fluid Mech. & Heat Transfer,* Vol. 2, Chapter 4, Hemisphere Publishing Co., New York (1991).

Preive, D.C. and Lin, M.M.J., *J. Colloid and Interface Sci.* **86**, 17 (1982).

Preive, D.C. and Lin, M.M.J., *J. Colloid and Interface Sci.* **76**, 32 (1980).

Preive, D.C. and Ruckenstein, E., *AIChE J.* **20**, 1178 (1974).

Rabinovich, Y.I. and Yoon, R. H., *Langmuir,* **10**, 1903 (1994).

Rabinovich, Y.I. and Derjaguin, B.V., *Colloids Surfaces.* **30**, 243 (1988).

Rajagopalan, R. and Kim, J., *J. Colloid and Interface Sci.* **83**, 428 (1981).

Rajagopalan, R. and Tien, C., *"Progress in Filtration and Separation"* (Wakerman, R. J., Ed.), Elsevier, Amsterdam (1979), pp.179-269.

Roache, P.J., *"Computational Fluid Dynamics"*, Hermosa Publisher, Albuquerque, New York (1972).

Ross, S. and Morrison, I. D., *"Colloid Systems and Interfaces"*, John Wiley, New York (1988).

Ruckenstein, E. and Chen, J. H., *J. Colloid and Interface Sci.* **128**, 592 (1989).

Ruckenstein, E., *J. Colloid and Interface Sci.* **66**, 531 (1978).

Ruckenstein, E. and Prieve, D.C., *J. Chem. Soc. Faraday II.* **69**, 1522 (1973).

Sanders, S., Ph. D. Dissertation, University of Alberta, Edmonton, AB, (1997).

Sanders, S., Chow, R. S. and Masliyah, J. H., *J. Colloid and Interface Sci.* **174**, 230 (1995).

Sjollema, J. and H.J. Busscher, *Colloids Surf.* **47**, 323 (1990).

Sjollema, J., Busscher, H.J. and Weerkamp, A.H., *Biofouling* **1**, 101 (1988).

Somasundaran, P., Shrotri, S. and Ananthapadmanabhan, K.P., *Colloids and Surf.* **142**, 83, (1998).

Song, L. and Elimelech, M., *J. Colloid and Interface Sci.* **173**, 165 (1995).

Soo, H. and Radke, C. J., *Chem. Eng. Sci.* **41**, 263 (1986).

Soo, H. and Radke, C. J., *J. Colloid and Interface Sci.* **102**, 462 (1984).

Spielman, L.A., *Ann. Rev. Fluid Mech.* **9**, 297 (1977).

Spielman, L.A. and Fitzpatrick, J.A., *J. Colloid and Interface Sci.* **46**, 22 (1974).

Spielman, L.A. and Fitzpatrick, J.A., *J. Colloid and Interface Sci.* **42**, 607 (1973).

Spielman, L.A. and Cukor, P.M., *J. Colloid and Interface Sci.* **43**, 51 (1973).

Spielman, L.A., *J. Colloid and Interface Sci.* **33**, 562 (1970).

Spielman, L.A. and Goren, S.L., *Environ. Sci. Technol.* **4**, 135 (1970).

Suzuki, A., Ho, N.F.H. and Higuchi, W.I., *J. Colloid and Interface Sci.* **29**, 552 (1969).

Tadros, Th. F. and Vincent, B., *"Encyclopedia of Emulsion Technology"*, Vol. 1, (Becher, P., Ed.) Marcel Dekker, Inc., New York (1983).

Takamura, K. and Chow, R.S., *Colloids Surf.* **15**, 35 (1985).

Takamura, K. and Chow, R. S., *J. Can. Pet. Technol.* **22**, 226 (1983).

Tien, C., *"Granular Filtration of Aerosols and Hydrosols"*, Butterworths, Stoneham, MA, (1989).

Tobiason, J., *Colloids Surf.* **39**, 53 (1989).

Umeyama, H. and Morokuma, K., *J. Am. Chem. Soc.* **99**, 1316 (1977).

van de Ven, T.G.M. and Kelemen, S.J., *J. Colloid and Interface Sci.* **181**, 118 (1996).

van Oss, C.J., *J. Dispersion Sci. Tech.* **11**, 491 (1990).

van de Ven, T.G.M., *"Colloidal Hydrodynamics"*, Academic Press, San Diego (1989).

Varennes, S. and van de Ven, T.G.M., *PhysicoChem. Hydrodyn.* **9**, 537 (1987).

Varennes, S. and van de Ven, T.G.M., *PhysicoChem. Hydrodyn.* **10**, 415 (1988).

Varennes, S. and van de Ven, T.G.M., *Colloids Surf.* **33**, 63 (1988).

Vincent, B., *J. Colloid and Interface Sci.* **42**, 270 (1973).

Visser, J., *Adv. Colloid Interface Sci.* **15**, 157 (1981).

Walz, J.Y., *Adv. Colloid Interface Sci.* **74**, 119 (1998).

Warszynski, P. and Adamczyk, Z., *J. Colloid and Interface Sci.* **187**, 283 (1997).

Warszynski, P. and van de Ven, T.G.M, *Adv. Colloid Interface Sci.* **36**, 33 (1991).

Warszynski, P. and van de Ven, T.G.M., *Faraday Discuss Chem. Soc.* **90**, 313 (1990).

Wnek, W. J., Gidaspow, D. and Wasan, D.T., *J. Colloid and Interface Sci.* **59**, 1 (1977).

Wu, X., Laroche, I., Masliyah, J., Czarnecki, J. and Dabros, T., *Colloid and Surf.* **174**, 133 (2000).

Yang, C., Ph.D. Dissertation, University of Alberta, Edmonton, AB, (2000).

Zebel, G., *J. Colloid and Interface Sci.* **20**, 552 (1965).

Zhou, Z.A., Hussien, H., Xu, Z., Czarnecki, J. and Masliyah, J.H., *J. Colloid and Interface Sci.* **197**, 242 (1998).

APPENDIX – A

Computer code for numerical solution of mass transfer

```
c       Program for numerically solving one-dimensional
c       mass transfer ODE equation in the impinging jet
c       This program has following important features
c       (1) In the model, a stagnation flow field is
c       assumed to be applicable. The external forces
c       include gravity force, Van der Waals interaction
c       electrical double layer interaction, and hydrophobic
c       interaction as well
c       (2)solving two coupled first-order ordinary differential
c       equations using Semi-implicit Extrapolation Method by Bader
c       and Deuflhard specially designed for very stiff ODE
c       (extrapolation is exactly the same as the original
c       Bulirsch-Stoer integrating routine)
c       (3) The numerical procedure for linear ODE is the same as that
c       employed by Prieve and Lin (J. Colloids & Interface Sci)
c       (4)
c       ------------------------------------------------
        program main
c       dimensions and other classifications
        implicit double precision (a-h, o-z)
        parameter (mx=30000)
        dimension xc(mx), yc(mx), yxc(mx), y(2)
        double precision n0, kb, lambda0, lambda, muf, kesy
        external derivs, stifbs
        data pi/3.1415926d0/, g0/9.8066d0/, e0/1.602d-19/,
     &    kb/1.381d-23/, lambda0/1.0d-7/, rhof/9.981d+2/,
     &    rhoa/1.25d+3/, muf/9.98d-4/, epus0/8.854d-12/,
     &    epusr/8.0d+1/, zi/1.0d0/, temp/2.93d+2/
c       ------------------------------------------------
c       inputing necessary data for all calculations
c       imputing the velocity field
c       ------------------------------------------------
c       initializing parameters
        epus=epus0*epusr
        drho=-(rhof-rhoa)
        ab=1.5d-6
        rb=1.275d-3
        re=1000.0d0
        ar=6.022d+23
        cs=0.01d0
```

```
      n0=1000*ar*cs
c     n0=6.023d+23
      c0=1.5d+9
c     pesib=-20.0d-3
c     pesic=-10.0d-3
c     ---------------------------------------------------
c     initializing the non-dimensional groups
      grav=0.002d0
      pe=0.0d0
      ad=0.0d0
      di=0.0d0
      da=0.0d0
      tao=0.0d0
      lambda=0.0d0
      hd=0.0d0
c     ---------------------------------------------------
c     setting the primary minimum
      x0=1.0d-4
c     ---------------------------------------------------
c     calculation of the average velocity at the exit of
c     tube and the Reynolds number
      vave=(re*muf)/(rb*rhof)
      vflow=vave*rb**2*pi
c     ---------------------------------------------------
c     calculation of the strength parameter for the stagnation
c     flow
      albar=5.3d0*re**0.5-8.13d0
      alpha=albar*vave/rb**2
c     ---------------------------------------------------
c     calculation of the diffusion coefficient using the
c     Stokes-Einstein equation
      dinf=kb*temp/(6.0d0*pi*muf*ab)
c     ---------------------------------------------------
c     calculation of the Peclet number
      pe=2.0d0*alpha*ab**3/dinf
c     ---------------------------------------------------
c     calculation of gravitation number
      grav=2.0d0/9.0d0*(drho*g0*ab**3)/(muf*dinf)
c     grav=0.0d5
c     calculation of the electrical double layer interaction
c     based on constant zeta potential model--(HHF model)
c     calculation of the double layer parameter
      di=(4*3.14*epus*ab*pesic*pesib)/(kb*temp)
c     di=1000.0d0
      da=(pesic-pesib)**2/(2.0d0*pesic*pesib)
c     da=0.0d0
c     calculation of the Debye-Huckel length
```

```
      kesy=((2.0d0*zi**2*e0**2*n0)/(epus*kb*temp))**0.5
      tao=kesy*ab
c     tao=58.2d0
c     defination of the EDL interaction function
      fedl=di*tao*(dexp(-tao*x0)/(1.0d0+dexp(-tao*x0))
     & -da*dexp(-2.0d0*tao*x0)/(1.0d0-dexp(-2.0d0*tao*x0)))
      fedlx=di*tao
     & *(-tao*dexp(-tao*x0)/(1.0d0+dexp(-tao*x0))
     & +tao*dexp(-2.0d0*tao*x0)/(1.0d0+dexp(-tao*x0))**2
     &   +da*2.0d0*tao*dexp(-2.0d0*tao*x0)
     & /(1.0d0-dexp(-2.0d0*tao*x0))+da*2.0d0*tao
     &  *dexp(-4.0d0*tao*x0)/(1.0d0-dexp(-2.0d0*tao*x0))**2)
c     write(*,*) 'fedl fedlx', fedl, fedlx
c     write(*,*)'di da', di, da
c     write(*,*) 'K, Ka', kesy, kesy*ab
c     ----------------------------------------------------------
c     calculation of Van der Waals interaction
c     calculation of the retardation parameter
      lambda=lambda0/ab
c     lambda=0.4d0
c     calculation of the adhession number
c     call hamaker(            ,a123)
      a123=1.0d-20
c     a123=0.0d0
c     ad=a123/(6.0d0*kb*temp)
c     ad=-0.1d0
      ad=0.412d0
c     defination of Van dee Waals interaction function
      fvdw=-ad*lambda*(lambda+22.232d0*x0)
     &      /(x0**2*(lambda+11.116d0*x0)**2)
      fvdwx=-ad*lambda*(22.232d0/(x0**2*(lambda+11.116d0*x0)**2)
     &     -(lambda+22.232d0*x0)*(2.0d0*x0*(lambda+11.116d0*x0)**2
     &       +2.0d0*11.116d0*x0**2*(lambda+11.116d0*x0))
     &      /(x0**4*(lambda+11.116d0*x0)**4))
c     write(*,*)'ad fvdw ', ad, fvdw
c     write(*,*) ' fvdwx, lambda', fvdwx, lambda
c     ----------------------------------------------------------
c     write(*,*)'vbar vflow', vave, vflow
c     write(*,*)'albar alpha', albar, alpha
c     write(*,*)'dinf pe', dinf, pe
c     ----------------------------------------------------------
c     calculation of hydrophobic interaction
c     ----------------------------------------------------------
      hd=0.0d0
      fhyp=-ad/x0**2
      vhyp=-ad/x0
c     ----------------------------------------------------------
```

```
c     To solve two coupled first-order ordinary differential
c     equations using Semi-implicit Extrapolation Method by Bader
c     and Deuflhard specially designed for very stiff ODE
c     (extrapolation is exactly the same as the original
c     Bulirsch-Stoer integrating routine)
      y0=0.0d0
      ym=1.0d0
      yguess=0.5d0*pe+grav
c     yguess=0.616d0*pe**(1/3)
c     write(*,*) 'y0, ym',y0, ym
c     write(*,*) 'grav yguess', grav, yguess
c     ----------------------------------------------------------
c     defination of functions for universal hydrodynamic coefficients
      a1=-0.443d0
      b1=1.299d0
      c1=-0.5568d0
      d1=0.32d0
c     ----------------------------------------------------------
      a2=1.455d0
      b2=1.259d0
      c2=0.7951d0
      d2=0.56d0
c     ----------------------------------------------------------
      a3=-0.487d0
      b3=5.423d0
      c3=-0.5905d0
      d3=37.83d0
c     ---------------------------------------------
c     defination of functions for universal hydrodynamic
c     coefficients
      fun1=dabs(1.0d0+a1*dexp(-b1*x0)+c1*dexp(-d1*x0**0.75))
      fun2=dabs(1.0d0+a2*dexp(-b2*x0)+c2*dexp(-d2*x0**0.5))
      fun3=dabs(1.0d0+a3*dexp(-b3*x0)+c3*dexp(-d3*x0**0.5))
c     ---------------------------------------------
c     write(*,*) 'f1, f2, f3', fun1, fun2, fun3
      eps=1.0d-6
      y(1)=y0
      y(2)=fun1*yguess
      y20=fun1*yguess
      kc=1
100   nvar=2
      xc(1)=x0
      yc(1)=y0
      yxc(1)=y20
c     write(*,*) 'y1, y2',y(1), y(2)
      do i=2, mx
c        xc(i)=xc(i-1)+xk**(i-1)*x0
```

```
c         x1=xc(i-1)
c         x2=xc(i)
          x1=x0+(i-2)*x0
          x2=x0+(i-1)*x0
c         x1=x0+(i-2)*x0*10.0d0
c         x2=x0+(i-1)*x0*10.0d0
          xc(i)=x2
          h1=(x2-x1)*1.0d-2
          hmin=h1*1.0d-12
          call odeint(y,nvar,x1,x2,eps,h1,hmin,nok,
     *         nbad,derivs,stifbs)
          yc(i)=y(1)
          yxc(i)=y(2)
        enddo
        if (dabs(yc(mx)-ym) .gt. eps) then
          y(1)=y0
          y20=y20*ym/yc(mx)
          y(2)=y20
          kc=kc+1
c       write(*,*) 'Cycle=',kc, yc(mx),ym
          goto 100
        endif
c       -------------------------------------------------------
c       calculation of Sherwood number and mass transfer flux
        sh=y20
        flux=100.0d0*y20*dinf*ym/ab
c       -------------------------------------------------------
      open (unit=2, file='vkc.out', status='unknown')
        do i=1, mx
          write(2,200) xc(i), yc(i), yxc(i)
        enddo
 200    format(f16.4,3x,f16.6,3x,f16.6)
c       -------------------------------------------------------
      open (unit=4, file='vk.out', status='unknown')
          write(4,400)x0, ab, re, pe, grav
          write(4,500)flux, sh, ad, hd
          write(4,500)1.0d0/kesy, tao, di, da
 400    format(f8.4,2x,f14.9,2x,f9.2,2x,f16.6,2x,f12.4)
 500    format(f16.12,3x,f16.6,3x,f16.6,3x,f16.6)
c       write(*,*) 'stop',kc, yc(mx), ym
        stop
        end
c       --------------------------------------------------
c*********************************************************************
c     filename:  STIFF.FOR
c *******************************************************************
      subroutine odeint(ystart,nvar,x1,x2,eps,h1,hmin,nok,
     *               nbad,derivs,stifbs)
      integer nbad,nok,nvar,kmaxx,maxstp,nmax
      real*8 eps,h1,hmin,x1,x2,ystart(nvar),tiny
      external derivs,stifbs
      parameter (maxstp=10000,nmax=10,kmaxx=100,tiny=1.d-30)
      integer i,kmax,kount,nstp
      real*8 dxsav,h,hdid,hnext,x,xsav,dydx(nmax),xp(kmaxx),y(nmax),
     *     yp(nmax,kmaxx),yscal(nmax)
      common /path/ kmax,kount,dxsav,xp,yp
      x=x1
      h=dsign(h1,x2-x1)
      nok=0
      nbad=0
      kount=0
      do 11 i=1,nvar
        y(i)=ystart(i)
11    continue
      if (kmax.gt.0) xsav=x-2.d0*dxsav
      do 16 nstp=1,maxstp
        call derivs(x,y,dydx)
        do 12 i=1,nvar
          yscal(i)=dabs(y(i))+dabs(h*dydx(i))+tiny
12      continue
        if(kmax.gt.0) then
          if(dabs(x-xsav).gt.dabs(dxsav)) then
            if(kount.lt.kmax-1) then
              kount=kount+1
              xp(kount)=x
              do 13 i=1,nvar
                yp(i,kount)=y(i)
13            continue
              xsav=x
            endif
          endif
        endif
        if((x+h-x2)*(x+h-x1).gt.0.d0) h=x2-x
        call stifbs(y,dydx,nvar,x,h,eps,yscal,hdid,hnext,derivs)
        if(hdid.eq.h) then
          nok=nok+1
        else
          nbad=nbad+1
        endif
        if((x-x2)*(x2-x1).ge.0.d0) then
          do 14 i=1,nvar
            ystart(i)=y(i)
14        continue
          if(kmax.ne.0) then
```

```
         kount=kount+1
         xp(kount)=x
         do 15 i=1,nvar
          yp(i,kount)=y(i)
15         continue
        endif
        return
       endif
       if(dabs(hnext).lt.hmin) then
        write(*,17)
        pause
       endif
       h=hnext
16     continue
      write(*,18)
      pause
17     format(' stepsize smaller than hmin in ODEINT')
18     format(' too many steps in ODEINT')
      return
      end
c
      subroutine pzextr(iest,xest,yest,yz,dy,nv)
      integer iest,nv,imax,nmax
      real*8 xest,dy(nv),yest(nv),yz(nv)
      parameter (imax=13,nmax=10)
      integer j,k1
      real*8 delta,f1,f2,q,d(nmax),qcol(nmax,imax),x(imax)
      save qcol,x
      x(iest)=xest
      do 11 j=1,nv
       dy(j)=yest(j)
       yz(j)=yest(j)
11     continue
      if(iest.eq.1) then
       do 12 j=1,nv
        qcol(j,1)=yest(j)
12       continue
      else
       do 13 j=1,nv
        d(j)=yest(j)
13       continue
       do 15 k1=1,iest-1
        delta=1.d0/(x(iest-k1)-xest)
        f1=xest*delta
        f2=x(iest-k1)*delta
        do 14 j=1,nv
         q=qcol(j,k1)
```

```
          qcol(j,k1)=dy(j)
          delta=d(j)-q
          dy(j)=f1*delta
          d(j)=f2*delta
          yz(j)=yz(j)+dy(j)
14         continue
15        continue
        do 16 j=1,nv
          qcol(j,iest)=dy(j)
16        continue
      endif
      return
      end
c
      SUBROUTINE stifbs(y,dydx,nv,x,htry,eps,yscal,hdid,hnext,derivs)
      INTEGER nv,NMAX,KMAXX,IMAX
      REAL*8 eps,hdid,hnext,htry,x,dydx(nv),y(nv),yscal(nv),
     *SAFE1,SAFE2,REDMAX,REDMIN,TINY,SCALMX
      EXTERNAL derivs
      PARAMETER
(NMAX=50,KMAXX=7,IMAX=KMAXX+1,SAFE1=.25d0,SAFE2=.7d0,
     *REDMAX=1.d-5,REDMIN=.7d0,TINY=1.d-30,SCALMX=.1d0)
CU    USES derivs,jacobn,simpr,pzextr
      INTEGER i,iq,k,kk,km,kmax,kopt,nvold,nseq(IMAX)
      REAL*8 eps1,epsold,errmax,fact,h,red,scale,work,wrkmin,xest,xnew,

*a(IMAX),alf(KMAXX,KMAXX),dfdx(NMAX),dfdy(NMAX,NMAX),err(KMAXX),
     *yerr(NMAX),ysav(NMAX),yseq(NMAX)
      LOGICAL first,reduct
      SAVE a,alf,epsold,first,kmax,kopt,nseq,nvold,xnew
      DATA first/.true./,epsold/-1.d0/,nvold/-1/
      DATA nseq /2,6,10,14,22,34,50,70/
      if(eps.ne.epsold.or.nv.ne.nvold)then
        hnext=-1.d29
        xnew=-1.d29
        eps1=SAFE1*eps
        a(1)=nseq(1)+1
        do 11 k=1,KMAXX
          a(k+1)=a(k)+nseq(k+1)
11        continue
        do 13 iq=2,KMAXX
          do 12 k=1,iq-1
            alf(k,iq)=eps1**((a(k+1)-a(iq+1))/((a(iq+1)-a(1)+1.d0)*
     *      (2*k+1)))
12          continue
13        continue
        epsold=eps
```

```
       nvold=nv
       a(1)=nv+a(1)
       do 14 k=1,KMAXX
         a(k+1)=a(k)+nseq(k+1)
14       continue
       do 15 kopt=2,KMAXX-1
         if(a(kopt+1).gt.a(kopt)*alf(kopt-1,kopt))goto 1
15       continue
1        kmax=kopt
      endif
      h=htry
      do 16 i=1,nv
        ysav(i)=y(i)
16      continue
      call jacobn(x,y,dfdx,dfdy,nv,nmax)
      if(h.ne.hnext.or.x.ne.xnew)then
        first=.true.
        kopt=kmax
      endif
      reduct=.false.
2       do 18 k=1,kmax
        xnew=x+h
        if(xnew.eq.x)pause 'stepsize underflow in stifbs'
        call simpr(ysav,dydx,dfdx,dfdy,nmax,nv,x,h,nseq(k),yseq,derivs)
        xest=(h/nseq(k))**2
        call pzextr(k,xest,yseq,y,yerr,nv)
        if(k.ne.1)then
          errmax=TINY
          do 17 i=1,nv
            errmax=dmax1(errmax,dabs(yerr(i)/yscal(i)))
17          continue
          errmax=errmax/eps
          km=k-1
          err(km)=(errmax/SAFE1)**(1.d0/(2*km+1))
        endif
        if(k.ne.1.and.(k.ge.kopt-1.or.first))then
          if(errmax.lt.1.d0) goto 4
          if(k.eq.kmax.or.k.eq.kopt+1)then
            red=SAFE2/err(km)
            goto 3
          else if(k.eq.kopt)then
            if(alf(kopt-1,kopt).lt.err(km))then
              red=1.d0/err(km)
              goto 3
            endif
          else if(kopt.eq.kmax)then
            if(alf(km,kmax-1).lt.err(km))then
          red=alf(km,kmax-1)*SAFE2/err(km)
          goto 3
         endif
        else if(alf(km,kopt).lt.err(km))then
         red=alf(km,kopt-1)/err(km)
         goto 3
        endif
       endif
18   continue
3    red=dmin1(red,REDMIN)
     red=dmax1(red,REDMAX)
     h=h*red
     reduct=.true.
     goto 2
4    x=xnew
     hdid=h
     first=.false.
     wrkmin=1.e35
     do 19 kk=1,km
       fact=dmax1(err(kk),SCALMX)
       work=fact*a(kk+1)
       if(work.lt.wrkmin)then
         scale=fact
         wrkmin=work
         kopt=kk+1
       endif
19   continue
     hnext=h/scale
     if(kopt.ge.k.and.kopt.ne.kmax.and..not.reduct)then
       fact=dmax1(scale/alf(kopt-1,kopt),SCALMX)
       if(a(kopt+1)*fact.le.wrkmin)then
         hnext=h/fact
         kopt=kopt+1
       endif
     endif
     return
     END
c
     SUBROUTINE simpr(y,dydx,dfdx,dfdy,nmax,n,xs,htot,nstep,yout,
    *derivs)
     INTEGER n,nmax,nstep,NMAXX
     REAL*8 htot,xs,dfdx(n),dfdy(nmax,nmax),dydx(n),y(n),yout(n)
     EXTERNAL derivs
     PARAMETER (NMAXX=50)
CU   USES derivs,lubksb,ludcmp
     INTEGER i,j,nn,indx(NMAXX)
     REAL*8 d,h,x,a(NMAXX,NMAXX),del(NMAXX),ytemp(NMAXX)
```

```
      h=htot/nstep
      do 12 i=1,n
       do 11 j=1,n
         a(i,j)=-h*dfdy(i,j)
11      continue
       a(i,i)=a(i,i)+1.d0
12    continue
      call ludcmp(a,n,NMAXX,indx,d)
      do 13 i=1,n
       yout(i)=h*(dydx(i)+h*dfdx(i))
13    continue
      call lubksb(a,n,NMAXX,indx,yout)
      do 14 i=1,n
       del(i)=yout(i)
       ytemp(i)=y(i)+del(i)
14    continue
      x=xs+h
      call derivs(x,ytemp,yout)
      do 17 nn=2,nstep
       do 15 i=1,n
         yout(i)=h*yout(i)-del(i)
15      continue
       call lubksb(a,n,NMAXX,indx,yout)
       do 16 i=1,n
         del(i)=del(i)+2.*yout(i)
         ytemp(i)=ytemp(i)+del(i)
16      continue
       x=x+h
       call derivs(x,ytemp,yout)
17    continue
      do 18 i=1,n
       yout(i)=h*yout(i)-del(i)
18    continue
      call lubksb(a,n,NMAXX,indx,yout)
      do 19 i=1,n
       yout(i)=ytemp(i)+yout(i)
19    continue
      return
      END
c
      SUBROUTINE ludcmp(a,n,np,indx,d)
      INTEGER n,np,indx(n),NMAX
      REAL*8 d,a(np,np),TINY
      PARAMETER (NMAX=500,TINY=1.0d-20)
      INTEGER i,imax,j,k
      REAL*8 aamax,dum,sum,vv(NMAX)
      d=1.d0
      do 12 i=1,n
        aamax=0.d0
        do 11 j=1,n
          if (dabs(a(i,j)).gt.aamax) aamax=dabs(a(i,j))
11        continue
        if (aamax.eq.0.d0) pause 'singular matrix in ludcmp'
        vv(i)=1.d0/aamax
12      continue
      do 19 j=1,n
        do 14 i=1,j-1
          sum=a(i,j)
          do 13 k=1,i-1
            sum=sum-a(i,k)*a(k,j)
13          continue
          a(i,j)=sum
14        continue
        aamax=0.d0
        do 16 i=j,n
          sum=a(i,j)
          do 15 k=1,j-1
            sum=sum-a(i,k)*a(k,j)
15          continue
          a(i,j)=sum
          dum=vv(i)*dabs(sum)
          if (dum.ge.aamax) then
            imax=i
            aamax=dum
          endif
16        continue
        if (j.ne.imax)then
          do 17 k=1,n
            dum=a(imax,k)
            a(imax,k)=a(j,k)
            a(j,k)=dum
17          continue
          d=-d
          vv(imax)=vv(j)
        endif
        indx(j)=imax
        if(a(j,j).eq.0.)a(j,j)=TINY
        if(j.ne.n)then
          dum=1.d0/a(j,j)
          do 18 i=j+1,n
            a(i,j)=a(i,j)*dum
18          continue
        endif
19      continue
```

```
      return
      END
c
      SUBROUTINE lubksb(a,n,np,indx,b)
      INTEGER n,np,indx(n)
      REAL*8 a(np,np),b(n)
      INTEGER i,ii,j,ll
      REAL*8 sum
      ii=0
      do 12 i=1,n
        ll=indx(i)
        sum=b(ll)
        b(ll)=b(i)
        if (ii.ne.0)then
          do 11 j=ii,i-1
            sum=sum-a(i,j)*b(j)
11        continue
        else if (sum.ne.0.d0) then
          ii=i
        endif
        b(i)=sum
12    continue
      do 14 i=n,1,-1
        sum=b(i)
        do 13 j=i+1,n
          sum=sum-a(i,j)*b(j)
13      continue
        b(i)=sum/a(i,i)
14    continue
      return
      END
c       ----------------------------------------------------------
        subroutine jacobn(x,y,dfdx,dfdy,n,nmax)
        implicit double precision (a-h,o-z)
        double precision n0, kb, lambda0, lambda, muf, kesy
        integer n, nmax, i
        dimension y(2), dydx(2), dfdx(2), dfdy(nmax,nmax)
        data pi/3.1415926d0/, g0/9.8066d0/, e0/1.602d-19/,
     &    kb/1.381d-23/, lambda0/1.0d-7/, rhof/9.981d+2/,
     &    rhoa/1.25d+3/, muf/9.98d-4/, epus0/8.854d-12/,
     &    epusr/8.0d+1/, zi/1.0d0/, temp/2.93d+2/
c       -----------------------------------------------------
c       inputing necessary data for all calculations
c       imputing the velocity field
c       -----------------------------------------------------
c       initializing parameters
        epus=epus0*epusr
```

```
       drho=-(rhof-rhoa)
       ab=1.5d-6
       rb=1.275d-3
      re=1000.0d0
      ar=6.022d+23
      cs=0.01d0
      n0=1000*ar*cs
        c0=1.5d+9
c     pesib=-20.0d-3
c     pesic=-10.0d-3
c       ---------------------------------------------
c       initializing the non-dimensional groups
        grav=0.002d0
        pe=0.0d0
        ad=0.0d0
        di=0.0d0
        da=0.0d0
        tao=0.0d0
        lambda=0.0d0
        hd=0.0d0
c       ---------------------------------------------
c       calculation of the average velocity at the exit of
c       tube and the Reynolds number
        vave=re*muf/(rb*rhof)
        vflow=vave*rb**2*pi
c       ------------------------------------------------
c       calculation of the strength parameter for the stagnation
c       flow
        albar=5.3d0*re**0.5-8.13d0
        alpha=albar*vave/rb**2
c       ------------------------------------------------
c       calculation of the diffusion coefficient using the
c       Stokes-Einstein equation
        dinf=kb*temp/(6.0d0*pi*muf*ab)
c       calculation of the Peclet number
        pe=2.0d0*alpha*ab**3/dinf
c       ------------------------------------------------
c       calculation of gravitation number
       grav=2.0d0/9.0d0*(drho*g0*ab**3)/(muf*dinf)
c      grav=0.0d0
c       ------------------------------------------------
c       calculation of the electrical double layer interaction
c       based on constant zeta potential model--(HHF model)
c       calculation of the double layer parameter
c      di=(4*3.14*epus*ab*pesic*pesib)/(kb*temp)
c      di=1000.0d0
      da=(pesic-pesib)**2/(2.0d0*pesic*pesib)
```

```
c    da=0.0d0
c      calculation of the Debye-Huckel length
       kesy=((2.0d0*zi**2*e0**2*n0)/(epus*kb*temp))**0.5
       tao=kesy*ab
c      tao=58.2d0
c      defination of the EDL interaction function
       fedl=di*tao*(dexp(-tao*x)/(1.0d0+dexp(-tao*x))
     &  -da*dexp(-2.0d0*tao*x)/(1.0d0-dexp(-2.0d0*tao*x)))
       fedlx=di*tao
     &  *(-tao*dexp(-tao*x)/(1.0d0+dexp(-tao*x))
     &  +tao*dexp(-2.0d0*tao*x)/(1.0d0+dexp(-tao*x))**2
     &    +da*2.0d0*tao*dexp(-2.0d0*tao*x)
     &  /(1.0d0-dexp(-2.0d0*tao*x))+da*2.0d0*tao
     &  *dexp(-4.0d0*tao*x)/(1.0d0-dexp(-2.0d0*tao*x))**2)
c      ------------------------------------------------------
c      calculation of Van der Waals interaction
c      calculation of the retardation parameter
       lambda=lambda0/ab
c      lambda=0.4d0
c      .calculation of the adhession number
c      call hamaker(           ,a123)
     a123=1.0d-20
c     ad=a123/(6.0d0*kb*temp)
     ad=0.412d0
c      defination of Van dee Waals interaction function
       fvdw=-ad*lambda*(lambda+22.232d0*x)
     &  /(x**2*(lambda+11.116d0*x)**2)
       fvdwx=-ad*lambda*(22.232d0/(x**2*(lambda+11.116d0*x)**2)
     &    -(lambda+22.232d0*x)*(2.0d0*x*(lambda+11.116d0*x)**2
     &    +2.0d0*11.116d0*x**2*(lambda+11.116d0*x))
     &    /(x**4*(lambda+11.116d0*x)**4))
c      ------------------------------------------------------
c      calculaytion of hydrophobic interactions
c      ------------------------------------------------------
       hd=0.0d0
       fhyp=-hd/x**2
       fhypx=2.0d0*hd/x**3
c      ------------------------------------------------------
c      defination of functions for universal hydrodynamic coefficients
       a1=-0.443d0
       b1=1.299d0
       c1=-0.5568d0
       d1=0.32d0
c      ------------------------------------------------------
       a2=1.455d0
       b2=1.259d0
       c2=0.7951d0
```

```
      d2=0.56d0
c     ----------------------------------------------------------
      a3=-0.487d0
      b3=5.423d0
      c3=-0.5905d0
      d3=37.83d0
c     ---------------------------------------------
c     defination of functions for universal hydrodynamic
c     coefficients
      fun1=dabs(1.0d0+a1*dexp(-b1*x)+c1*dexp(-d1*x**0.75))
      fun2=dabs(1.0d0+a2*dexp(-b2*x)+c2*dexp(-d2*x**0.5))
      fun3=dabs(1.0d0+a3*dexp(-b3*x)+c3*dexp(-d3*x**0.5))
      fun1x=-a1*b1*dexp(-b1*x)
     &  -0.75d0*c1*d1*x**(-0.25)*dexp(-d1*x**0.75)
      fun2x=-a2*b2*dexp(-b2*x)
     &    -0.5d0*c2*d2*x**(-0.5)*dexp(-d2*x**0.5)
      fun3x=-a3*b3*dexp(-b3*x)
     &    -0.5d0*c3*d3*x**(-0.5)*dexp(-d3*x**0.5)
c     ---------------------------------------------
c     defination of the components of the Jacobi matrix
c     -------------------------------------------------
      dydx(1)=(y(2)/fun1-0.5d0*pe*fun2*(1.0d0+x)**2*y(1)
     &      +(grav+fedl+fvdw+fhyp)*y(1))
      dydx(2)=pe*fun3*(1.0d0+x)*y(1)
     dfdx(1)=dydx(2)/fun1-y(2)*fun1x/fun1**2-pe*fun2*(1.0d0+x)*y(1)
     &    -0.5d0*pe*fun2x*(1.0d0+x)**2*y(1)
     &        -0.5d0*pe*fun2*(1.0d0+x)**2*dydx(1)
     &        +(fedlx+fvdwx+fhypx)*y(1)+(grav+fedl+fvdw+fhyp)*dydx(1)
      dfdx(2)=pe*fun3x*(1.0d0+x)*y(1)+pe*fun3*y(1)
     &      +pe*fun3*(1.0d0+x)*dydx(1)
c     dfdx(1)=dydx(2)/fun1-pe*fun2*(1.0d0+x)*y(1)
c    &        -0.5d0*pe*fun2*(1.0d0+x)**2*dydx(1)
c    &        +(fedlx+fvdwx+fhypx)*y(1)+(grav+fedl+fvdw+fhyp)*dydx(1)
c     dfdx(2)=pe*fun3*y(1)+pe*fun3*(1.0d0+x)*dydx(1)
      dfdy(1,1)=-0.5d0*pe*fun2*(1.0d0+x)**2+(grav+fedl+fvdw+fhyp)
      dfdy(1,2)=1.0d0/fun1
      dfdy(2,1)=pe*fun3*(1.0d0+x)
      dfdy(2,2)=0.0d0
      return
      end
c     ---------------------------------------------------------
      subroutine derivs(x,y,dydx)
      implicit double precision (a-h,o-z)
      double precision n0, kb, lambda0, lambda, muf, kesy
      dimension y(2), dydx(2)
      data pi/3.1415926d0/, g0/9.8066d0/, e0/1.602d-19/,
     &   kb/1.381d-23/, lambda0/1.0d-7/, rhof/9.981d+2/,
     &     rhoa/1.25d+3/, muf/9.98d-4/, epus0/8.854d-12/,
     &     epusr/8.0d+1/, zi/1.0d0/, temp/2.93d+2/
c      ---------------------------------------------------
c      inputing necessary data for all calculations
c      imputing the velocity field
c      ---------------------------------------------------
c      initializing parameters
       epus=epus0*epusr
      drho=-(rhof-rhoa)
      ab=1.5d-6
     rb=1.275d-3
     re=1000.0d0
    ar=6.022d+23
    cs=0.01d0
    n0=1000*ar*cs
   c0=1.5d+9
c   pesib=-20.0d-3
c   pesic=-10.0d-3
c      ---------------------------------------------------
c      initializing the non-dimensional groups
       grav=0.002d0
       pe=0.0d0
       ad=0.0d0
       di=0.0d0
       da=0.0d0
       tao=0.0d0
       lambda=0.0d0
       hd=0.0d0
c      ---------------------------------------------------
c      calculation of the average velocity at the exit of
c      tube and the Reynolds number
       vave=re*muf/(rb*rhof)
       vflow=vave*rb**2*pi
c      ---------------------------------------------------
c      calculation of the strength parameter for the stagnation
c      flow
       albar=5.3d0*re**0.5-8.13d0
       alpha=albar*vave/rb**2
c      ---------------------------------------------------
c      calculation of the diffusion coefficient using the
c      Stokes-Einstein equation
       dinf=kb*temp/(6.0d0*pi*muf*ab)
c      calculation of the Peclet number
       pe=2.0d0*alpha*ab**3/dinf
c      ---------------------------------------------------
c      calculation of gravitation number
      grav=2.0d0/9.0d0*(drho*g0*ab**3)/(muf*dinf)
```

```
c      grav=0.0d0
c       -------------------------------------------------------
c       calculation of the electrical double layer interaction
c       based on constant zeta potential model--(HHF model)
c       calculation of the double layer parameter
       di=(4*3.14*epus*ab*pesic*pesib)/(kb*temp)
c      di=1000.0d0
c     da=(pesic-pesib)**2/(2.0d0*pesic*pesib)
     da=0.0d0
c       calculation of the Debye-Huckel length
        kesy=((2.0d0*zi**2*e0**2*n0)/(epus*kb*temp))**0.5
        tao=kesy*ab
c       tao=58.2d0
c       defination of the EDL interaction function
        fedl=di*tao*(dexp(-tao*x)/(1.0d0+dexp(-tao*x))
     &     -da*dexp(-2.0d0*tao*x)/(1.0d0-dexp(-2.0d0*tao*x)))
        vedl=0.5d0*di*(dlog((1.0d0+dexp(-tao*x))
     &     /(1.0d0-dexp(-tao*x)))
     &     +(da+1.0d0)*dlog(1.0d0-dexp(-2.0d0*tao*x)))
c       -------------------------------------------------------
c       calculation of Van der Waals interaction
c       calculation of the retardation parameter
        lambda=lambda0/ab
c       lambda=0.4d0
c       calculation of the adhession number
c       call hamaker(          ,a123)
      a123=1.0d-20
c      ad=a123/(6.0d0*kb*temp)
      ad=0.412d0
c       defination of Van dee Waals interaction function
c       fvdw=-ad*4.0d0/(x**2*(x+2.0d0)**2)
c       vvdw=-ad*(1.0d0/x+1.0d0/(x+2.0d0)+dlog(x/(x+2.0d0)))
        fvdw=-ad*lambda*(lambda+22.232d0*x)
     &     /(x**2*(lambda+11.116d0*x)**2)
        vvdw=-ad*(1.0d0/x-11.116d0/(11.116d0*x+lambda))
c       -------------------------------------------------------
c       calculation of hydrophobic interaction
        hd=0.0d0
        fhyp=-hd/x**2
        vhyp=-hd/x
c--------------------------------------------------------------
c       defination of functions for universal hydrodynamic coefficients
c       -------------------------------------------------------
        a1=-0.443d0
        b1=1.299d0
        c1=-0.5568d0
        d1=0.32d0
```

```
c       -------------------------------------------------------
        a2=1.455d0
        b2=1.259d0
        c2=0.7951d0
        d2=0.56d0
c       -------------------------------------------------------
        a3=-0.487d0
        b3=5.423d0
        c3=-0.5905d0
        d3=37.83d0
c       ---------------------------------------------
c       defination of functions for universal hydrodynamic
c       coefficients
        fun1=dabs(1.0d0+a1*dexp(-b1*x)+c1*dexp(-d1*x**0.75))
        fun2=dabs(1.0d0+a2*dexp(-b2*x)+c2*dexp(-d2*x**0.5))
        fun3=dabs(1.0d0+a3*dexp(-b3*x)+c3*dexp(-d3*x**0.5))
c       ---------------------------------------------
c       expressing the odinary differential equations
c       ---------------------------------------------
        dydx(1)=(y(2)/fun1-0.5d0*pe*fun2*(1.0d0+x)**2*y(1)
    &        +(grav+fedl+fvdw+fhyp)*y(1))
        dydx(2)=pe*fun3*(1.0d0+x)*y(1)
        return
        end
c       -----------------------------------------------
```

APPENDIX – B

Raw Data: SRCD Data Tables

Table 1
Raw data; SRCD for latex particles
Latex particle - hydrophilic glass collector
$a_p = 1.45\ \mu m$
Area =0.283 mm^2
pH = 5.8 and NaCl = 0.01M
Concentration = 6.2×10^6 particles / ml

Time seconds	Re 50-1	SRCD parti/mm^2	Re 50-2	SRCD parti/mm^2	Re 50-3	SRCD parti/mm^2	Re 50-4	SRCD parti/mm^2
0.00	0.00	0.00	0.00	0.00	0.00	0.00	0.00	0.00
30.00	17.00	60.09	17.00	60.09	17.00	60.09	16.00	56.56
60.00	34.00	120.18	38.00	134.32	37.00	130.79	40.00	141.39
90.00	58.00	205.02	52.00	183.81	78.00	275.72	55.00	194.41
120.00	74.00	261.58	76.00	268.65	98.00	346.41	77.00	272.18
150.00	98.00	346.41	96.00	339.34	124.00	438.32	95.00	335.81
180.00	122.00	431.25	110.0	388.83	136.00	480.74	120.00	424.18
195.00	132.00	466.60	125.0	441.85				
210.00								
	slope	2.33	slope	2.19	slope	2.79	slope	2.28
	Sh	3.66	Sh	3.45	Sh	4.38	Sh	3.59

Time seconds	Re 75-1	SRCD parti/mm^2	Re 75-2	SRCD parti/mm^2	Re 75-3	SRCD parti/mm^2	Re 75-4	SRCD parti/mm^2
0.00	0.00	0.00	0.00	0.00	0.00	0.00	0.00	0.00
30.00	22.00	77.77	60.00	212.09	31.00	109.58	42.00	148.46
60.00	43.00	152.00	86.00	303.99	65.00	229.76	92.00	325.20
90.00	65.00	229.76	127.00	448.92	97.00	342.88	130.00	459.53
120.00	85.00	300.46	160.00	565.57	130.00	459.53	162.00	572.64
150.00	102.00	360.55	187.00	661.01	155.00	547.90	190.00	671.62
180.00	111.00	392.36			178.00	629.20	215.00	759.99
	slope	2.36	slope	4.69	slope	3.64	slope	4.54
	Sh	3.70	Sh	7.36	Sh	5.73	Sh	7.12

Time	Re	SRCD	Re	SRCD	Re	SRCD
seconds	100-1	parti/mm^2	100-2	parti/mm^2	100-3	parti/mm^2
0.00	0.00	0.00	0.00	0.00	0.00	0.00
30.00	48.00	169.67	48.00	169.67	52.00	183.81
60.00	100.00	353.48	112.00	395.90	105.00	371.16
90.00	148.00	523.15	165.00	583.24	155.00	547.90
120.00	200.00	706.96	210.00	742.31	210.00	742.31
150.00	234.00	827.15	250.00	883.70	260.00	919.05
180.00	274.00	968.54	285.00	1007.42	287.00	1014.49
	slope	5.58	slope	5.91	slope	5.94
	Sh	8.76	Sh	9.23	Sh	9.33

Time	Re	SRCD	Re	SRCD	Re	SRCD	Re	SRCD
seconds	150-1	parti/mm^2	150-2	parti/mm^2	150-3	parti/mm^2	150-4	parti/mm^2
0.00	0.00	0.00	0.00	0.00	0.00	0.00	0.00	0.00
30.00	82.00	289.86	120.00	424.18	115.00	406.50	112.00	395.90
60.00	172.00	607.99	225.00	795.33	225.00	795.33	218.00	770.59
90.00	227.00	802.40	325.00	1148.82	320.00	1131.14	325.00	1148.82
120.00	296.00	1046.31	407.00	1438.67	380.00	1343.23	410.00	1449.28
150.00	348.00	1230.12	437.00	1544.72	440.00	1555.32	450.00	1590.67
180.00	397.00	1403.32	465.00	1643.69	500.00	1767.41	510.00	1802.76
slope		8.30		13.00		11.96		12.42
Sh		13.04		20.41		18.78		19.50

Time	Re	SRCD	Re	SRCD	Re	SRCD	Re	SRCD
seconds	200-1	parti/mm^2	200-2	parti/mm^2	200-3	parti/mm^2	200-4	parti/mm^2
0.00	0.00	0.00	0.00	0.00	0.00	0.00	0.00	0.00
15.00	75.00	265.11	100.00	353.48	100.00	353.48	70.00	247.44
30.00	150.00	530.22	210.00	742.31	190.00	671.62	135.00	477.20
45.00	226.00	798.87	330.00	1166.49	250.00	883.70	200.00	706.96
60.00	302.00	1067.52	410.00	1449.28	310.00	1095.79	260.00	919.05
75.00	364.00	1286.67	475.00	1679.04	370.00	1307.88	318.00	1124.07
90.00	424.00	1498.76	505.00	1785.08	400.00	1413.93	376.00	1329.09
120.00	510.00	1802.76	600.00	2120.89	525.00	1855.78	461.00	1629.55
150.00	588.00	2078.47			575.00	2032.52	517.00	1827.50
slope		17.16		24.74		20.70		15.55
Sh		26.93		38.85		32.50		24.39

Time	Re	SRCD	Re	SRCD	Re	SRCD	Re	SRCD
seconds	260-1	parti/mm^2	260-2	parti/mm^2	260-3	parti/mm^2	260-4	parti/mm^2
0.00	0.00	0.00	0.00	0.00	0.00	0.00	0.00	0.00
15.00	80.00	282.79	62.00	219.16	155.00	547.90	140.00	494.87
30.00	155.00	547.90	124.00	438.32	258.00	911.98	260.00	919.05
45.00	220.00	777.66	184.00	650.41	356.00	1258.40	340.00	1201.84
60.00	280.00	989.75	232.00	820.08	425.00	1502.30	405.00	1431.60
75.00	320.00	1131.14	280.00	989.75	520.00	1838.11	470.00	1661.36
90.00	360.00	1272.53	320.00	1131.14	577.00	2039.59	511.00	1806.29
105.00	390.00	1378.58	368.00	1300.81	639.00	2258.75	551.00	1947.68
120.00	420.00	1484.62	402.00	1421.00	690.00	2439.02	586.00	2071.40
135.00			437.00	1544.72				
150.00			470.00	1661.36				
slope		17.67		14.06		29.27		28.28
Sh		27.80		22.23		45.95		44.40

End of latex SRCD table

Table 2

Asphaltene emulsion - hydrophilic glass collector

Area =0.283 mm^2

For pH = 3.5, NaCl = 0.01M, a_p=1.5 μm

Concentration of particles = 2.1×10^6 particles / ml

Time seconds	Surface 1st	Re=62 no of parti	SRCD parti/mm^2
0.00		0.00	0.00
15.00		6.00	21.21
30.00		11.00	38.88
45.00		16.00	56.56
60.00		22.00	77.77
75.00		28.00	98.97
90.00		33.00	116.65
120.00		46.00	162.60
180.00		66.00	233.30
Slope	1.30	Sh	6.76

Time seconds	Surface 2nd	Re=62 no of parti	SRCD parti/mm^2
0.00		0.00	0.00
15.00		7.00	24.74
30.00		12.00	42.42
45.00		19.00	67.16
60.00		25.00	88.37
75.00		31.00	109.58
90.00		36.00	127.25
120.00		48.00	169.67
180.00		69.00	243.90
Slope	1.47	Sh	7.64

Time seconds	Surface 3rd	Re=62 no of parti	SRCD parti/mm^2
0.00		0.00	0.00
15.00		7.00	24.74
30.00		13.00	45.95
45.00		20.00	70.70
60.00		28.00	98.97
75.00		34.00	120.18
90.00		42.00	148.46
120.00		56.00	197.95
180.00		84.00	296.92
Slope	1.60	Sh	8.32

Time	Surface	Re=100	SRCD
seconds	1st	no of parti	parti/mm^2
0.00		0.00	0.00
30.00		21.00	74.23
45.00		33.00	116.65
60.00		42.00	148.46
90.00		62.00	219.16
120.00		81.00	286.32
150.00		101.00	357.02
180.00		115.00	406.50
Slope	2.51	Sh	13.00

Time	Surface	Re=100	SRCD
seconds	2nd	no of parti	parti/mm^2
0.00		0.00	0.00
15.00		11.00	38.88
30.00		20.00	70.70
45.00		31.00	109.58
60.00		41.00	144.93
90.00		59.00	208.55
120.00		85.00	300.46
150.00		100.00	353.48
180.00		110.00	388.83
Slope	2.42	Sh	12.58

Time	Surface	Re=150	SRCD
seconds	1st	no of parti	parti/mm^2
0.00		0.00	0.00
15.00		12.00	42.42
30.00		25.00	88.37
45.00		37.00	130.79
60.00		50.00	176.74
75.00		61.00	215.62
90.00		72.00	254.51
120.00		95.00	335.81
180.00		148.00	523.15
Slope	2.90	Sh	15.08

Time	Surface	Re=150	SRCD
seconds	2nd	no of parti	parti/mm^2
0.00		0.00	0.00
15.00		13.00	45.95
30.00		26.00	91.91
45.00		38.00	134.32
60.00		49.00	173.21
90.00		71.00	250.97
120.00		95.00	335.81
180.00		115.00	406.50
Slope	2.95	Sh	15.34

Time	Surface	Re=200	SRCD
seconds	1st	no of parti	parti/mm^2
0.00		0.00	0.00
15.00		15.00	53.02
30.00		29.00	102.51
45.00		45.00	159.07
60.00		59.00	208.55
90.00		81.00	286.32
120.00		106.00	374.69
180.00		128.00	452.46
Slope	3.50	Sh	18.20

Time	Surface	Re=200	SRCD
seconds	2nd	no of parti	parti/mm^2
0.00		0.00	0.00
15.00		15.00	53.02
30.00		32.00	113.11
45.00		48.00	169.67
60.00		62.00	219.16
90.00		91.00	321.67
120.00		115.00	406.50
180.00		166.00	586.78
Slope	3.70	Sh	19.24

Time	Surface	Re=255	SRCD
seconds	1st	no of parti	parti/mm^2
0.00		0.00	0.00
15.00		28.00	98.97
30.00		56.00	197.95
45.00		85.00	300.46
60.00		115.00	406.50
75.00		144.00	509.01
90.00		169.00	597.38
105.00		191.00	675.15
120.00		206.00	728.17
150.00		216.00	763.52
Slope	6.75	Sh	35.10

Time	Surface	Re=255	SRCD
seconds	2nd	no of parti	parti/mm^2
0.00		0.00	0.00
15.00		31.00	109.58
30.00		61.00	215.62
45.00		91.00	321.67
60.00		122.00	431.25
75.00		153.00	540.83
90.00		178.00	629.20
105.00		201.00	710.50
120.00		215.00	759.99
144.00		225.00	795.33
Slope	7.20	Sh	37.44

Time	Surface	Re=295	SRCD
seconds	1st	no of parti	parti/mm^2
0.00		0.00	0.00
15.00		52.00	183.81
30.00		101.00	357.02
45.00		151.00	533.76
60.00		202.00	714.03
75.00		251.00	887.24
90.00		285.00	1007.42
105.00		305.00	1078.12
120.00		312.00	1102.86
Slope	11.90	Sh	61.88

Time	Surface	Re=295	SRCD
seconds	2nd	no of parti	parti/mm^2
0.00		0.00	0.00
15.00		48.00	169.67
30.00		96.00	339.34
45.00		143.00	505.48
60.00		190.00	671.62
75.00		237.00	837.75
90.00		269.00	950.87
105.00		291.00	1028.63
120.00		299.00	1056.91
Slope	11.20	Sh	58.24

Time	Surface	Re=370	SRCD
seconds	1st	no of parti	parti/mm^2
0.00		0.00	0.00
15.00		59.00	208.55
30.00		117.00	413.57
45.00		176.00	622.13
60.00		236.00	834.22
75.00		279.00	986.21
90.00		320.00	1131.14
105.00		360.00	1272.53
120.00		365.00	1290.21
Slope	13.90	Sh	72.28

Time	Surface	Re=370	SRCD
seconds	2nd	no of parti	parti/mm^2
0.00		0.00	0.00
15.00		72.00	254.51
30.00		142.00	501.94
45.00		212.00	749.38
60.00		281.00	993.28
75.00		350.00	1237.19
90.00		390.00	1378.58
Slope	16.56	Sh	80.91

Time	Surface	Re=410	SRCD
seconds	1st	no of parti	parti/mm^2
0.00		0.00	0.00
15.00		76.00	268.65
30.00		150.00	530.22
45.00		231.00	816.54
60.00		312.00	1102.86
75.00		374.00	1322.02
90.00		410.00	1449.28
120.00		441.00	1558.85
Slope	18.20	Sh	94.64

Time	Surface	Re=410	SRCD
seconds	2nd	no of parti	parti/mm^2
0.00		0.00	0.00
15.00		78.00	275.72
30.00		152.00	537.29
45.00		227.00	802.40
60.00		301.00	1063.98
90.00		348.00	1230.12
120.00		382.00	1350.30
Slope	17.80	Sh	92.56

Time	Surface	Re=545	SRCD
seconds	1st	no of parti	parti/mm^2
0.00		0.00	0.00
15.00		77.00	272.18
30.00		155.00	547.90
45.00		231.00	816.54
60.00		300.00	1060.45
90.00		385.00	1360.90
120.00		411.00	1452.81
Slope	18.20	Sh	94.64

Time	Surface	Re=545	SRCD
seconds	2nd	no of parti	parti/mm^2
0.00		0.00	0.00
15.00		86.00	303.99
30.00		169.00	597.38
45.00		245.00	866.03
60.00		331.00	1170.02
Slope	19.50	Sh	101.40

Table 3

Asphaltene emulsion - hydrophilic glass collector
Area =0.283 mm^2
For pH = 8.0, NaCl = 0.001M, a_p=1.5 μm
Concentration of particles = 8.1×10^6 particles / ml

Time	Surface	Re=150	SRCD
seconds	1st	no of particles	parti/mm^2
0		0	0.00
10		59	208.55
20		121	427.71
30		179	632.73
40		241	851.89
50		298	1053.38
60		353	1247.79
70		405	1431.60
80		440	1555.32
90		453	1601.27
Slope	21.02	Sh	27.54

Time	Surface	Re=210	SRCD	Time	Surface	Re=210	SRCD
seconds	1st	no of particles	parti/mm^2	seconds	2nd	no of particles	parti/mm^2
0		0	0.00	0		0	0.00
10		76	268.65	10		82	289.86
20		141	498.41	20		161	569.11
30		214	756.45	30		239	844.82
40		287	1014.49	40		316	1117.00
50		351	1240.72	50		375	1325.56
60		394	1392.72	60		419	1481.09
70		428	1512.90	90		491	1735.60
90		485	1714.39				
Slope	25.08	Sh	32.85	Slope	27.38	Sh	35.87

Time	Surface	Re=278	SRCD	Time	Surface	Re=278	SRCD
seconds	1st	no of particles	parti/mm^2	seconds	2nd	no of particles	parti/mm^2
0		0	0.00	0		0	0.00
10		95	335.81	10		107	378.23
20		188	664.55	20		205	724.64
30		283	1000.35	30		301	1063.98
40		365	1290.21	40		381	1346.77
50		451	1594.20	50		443	1565.92
60		482	1703.78	60		485	1714.39
Slope	32.36	Sh	42.39	90		558	1972.43
				slope	33.16	Sh	43.44

Time	Surface	Re=315	SRCD	Time	Surface	Re=315	SRCD
seconds	1st	no of particle	parti/mm^2	seconds	2nd	no of particles	parti/mm^2
0		0	0.00	0		0	0.00
10		103	364.09	10		101	357.02
20		204	721.10	20		197	696.36
30		297	1049.84	30		296	1046.31
40		371	1311.42	40		385	1360.90
50		429	1516.44	50		447	1580.06
60		468	1654.29	60		489	1728.53
slope	34.01	Sh	44.55	slope	34.44	Sh	45.12

Time	Surface	Re=420	SRCD	Time	Surface	Re=420	SRCD
seconds	1st	no of particles	parti/mm^2	seconds	2nd	no of particles	parti/mm^2
0		0	0.00	0		0	0.00
10		98	346.41	10		103	364.09
20		198	699.89	20		204	721.10
30		295	1042.77	30		298	1053.38
40		398	1406.86	40		371	1311.42
50		501	1770.94	50		429	1516.44
60		572	2021.92	60		468	1654.29
70		629	2223.40	slope	35.47	Sh	46.47
80		676	2389.54				
90		710	2509.72				
slope	35.19	Sh	46.1				

Time	Surface	Re=505	SRCD	Time	Surface	Re=505	SRCD
seconds	1st	no of particles	parti/mm^2	seconds	2nd	no of particles	parti/mm^2
0		0	0.00	0		0	0.00
10		142	501.94	10		148	523.15
20		275	972.07	20		293	1035.70
30		427	1509.37	30		415	1466.95
40		492	1739.13	40		521	1841.64
50		568	2007.78	50		596	2106.75
60		591	2089.08	60		605	2138.56
slope	49.82	Sh	65.26	slope	49.97	Sh	65.46

Table 4

Asphaltene emulsion - hydrophobic glass collector
Area =0.283 mm^2
For pH = 8.5, NaCl = 0.01M, a_p=1.5 μm
Concentration of particles = 7.1×10^6 particles / ml

Time	Surface	Re=100	SRCD	Time	Surface	Re=100	SRCD
seconds	1st	no of parti	parti/mm^2	seconds	2nd	no of parti	parti/mm^2
0		0	0.00	0		0	0.00
30		3	10.60	30		4	14.14
60		6	21.21	60		7	24.74
90		8	28.28	90		11	38.88
120		10	35.35	120		14	49.49
180		15	53.02	180		21	74.23
Slope	0.3	Sh	0.44	Slope	0.42	Sh	0.61

Time	Surface	Re=150	SRCD	Time	Surface	Re=150	SRCD
seconds	1st	no of parti	parti/mm^2	seconds	2nd	no of parti	parti/mm^2
0		0	0.00	0		0	0.00
30		6	21.21	30		7	24.74
60		12	42.42	60		13	45.95
90		17	60.09	90		19	67.16
120		23	81.30	120		24	84.84
150		29	102.51	150		31	109.58
180		35	123.72	180		37	130.79
Slope	0.69	Sh	1.00	Slope	0.73	Sh	1.06

Time	Surface	Re=200	SRCD	Time	Surface	Re=200	SRCD
seconds	1st	no of parti	parti/mm^2	seconds	2nd	no of parti	parti/mm^2
0		0	0.00	0		0	0.00
30		14	49.49	30		15	53.02
60		26	91.91	60		29	102.51
90		40	141.39	90		43	152.00
120		53	187.35	120		58	205.02
150		65	229.76	150		71	250.97
180		79	279.25	180		88	311.06
Slope	1.55	Sh	2.25	Slope	1.7	Sh	2.47

Time	Surface	Re=255	SRCD	Time	Surface	Re=255	SRCD
seconds	1st	no of parti	parti/mm^2	seconds	2nd	no of parti	parti/mm^2
0		0	0.00	0		0	0.00
30		20	70.70	30		22	77.77
60		39	137.86	60		42	148.46
90		57	201.48	90		63	222.69
120		78	275.72	120		87	307.53
150		95	335.81	150		107	378.23
180		108	381.76	180		126	445.39
Slope	2.2	Sh	3.19	Slope	2.5	Sh	3.63

Time	Surface	Re=370	SRCD	Time	Surface	Re=370	SRCD
seconds	1st	no of parti	parti/mm^2	seconds	2nd	no of parti	parti/mm^2
0		0	0.00	0		0	0.00
30		27	95.44	30		24	84.84
60		48	169.67	60		45	159.07
90		79	279.25	90		69	243.90
120		112	395.90	120		95	335.81
150		135	477.20	150		120	424.18
180		165	583.24	180		144	509.01
Slope	3.2	Sh	4.64	Slope	2.8	Sh	4.06

Time	Surface	Re=410	SRCD	Time	Surface	Re=410	SRCD
seconds	1st	no of parti	parti/mm^2	seconds	2nd	no of parti	parti/mm^2
0		0	0.00	0		0	0.00
30		26	91.91	30		35	123.72
60		53	187.35	60		68	240.37
90		82	289.86	90		97	342.88
120		109	385.30	120		128	452.46
150		138	487.80	150		145	512.55
180		163	576.18	180		165	583.24
Slope	3.21	Sh	4.66	Slope	3.82	Sh	5.54

Time	Surface	Re=505	SRCD	Time	Surface	Re=505	SRCD
seconds	1st	no of parti	parti/mm^2	seconds	2nd	no of parti	parti/mm^2
0		0	0.00	0		0	0.00
30		95	335.81	30		78	275.72
60		188	664.55	60		155	547.90
90		275	972.07	90		235	830.68
120		355	1254.86	120		273	965.01
150		405	1431.60	150		303	1071.05
180		419	1481.09	180		321	1134.68
Slope	10.2	Sh	14.79	Slope	9.2	Sh	13.34

Table 5
Asphaltene emulsion - hydrophobic glass collector
Area =0.283 mm^2
For pH = 3.5, NaCl = 0.01M, a_p=1.5 μm
Concentration of particles = 2.1×10^6 particles / ml

Time	Surface	Re=62	SRCD
seconds	1st	no of parti	parti/mm^2
0		0	0.00
30		22	77.77
60		46	162.60
90		66	233.30
120		84	296.92
155		99	349.95
180		110	388.83
slope	2.63	Sh	13.08

Time	Surface	Re=62	SRCD
seconds	2nd	no of parti	parti/mm^2
0		0	0.00
15		9	31.81
30		17	60.09
45		26	91.91
60		35	123.72
90		53	187.35
120		70	247.44
180		96	339.34
slope	2.1	Sh	10.50

Time	Surface	Re=62	SRCD
seconds	3rd	no of parti	parti/mm^2
0		0	0.00
30		22	77.77
60		42	148.46
120		75	265.11
180		97	342.88
Slope	2.4	Sh	11.35

Time	Surface	Re=150	SRCD
seconds	1st	no of parti	parti/mm^2
0		0	0.00
30		42	148.46
45		66	233.30
60		89	314.60
120		142	501.94
180		175	618.59
slope	5.2	Sh	25.90

Time	Surface	Re=150	SRCD
seconds	2nd	no of parti	parti/mm^2
0		0	0.00
30		38	134.32
60		74	261.58
120		98	346.41
180		119	420.64
slope	4.4	Sh	21.9

Time	Surface	Re=200	SRCD
seconds	1st	no of parti	parti/mm^2
0		0	0.00
30		37	130.79
60		71	250.97
120		110	388.83
180		139	491.34
Slope	4.2	Sh	20.90

Time	Surface	Re=200	SRCD
seconds	2nd	no of parti	parti/mm^2
0		0	0.00
30		45	159.07
60		86	303.99
120		118	417.11
180		145	512.55
Slope	5.1	Sh	25.40

Time	Surface	Re=255	SRCD
seconds	1st	no of parti	parti/mm^2
0		0	0.00
15		49	173.21
30		95	335.81
45		145	512.55
60		191	675.15
75		235	830.68
90		259	915.52
105		284	1003.89
120		306	1081.65
150		354	1251.33
Slope	11.3	Sh	56.27

Time	Surface	Re=255	SRCD
seconds	2nd	no of parti	parti/mm^2
0		0	0.00
15		41	144.93
30		84	296.92
45		125	441.85
60		165	583.24
75		190	671.62
90		215	759.99
105		240	848.36
120		262	926.12
144		297	1049.84
Slope	9.8302	Sh	48.95

Time	Surface	Re=295	SRCD
seconds	1st	no of parti	parti/mm^2
0		0	0.00
15		65	229.76
30		128	452.46
45		189	668.08
60		252	890.77
75		290	1025.10
90		325	1148.82
105		355	1254.86
120		375	1325.56
Slope	14.9	Sh	74.2

Time	Surface	Re=295	SRCD
seconds	2nd	no of parti	parti/mm^2
0		0	0
15		58	205.01
30		121	427.71
45		175	618.59
60		235	830.68
75		285	1007.42
90		292	1032.16
105		326	1152.35
120		351	1240.72
Flux Jo	13.7	Sh	68.2

Time	Surface	Re=370	SRCD
seconds	1st	no of parti	parti/mm^2
0		0	0.00
15		65	229.76
30		128	452.46
45		186	657.48
60		247	873.10
75		278	982.68
90		323	1141.75
105		359	1269.00
120		383	1353.84
Slope	14.7	Sh	74.20

Time	Surface	Re=370	SRCD
seconds	2nd	no of parti	parti/mm^2
0		0	0
15		85	300.4595
30		168	593.8494
45		245	866.0304
60		335	1184.164
75		379	1339.696
90		402	1420.997
Slope	19.9	Sh	99.1

Time	Surface	Re=410	SRCD
seconds	1st	no of parti	parti/mm^2
0		0	0.00
15		88	311.06
30		171	604.45
45		251	887.24
60		331	1170.02
75		374	1322.02
90		419	1481.09
120		460	1626.02
Slope	19.7	Sh	98.10

Time	Surface	Re=410	SRCD
seconds	2nd	no of parti	parti/mm^2
0		0	0.00
15		89	314.60
30		179	632.73
45		265	936.73
60		295	1042.77
90		335	1184.16
120		368	1300.81
Slope	20.9	Sh	104.08

Time	Surface	Re=545	SRCD
seconds	1st	no of parti	parti/mm^2
0		0	0.00
15		93	328.74
30		183	646.87
45		265	936.73
60		303	1071.05
90		349	1233.65
120		358	1265.46
Slope	21.1	Sh	105.80

Time	Surface	Re=545	SRCD
seconds	2nd	no of parti	parti/mm^2
0		0	0.00
15		93	328.74
30		185	653.94
45		275	972.07
60		318	1124.07
90		352	1244.26
120		375	1325.56
Slope	21.7	Sh	108.10

Table 6
Asphaltene emulsion – hydrophobic glass collector
Area =0.283 mm^2
For pH = 8.0, NaCl = 0.001M, a_p=1.5 μm
Concentration of particles = 8.1×10^6 particles / ml

Time	Surface	Re=46	SRCD	Time	Surface	Re=46	SRCD
seconds	1st	no of particles	parti/mm^2	seconds	2nd	no of particles	parti/mm^2
0		0	0.00	0		0	0.00
10		15	53.02	10		12	42.42
20		29	102.51	20		25	88.37
30		46	162.60	30		39	137.86
40		61	215.62	40		54	190.88
60		88	311.06	60		75	265.11
90		121	427.71	90		115	406.50
120		145	512.55	120		158	558.50
slope	5.26	Sh	6.9	slope	4.59	Sh	6.01

Time	Surface	Re=96	SRCD	Time	Surface	Re=96	SRCD
seconds	1st	no of particles	parti/mm^2	seconds	2nd	no of particles	parti/mm^2
0		0	0.00	0		0	0.00
10		37	130.79	10		37	130.79
20		67	236.83	20		71	250.97
30		97	342.88	30		106	374.69
40		131	463.06	40		137	484.27
50		164	579.71	50		169	597.38
60		191	675.15	60		199	703.43
70		226	798.87	70		227	802.40
80		259	915.52	80		255	901.38
90		280	989.75	90		281	993.28
100		301	1063.98	120		333	1177.09
110		311	1099.33	130		345	1219.51
120		317	1120.54	slope	11.98	Sh	15.69
slope	11.45	Sh	15				

Time	Surface	Re=150	SRCD	Time	Surface	Re=150	SRCD
seconds	1st	no of particles	parti/mm^2	seconds	2nd	no of particles	parti/mm^2
0		0	0.00	0		0	0.00
10		59	208.55	10		65	229.76
20		113	399.43	20		125	441.85
30		167	590.31	30		182	643.34
40		213	752.92	40		234	827.15
50		251	887.24	50		266	940.26
60		273	965.01	60		291	1028.63
90		293	1035.70	90		312	1102.86
slope	18.59	Sh	24.35	slope	20.1	Sh	26.33

Time	Surface	Re=210	SRCD	Time	Surface	Re=210	SRCD
seconds	1st	no of particles	parti/mm^2	seconds	2nd	no of particles	parti/mm^2
0		0	0.00	0		0	0.00
15		102	360.55	15		82	289.86
20		131	463.06	20		110	388.83
30		199	703.43	30		169	597.38
40		256	904.91	40		208	735.24
50		295	1042.77	50		229	809.47
60		327	1155.89	60		246	869.57
90		369	1304.35	90		260	919.05
slope	23.03	Sh	30.17	Slope	19.03	Sh	24.93

Time	Surface	Re=278	SRCD	Time	Surface	Re=278	SRCD
seconds	1st	no of particles	parti/mm^2	seconds	2nd	no of particles	parti/mm^2
0		0	0.00	0		0	0
10		82	289.86	10		83	293.3899
20		163	576.18	20		162	572.6405
30		244	862.50	30		238	841.2867
40		316	1117.00	40		290	1025.097
50		361	1276.07	50		342	1208.908
60		403	1424.53	60		374	1322.022
80		426	1505.83	80		415	1466.949
slope	28.33	Sh	37.11	slope	28.3	Sh	37.07

Time	Surface	Re=310	SRCD	Time	Surface	Re=310	SRCD
seconds	1st	no of particles	parti/mm^2	seconds	2nd	no of particles	parti/mm^2
0		0	0.00	0		0	0.00
10		94	332.27	10		95	335.81
20		178	629.20	20		183	646.87
30		251	887.24	30		272	961.47
40		308	1088.72	40		320	1131.14
60		344	1215.98	50		352	1244.26
90		383	1353.84	60		379	1339.70
slope	30.37	Sh	39.78	90		418	1477.55
				slope	32.24	Sh	42.23

Time	Surface	Re=420	SRCD	Time	Surface	Re=420	SRCD
seconds	1st	no of particles	parti/mm^2	seconds	2nd	no of particles	parti/mm^2
0		0	0.00	0		0	0.00
10		118	417.11	10		99	349.95
20		211	745.85	20		201	710.50
30		286	1010.96	30		288	1018.03
40		338	1194.77	40		351	1240.72
50		374	1322.02	50		384	1357.37
60		409	1445.74	60		404	1428.07
slope	38.18	Sh	50.01	slope	34.47	Sh	45.44

Time	Surface	Re=505	SRCD
seconds	1st	no of particles	parti/mm^2
0		0	0.00
10		149	526.69
20		268	947.33
30		367	1297.28
40		436	1541.18
50		478	1689.64
60		502	1774.48
Slope	48.43	Sh	63.44

End of hydrophobic collector data

Table 7

Asphaltene emulsion – asphaltene coated collector

Area =0.283 mm^2

For pH = 3.5, NaCl = 0.01M, a_p=1.5 μm

Concentration of particles =3.1×10^6 particles / ml

Time	Collector	Re=45	SRCD	Time	Collector	Re=45	SRCD
seconds	Asph -1	no of parti	parti/mm^2	seconds	Asph -2	no of parti	parti/mm^2
0		0	0	0		0	0
30		14	49.48	30		23	81.30
60		27	95.44	60		44	155.53
90		41	144.92	90		66	233.29
120		54	190.88	120		75	265.11
150		70	247.43	150		93	328.73
180		86	303.99	180		109	385.29
210		102	360.55	210		126	445.38
slope	1.67	Sh	5.14	slope	2.2	Sh	6.78

Time	Collector	Re=96	SRCD	Time	Collector	Re=96	SRCD
seconds	Asph -1	no of parti	parti/mm^2	seconds	Asph -2	no of parti	parti/mm^2
0		0	0	0		0	0
30		34	120.18	30		35	123.72
60		72	254.51	60		66	233.30
90		105	371.16	90		99	349.95
120		140	494.87	120		134	473.67
150		174	615.06	150		169	597.38
180		200	706.96	180		205	724.64
210		219	774.13	210		222	784.73
slope	4.12	Sh	12.57	slope	3.98	Sh	12.26

Time	Collector	Re=150	SRCD	Time	Collector	Re=150	SRCD
seconds	Asph -1	no of parti	parti/mm^2	seconds	Asph -2	no of parti	parti/mm^2
0		0	0.00	0		0	0.00
15		32	113.11	15		38	134.32
30		63	222.69	30		67	236.83
45		97	342.88	45		105	371.16
60		130	459.53	60		141	498.41
75		162	572.64	75		176	622.13
90		191	675.15	90		211	745.85
120		246	869.57	120		268	947.33
150		296	1046.31	slope	8.12	Sh	25.01
180		338	1194.77				
slope	7.57	Sh	23.32				

Time	Collector	Re=215	SRCD	Time	Collector	Re=215	SRCD
seconds	Asph -1	no of parti	parti/mm^2	seconds	Asph -2	no of parti	parti/mm^2
0		0	0.00	0		0	0.00
15		49	173.21	15		51	180.28
30		97	342.88	30		106	374.69
45		146	516.08	45		161	569.11
60		192	678.69	60		215	759.99
75		236	834.22	75		264	933.19
90		278	982.68	90		317	1120.54
120		337	1191.23	120		378	1336.16
150		365	1290.21	150		415	1466.95
slope	11.13	Sh	34.28	slope	12.5	Sh	38.5

Time	Collector	Re=315	SRCD	Time	Collector	Re=315	SRCD
seconds	Asph -1	no of parti	parti/mm^2	seconds	Asph -2	no of parti	parti/mm^2
0		0	0.00	0		0	0.00
15		77	272.18	15		74	261.58
30		159	562.04	30		147	519.62
45		229	809.47	45		219	774.13
60		294	1039.24	60		288	1018.03
75		361	1276.07	75		352	1244.26
90		416	1470.48	90		412	1456.34
120		465	1643.69	120		469	1657.83
slope	17.41	Sh	53.62	slope	16.9	Sh	52.05

Time	Collector	Re=410	SRCD	Time	Collector	Re=410	SRCD
seconds	Asph -1	no of parti	parti/mm^2	seconds	Asph -2	no of parti	parti/mm^2
0		0	0.00	0		0	0.00
15		94	332.27	15		91	321.67
30		185	653.94	31		179	632.73
45		274	968.54	45		267	943.80
60		356	1258.40	60		345	1219.51
75		421	1488.16	75		416	1470.48
90		483	1707.32	90		454	1604.81
120		526	1859.31	120		501	1770.94
slope	21.3	Sh	65.6	slope	20.13	Sh	61.97

Time	Collector	Re=505	SRCD	Time	Collector	Re=505	SRCD
seconds	Asph -1	no of parti	parti/mm^2	seconds	Asph -2	no of parti	parti/mm^2
0		0	0.00	0		0	0.00
15		124	438.32	15		119	420.64
30		243	858.96	30		231	816.54
45		352	1244.26	45		337	1191.23
60		443	1565.92	60		436	1541.18
75		505	1785.08	75		498	1760.34
90		534	1887.59	90		529	1869.92
slope	28.04	Sh	86.36	slope	26.8	Sh	82.54

Time	Collector	Re=625	SRCD	Time	Collector	Re=625	SRCD
seconds	Asph -1	no of parti	parti/mm^2	seconds	Asph -2	no of parti	parti/mm^2
0		0	0.00	0		0	0
15		157	554.97	10		102	360.55
30		318	1124.07	20		189	668.08
45		445	1572.99	30		288	1018.03
60		581	2053.73	40		376	1329.09
75		659	2329.45	50		437	1544.72
90		689	2435.49	60		476	1682.57
slope	35.82	Sh	110.33	70		517	1827.50
				80		529	1869.92
				slope	33.94	Sh	104.53

Table 8

Asphaltene emulsion – bitumen coated collector
Area =0.283 mm^2
For pH = 3.5, NaCl = 0.01M, a_p=1.5 μm
Concentration of particles =3.1×10^6 particles / ml

Time	Collector	Re=96	SRCD
seconds		no of parti	parti/mm^2
0		0	0.00
30		27	95.44
60		52	183.81
90		77	272.18
120		99	349.95
150		123	434.78
210		147	519.62
240		167	590.31
270		177	625.66
slope	2.94	Sh	10.29

Time	Collector	Re=150	SRCD
seconds		no of parti	parti/mm^2
0		0	0.00
15		22	77.77
30		45	159.07
45		62	219.16
60		85	300.46
75		107	378.23
90		127	448.92
120		147	519.62
150		155	547.90
slope	5.01	Sh	17.5

Time	Collector	Re=215	SRCD
seconds		no of parti	parti/mm^2
0		0	0.00
15		39	137.86
30		81	286.32
45		119	420.64
60		155	547.90
75		195	689.29
90		235	830.68
120		298	1053.38
150		338	1194.77
180		359	1269.00
slope	9.23	Sh	32.86

Time	Collector	Re=315	SRCD
seconds		no of parti	parti/mm^2
0		0	0.00
15		52	183.81
30		101	357.02
45		149	526.69
60		198	699.89
75		242	855.43
90		289	1021.56
120		361	1276.07
150		379	1339.70
180		389	1375.04
slope	11.58	Sh	41.22

Time	Collector	Re=215	SRCD
seconds		no of parti	parti/mm^2
0		0	0
15		39	137.8579
30		81	286.3203
45		119	420.6433
60		155	547.8968
75		195	689.2895
90		235	830.6822
120		298	1053.376
150		338	1194.768
180		359	1269
slope	9.23	Sh	32.86

Time	Collector	Re=315	SRCD
seconds		no of parti	parti/mm^2
0		0	0
15		52	183.8105
30		101	357.0166
45		149	526.6879
60		198	699.894
75		242	855.4259
90		289	1021.562
120		361	1276.069
150		379	1339.696
180		389	1375.044
slope	11.58	Sh	41.22

Time	Collector	Re=625	SRCD
seconds		no of parti	parti/mm^2
0		0	0.00
10		91	321.67
20		173	611.52
30		260	919.05
40		348	1230.12
50		415	1466.95
60		447	1580.06
slope	30.74	Sh	109.43